Principles for Designing Robust and Stable Synthetic Microbial Consortia

Thesis by
Xinying Ren

In Partial Fulfillment of the Requirements for the
Degree of
Doctor of Philosophy

Caltech

CALIFORNIA INSTITUTE OF TECHNOLOGY
Pasadena, California

2021
Defended March 1, 2021

© 2021

Xinying Ren
ORCID: 0000-0002-8852-6722

ACKNOWLEDGEMENTS

ABSTRACT

Engineering stable microbial consortia with robust functions are useful in many areas, including bioproduction and human health. Robust and stable properties depend on proper control of dynamics ranging from single cell-level to population-environment interactions. In this thesis, I discuss principles of building microbial consortia with synthetic circuits in two design scenarios.

First, for one microbial population, strong disturbances in environments often severely perturb cell states and lead to heterogeneous responses. Single cell-level design of control circuits may fail to induce a uniform response as needed. I demonstrate that cell-cell signaling systems can facilitate coordination among cells and achieve robust population-level behaviors. Moreover, I show that heterogeneity can be harnessed for robust adaptation at population-level via a bistable state switch.

Second, multi-species consortia are intrinsically unstable due to competitive exclusion. Previous theoretical investigations based on models of pairwise interactions mainly explored what interaction network topology ensures stable coexistence. Yet neglecting detailed interaction mechanisms and spatial context results in contradictory predictions. Focusing on chemical-mediated interaction, I show that detailed mechanisms of chemical consumption/accumulation and chemical-induced growth/death, interaction network topology and spatial structures of environments all are critical factors to maintain stable coexistence. With a two population-system, I demonstrate that the same interaction network topology can exhibit qualitatively different or even opposite behaviors due to interaction mechanisms and spatial conditions.

PUBLISHED CONTENT AND CONTRIBUTIONS

Ren, Xinying and Richard M Murray (2020). "Layered Feedback Control Improves Robust Functionality across Heterogeneous Cell Populations". In: *bioRxiv*.
X.R. conceived the project, performed the research, and wrote the manuscript.

Ren, Xinying, Christian Cuba Samaniego, et al. (2020). "Bistable State Switch Enables Ultrasensitive Feedback Control in Heterogeneous Microbial Populations". In: *bioRxiv*.
X.R. and C.C.M. conceived the project. X.R. developed models, ran simulations, and wrote the manuscript.

Ren, Xinying and Richard M Murray (2019). "Cooperation enhances robustness of coexistence in spatially structured consortia". In: *2019 18th European Control Conference (ECC)*. IEEE, pp. 2651–2656.
X.R. conceived the project, performed the research, and wrote the manuscript.

– (2018). "Role of interaction network topology in controlling microbial population in consortia". In: *2018 IEEE Conference on Decision and Control (CDC)*. IEEE, pp. 2691–2697.
X.R. conceived the project, performed the research, and wrote the manuscript.

Ren, Xinying, Ania-Ariadna Baetica, et al. (2017). "Population regulation in microbial consortia using dual feedback control". In: *2017 IEEE 56th Annual Conference on Decision and Control (CDC)*. IEEE, pp. 5341–5347.
X.R. conceived the project, developed models and ran simulations. X.R., A.A.B. and A.S. wrote the manuscript.

TABLE OF CONTENTS

C h a p t e r   1

INTRODUCTION

The field of synthetic biology involves redesigning and engineering organisms for novel and useful functions. Synthetic organisms of bacteria, yeast and mammalian cells can have diverse applications in biofuel production (Alper and Stephanopoulos, 2009; H. Zhang et al., 2015; Zhou et al., 2015), biosensing (Meyer et al., 2015; Xiu et al., 2017), therapeutics (J. C. Anderson et al., 2006; Lu and Collins, 2007), novel biomaterials (Widmaier et al., 2009; Khalil and Collins, 2010), etc. Synthetic gene circuits are used to modulate dynamics of living organisms, of which standardized and modular circuit components are combined to achieve complex functions.

Building synthetic circuits to realize desired functions relies on specific molecular implementations, which often involves an iterative process of trial and error and is in general difficult from the engineering perspective. Therefore, developing design principles becomes important and helpful. Based on fundamental understanding of biology, theory and mathematical models that capture essential dynamics of synthetic systems can provide key insights on circuit designs.

Since the original synthetic gene circuits of an oscillator (Elowitz and Leibler, 2000) and a toggle switch (Gardner, Cantor, and Collins, 2000), a multitude of novel behaviors have been created in single cells and single populations in the past decades. Yet until recently, engineering multicellular systems that involve multiple cell populations starts to be recognized in the field of synthetic biology. Compared to single cells or single populations, multiple cell populations have more potential in generating complex dynamics and fulfilling complicated functions through a division of labor (Brenner, You, and Arnold, 2008; Johns et al., 2016; Lindemann et al., 2016; Roell et al., 2019). In particular, studies of synthetic microbial consortia are emerging because of their advantages in long-term survival. It has been a major issue in engineering microbial populations that synthetic circuits may induce a significant burden in host cells that leads to reduced biosynthesis, slow growth and even failure to maintain a population density in long terms (Ceroni, Algar, et al., 2015; Borkowski et al., 2016). However, due to a division of labor among multiple microbial populations, host cells in a consortium can obtain more fitness benefits with a reduced burden from synthetic circuits (Gestel, Vlamakis, and Kolter, 2015;

West and Cooper, 2016).

Despite great advantages of synthetic microbial consortia, there are significant challenges associated with engineering multiple interacting populations with controlled behaviors. First, many desired functions depend on reliable and robust dynamics of synthetic cell populations, especially in complicated and fluctuating environments. Compared to single cells or single populations, there exist more diverse sources of uncertainties and disturbances in microbial consortia, ranging from noises in gene expression and heterogeneous cell states to cell-cell interactions and population-environment interactions. The second challenge is that the performance of microbial consortia requires fine-tuning of not only single populations' behaviors but also the composition and density ratio of multiple populations. In a consortium where the desired function is divided into subtasks among multiple populations, each population needs to grow and maintain a certain density in prior to fulfilling their subtasks (Jones and Xin Wang, 2018; Jawed, Yazdani, and Koffas, 2019). Thus, factors that affect the population density become crucial and may require proper control, including cell growth/death kinetics, cell metabolic states, resource allocation in environments and spatial structures of consortia. The third challenge lies in maintaining stable coexistence of synthetic microbial populations where they do not outcompete each other in co-cultures. Natural microbial consortia can maintain stable coexistence without competition exclusion through cell-cell interactions, yet these interactions are often complicated and inexplicit (Burmølle et al., 2006; Woyke et al., 2006; Kuramitsu et al., 2007; Relman, 2012; Clemente et al., 2015). To engineer stable and coexisting populations, we need to understand how cell-cell interactions affect population dynamics and to reprogram interaction networks for dynamics modulation. More challenges include: mutation and cheater populations may jeopardize desired functions by dominating the consortia in long terms (Travisano and Velicer, 2004; Escalante et al., 2015); the lack of orthogonal synthetic cell-cell interaction components makes it hard to achieve explicit interactions without cross-talks in implementations (Wu, Menn, and Xiao Wang, 2014; Scott and Hasty, 2016).

This thesis mainly attempts to explore design principles of synthetic microbial consortia that tackle the three main challenges mentioned above: achieving stable and robust population-level dynamics, densities and coexistence.

Existing design principles for stable and robust cellular behaviors are proposed in theoretical studies (W. Ma et al., 2009; Drengstig et al., 2012; Briat, Gupta, and

Khammash, 2016; Xiao and Doyle, 2018), and are verified in experiments with synthetic circuits (Aoki et al., 2019; Agrawal et al., 2019). These principles mostly focus on controlling a certain gene expression level by engineering intracellular gene regulation networks in single cells, so are considered as single cell-level design principles. Single cell-level design principles are not very helpful for synthetic microbial consortia for various reasons. First, merely intracellular gene regulation cannot modulate population-level dynamics and densities or cell-cell interactions in microbial consortia. Second, the assumptions of homogeneous metabolic states and ideal growth for all individual cells in single cell-level designs become unrealistic in a co-culture of multiple cell populations. The growth and metabolic states of cells are constantly affected by other populations and fluctuating environments. In extreme conditions, some populations may become stressed and lose circuit functions or be outcompeted by others. Third, single cell-level designs often ignore the spatial context given the homogeneous assumption, while the spatial structure of microbial consortia plays a significant role in their stability, robustness and performance.

Therefore, design principles of stable and robust microbial consortia require a new perspective that involves regulation of multiple levels of dynamics, including intracellular gene expression, cellular metabolism and growth, cell-cell interactions, and spatial structures in environments. In Chapter 2, design principles are introduced for stable and robust population-level dynamics and densities, specifically in populations with heterogeneous cell metabolic states. In Chapter 3, I present how to design cell-cell interactions among multiple populations to achieve stable coexistence. In Chapter 4, the role of spatial structures in consortia stability is discussed.

In Chapter 2, I explore design principles for robust behaviors in one microbial population. Motivated by feedback control theory, I introduce the general feedback circuit design at single cell-level via intracellular gene regulation and at population-level via cell-cell signaling systems. A set of synthetic circuit designs for population density-dependent functions are demonstrated as examples. Two specific population-level design principles, signal integral feedback and bistable state switching feedback, are proposed and demonstrated to exhibit robust adaption to environmental disturbances in both homogeneous and heterogeneous populations. A layered feedback design by combining single cell-level and population-level control circuits is also shown with enhanced robustness performance under intracellular noises as well as environmental disturbances.

Chapter 3 focuses on designing cell-cell interactions for stable coexistence of mul-

tiple populations in well-mixed environments. I first review classical mathematical models and common experimental approaches to study microbial population coexistence. A mechanistic model of chemical-mediated interactions is proposed to study how chemicals produced by populations can modulate cell growth and death kinetics for stable coexistence. In a two population-system, I show that stable coexistence can be achieved in both mutually competitive and cooperative populations. Yet the stability conditions differ based on specific mechanisms, such as chemicals being accumulative or consumed and degraded, chemicals activating cell death or inhibiting cell growth, etc.

Chapter 4 addresses the population interaction design problem in a spatial context. I explore principles for stable coexistence and robust functionality in two directions. On one hand, defined spatial distributions of microbial populations can determine strengths of cell-cell interactions that are mediated by diffusible signaling molecules. Thus, the accurate and robust outputs of desired functions in microbial consortia depend on spatial distributions. On the other hand, microbial populations can self-organize into various spatial structures based on their interactions. Modeling and simulation results suggest that unlike in well-mixed environments, intermixing spatial patterns generated by cooperative populations facilitate more stable coexistence.

Chapter 2

ROBUST CONTROL OF POPULATION-LEVEL BEHAVIORS

2.1 Motivation

Advances in synthetic biology have improved our ability to engineer genetic circuits and build multicellular systems with controllable and complex, non-native functionalities. For example, researchers have developed engineered microbial consortia to ferment the sugars more efficiently using two *Escherichia coli* strains (Eiteman, S. A. Lee, and Altman, 2008). Two engineered *Bacillus subtilis* strains have been shown to exhibit the desired enzymatic activity that requires multiple steps of metabolic process in co-cultures (Arai et al., 2007). Synthetic microbial consortia have also been used to study evolution and stability of natural ecosystems by engineering interactions among cell strains and observing diverse behaviors of co-adaptation and co-evolution in controlled environments (Shou, S. Ram, and Vilar, 2007; Balagaddé et al., 2008).

One major challenge for engineering synthetic consortia is to realize reliable and robust population-level behaviors, which usually depend on homeostasis in gene expression and population density given various uncertainties and disturbances in cellular dynamics and from fluctuating environments. For example, using engineered bacterial populations as drug-delivery devices requires efforts of controlling the bioproduction rate in cells to ensure a robust drug release dosage in the changing environment of host organisms (Ozdemir et al., 2018). In biofilm-based microbial consortia, multiple cell populations depend on long-term coexistence to cooperatively adapt to outside attack and environmental stress (Burmølle et al., 2006). Thus, robust control mechanisms on gene expression and population density are needed for synthetic microbial consortia to deal with noises in cellular gene expression, variations in cell metabolic states and growth, and environmental disturbances.

In dynamical systems and control research, feedback control is instrumental in achieving robustness, and has been also applied to understand homeostasis in natural biological systems and to design synthetic organisms. Previous theoretical studies have predicted that circuits based on gene regulation networks with feedback can achieve robust gene expression despite of cellular noises and disturbances (Ang, Bagh, et al., 2010; Drengstig et al., 2012; Briat, Gupta, and Khammash, 2016;
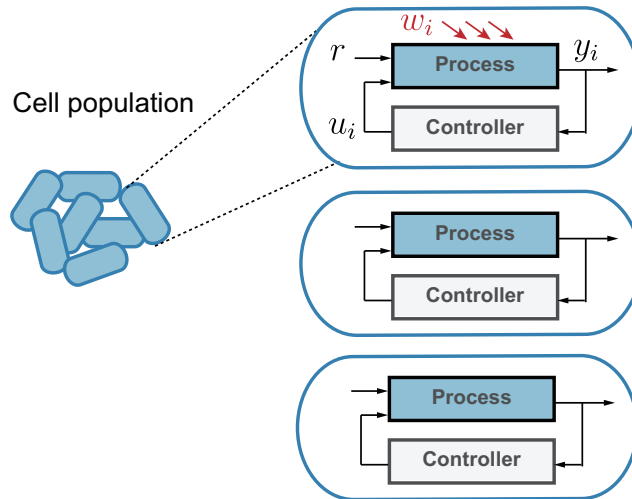
Figure 2.1: Schematic diagram of single cell-level feedback control. Cells in a homogeneous cell population can be considered as identical feedback control systems.

Xiao and Doyle, 2018). Experimental results have also demonstrated that feedback control circuits can exhibit robust adaptation to disturbances in gene expression (Hsiao et al., 2015; Aoki et al., 2019).

These feedback control circuits are usually designed at single cell-level, which involves only intracellular gene regulation in individual cells. Single cell-level design is useful for achieving population-level functions in homogeneous cell populations because population-level behaviors are considered as the sum or the average of identical individual cells. For example, robust population-level gene expression is ensured if the feedback control circuit guarantees robustness in gene expression at single cell-level, since all cells exhibit robust adaptation to disturbances in the same way in a homogeneous population.

We illustrate single cell-level design of feedback control circuits in a homogeneous population in Figure 2.1, where all cells have the same circuit (controller) that regulates the target gene expression (process). In the i-th cell, the controller output u_i can steer the process output y_i to track the reference r, while the process dynamics is perturbed by a homogeneous disturbance w_i. In this homogeneous population, the population-level gene expression is robust to the disturbance w_i when the single cell-level gene expression in all individual cells is robust to the disturbance.

However, in many other scenarios, a cell population may exhibit heterogeneous dynamics and response to disturbances, for example, when cells are under heteroge-
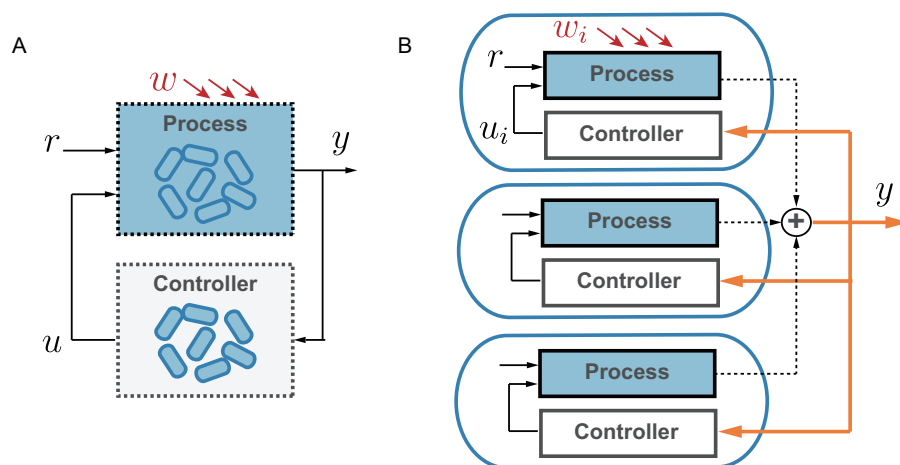
Figure 2.2: Schematic diagram of population-level feedback control. (A) Block diagram of a feedback control system at population-level. (B) Implementation of the feedback controller using a sending-receiving module.

neous disturbances in environments (Toyofuku et al., 2016; Schreiber et al., 2016), or under severe stress and enter heterogeneous phenotypes (Balaban et al., 2004; Kussell and Leibler, 2005; Satija and Shalek, 2014; Holland et al., 2014). In these cases, single cell-level design is not sufficient for robust population-level behaviors.

Population-level design provides a new approach for building control circuits in synthetic multicellular systems and microbial consortia. Unlike single cell-level design, population-level design focuses on the collective behavior of all cells in a population instead of each individual cell. Figure 2.2 (left) illustrates the main idea of population-level feedback control circuit design. The population can be considered to have an overall gene expression process with an output y that is perturbed by an integrated disturbance w from various sources. The control circuit should function as a population-level feedback controller with an output u that steers the population-level gene expression level y to the reference r. In real implementations, the control circuits are embedded in all individual cells with the key component of a sending-receiving module, as shown in Figure 2.2 (right). The sending-receiving module (dashed lines and orange solid lines) generates a global signal that directly measures the population-level gene expression y and the control circuit in each cell can respond to the global signal. When any disturbance perturbs the population-level expression dynamics of the target gene, all cells should be able to sense the integrated disturbance via the global signal and respond collectively no matter the disturbance is homogeneous or heterogeneous, from cellular noises or environmental fluctuations.

In this chapter, we first present single cell-level and population-level design of feedback control circuits for robust population-level behaviors in Section 2.2 and 2.3. We demonstrate the robustness performance and limitations of these two types of circuit design in homogeneous and heterogeneous populations with simple examples. In Section 2.4, we propose detailed circuits of population-level design based on cell-cell signaling systems, and show that population-level design can achieve robust control of population density and density-dependent functions. To further provide general design guidance, we propose two design principles for robust population-level control: signal integral feedback in Section 2.5 and bistable state switching feedback in Section 2.6. In Section 2.7, we illustrate a layered circuit design principle that combines single cell-level and population-level feedback, and show that layered feedback improves robustness performance to more diverse disturbances and uncertainties.

2.2 Single cell-level control circuit design

Consider a cell population of N cells. The desired population-level behavior (control objective) is the production of a target chemical X. The population-level production depends on each single cell's production and the total cell number, so it is a population density-dependent function.

At single cell-level, the process of expressing the target gene and producing the target chemical X in each cell has noises and uncertainties. To obtain robust production in each individual cell despite these noises and uncertainties, we design a single cell-level feedback control circuit based on intracellular gene regulation, shown in Figure 2.3. Figure 2.3A is a control diagram where y_i represents the target X production level, u_i represents the control actuation to regulate y_i according to the reference r, and w_i represents the uncertainty or disturbance in the ith cell. Figure 2.3B illustrates the intracellular gene regulation in the single cell-level design. The uncertainty and disturbance w_i arises from bursty biochemical reactions in cells that affect the target production of X in the ith cell. The controller for robust production is usually implemented through regulation from other chemical species Z.

For simplicity, we assume the regulation circuit has one control species Z. We denote the concentration of X and Z in the ith cell by x_i and z_i, where $i = 1, 2, ..., N$. The population-level production is defined as the total concentration of X, denoted
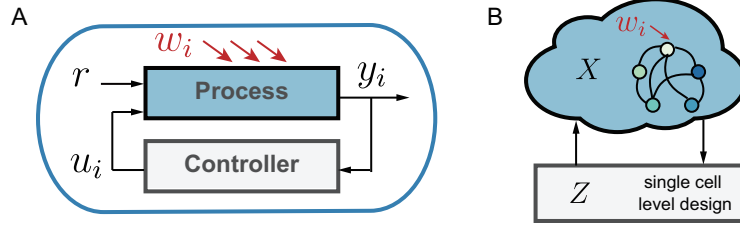
Figure 2.3: Schematic diagram of single cell-level circuit design. (A) Block diagram of a feedback control system in a single cell. (B) Circuit design of a feedback controller using intracellular gene regulation with control species Z.

by y:

$$y = \sum_{i=1}^{N} x_i. \tag{2.1}$$

Homogeneous cell population

In a homogeneous cell population shown in Figure 2.4A, the cellular noise and uncertainty of the target gene expression and chemical production of X is defined as w_i in the ith cell. Each cell's expression of X is under regulation of the control species Z, so the dynamics of x_i can be modeled by a function $f(x_i, z_i, w_i)$. The control species Z senses the target X to actuate regulation, so we model the dynamics of z_i in each cell as $u(x_i, z_i)$. Thus, the dynamics of the cell population can be modeled using ordinary differential equations:

$$\begin{aligned}
\frac{\mathrm{d}x_i}{\mathrm{d}t} &= f(x_i, z_i, w_i), \\
\frac{\mathrm{d}z_i}{\mathrm{d}t} &= u(x_i, z_i).
\end{aligned} \tag{2.2}$$

We assume the feedback controller is well-designed at single cell-level to ensure each individual cell has a stable gene expression and maintains a robust X concentration at a constant value μ despite the noise and uncertainty in X expression. In other words, there is a stable and robust steady state of $x_i(\infty)$ in each cell, where $x_i(\infty) = \mu$. Therefore, the population-level production of X is guaranteed to be robust to the cellular noise and uncertainty in this homogeneous population, i.e., $y(\infty) = N\mu$.

For example, we consider a circuit with an integral feedback controller, as presented in Figure 2.4B. In this circuit, X activates Z production and Z represses X production, forming a negative loop. We assume Z is a self-activating species with a constant production rate $\frac{1}{\mu}$. Meanwhile, the production of X in the ith cell is perturbed by an unknown cellular noise w_i, with a uncertain production rate $\alpha(w_i)$. Both species of

A   Homogeneous cell population
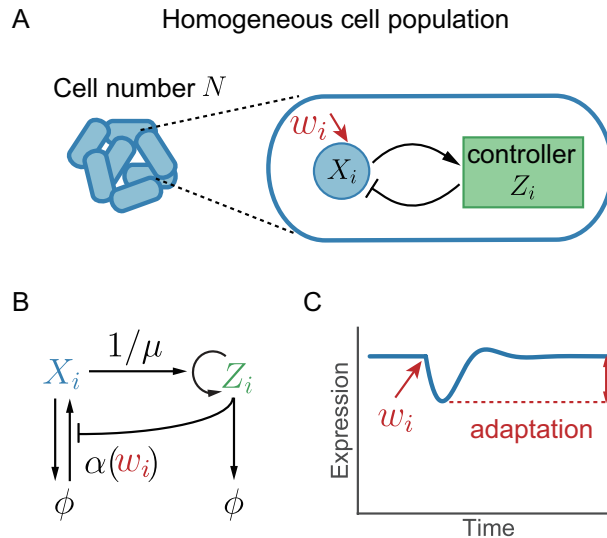
Figure 2.4: Single cell-level circuit design in a homogeneous cell population. (A) Schematic diagram of a circuit design with negative feedback in the ith cell in a homogeneous population. (B) An example circuit of gene regulation that implements integral feedback control on X concentration in the ith cell. Pointed arrows denote activation and blunt-end arrows denote repression. (C) The simulation of a single cell's expression of X and adaptation to a step disturbance w_i.

X and Z have self-degradation and dilution due to cell growth and division. Then, we can model the dynamics of the ith cell as

$$\frac{\mathrm{d}x_i}{\mathrm{d}t} = f\left(x_i, z_i, w_i\right) = \frac{\alpha(w_i)}{z_i} - x_i,$$
$$\frac{\mathrm{d}z_i}{\mathrm{d}t} = u\left(x_i, z_i\right) = \frac{1}{\mu}x_i z_i - z_i. \tag{2.3}$$

At steady state, we can solve $\frac{\mathrm{d}x_i}{\mathrm{d}t} = 0$, $\frac{\mathrm{d}z_i}{\mathrm{d}t} = 0$ and obtain a stable solution:

$$x_i(\infty) = \mu,$$
$$z_i(\infty) = \frac{\alpha(w_i)}{\mu}. \tag{2.4}$$

It shows that in the ith cell, the target chemical concentration x_i always robustly converges to a stable and constant value of μ, without being affected by the noise w_i. This is because the control species Z functions as an integral feedback controller that generates control actuation to X production according to the perturbation by w_i.

We can further obtain the population-level production at steady state since all cells are homogeneous:

$$y(\infty) = N\mu. \tag{2.5}$$

In Figure 2.4C, the simulation shows that the X concentration in each single cell achieves perfect adaptation to a step disturbance w_i with zero error at steady state. Thus, in a homogeneous population with a constant cell number N, the population-level production should also exhibit a robust level with similar adaptation.

Heterogeneous cell population

However, genetically identical cells can exhibit heterogeneous phenotypes in a population. A major scenario is when a cell population is faced with environmental disturbances. Many environmental disturbances induce stress in cells. When cells are stressed, they may switch metabolic states and exhibit distinct phenotypes. For example, in an wild type *Escherichia coli* population under antibiotic treatment, a small fraction of cells enter into the persister state with low metabolism and shut down other cellular functions (Balaban et al., 2004; Keren et al., 2004). Similarly, synthetic microbial populations may become heterogeneous in target gene expression when they are perturbed by environmental disturbances such as heat shock, starvation and antimicrobial stress. In these conditions, a fraction of cells may no longer express the target gene due to metabolic state change and become 'non-producing' or dysfunctional.

We next investigate if single cell-level design of control circuits can deal with environmental disturbances that lead to 'non-producing' phenoypes and achieve robust population-level target production in a heterogeneous population.

For simplicity, we consider two emerging phenotypes after the environmental disturbance w: the 'producing' and the 'non-producing' phenotypes in a population of N cells, illustrated in Figure 2.5A. Cells of both phenotypes are genetically identical with the same synthetic control circuit that involves regulation by a species Z. The 'producing' phenotype can produce X normally, and we model the dynamics of X concentration x_i in the ith 'producing' cell by a function $f(x_i, z_i, w)$. On the other hand, cells exhibiting the 'non-producing' phenotype stop producing X due to severe stress and become dysfunctional in the production of the target chemical X. We define a function $f'\left(x'_j, z_j, w\right)$ to describe the dynamics of X concentration x'_j in the jth 'non-producing' cell. Since 'non-producing' cells do not produce X, there is only self-degradation and dilution of X and we can set $f'\left(x'_j, z_j, w\right) \leq 0$. Assume that cell numbers of both phenotypes in this heterogeneous population are
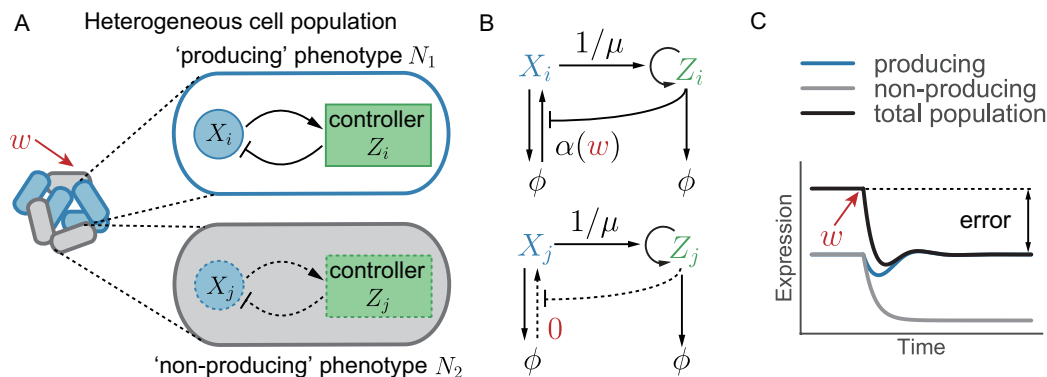
Figure 2.5: Single cell-level circuit design in a heterogeneous cell population. (A) Schematic diagram of two emerging phenotypes after a cell population is perturbed by an environmental disturbance w. Dashed lines in the 'non-producing' cell represents the circuit regulation is not properly functional due to cell's metabolic state change under stress. (B) An example circuit of gene regulation that implements integral feedback control on X concentration in two cell phenotypes. The upper is in the ith 'producing' cell and the lower is in the jth 'non-producing' cell where the X production rate becomes zero. (C) The simulation of two phenotypes' production and the total population-level production of X after a perturbation from a step disturbance w.

N_1 and N_2, we can write down the ODE model of all cells:

$$
\begin{aligned}
\text{'producing' cells:} \quad & \frac{\mathrm{d}x_i}{\mathrm{d}t} = f\left(x_i, z_i, w\right), \\
& \frac{\mathrm{d}z_i}{\mathrm{d}t} = u\left(x_i, z_i\right), \\
\text{'non-producing' cells:} \quad & \frac{\mathrm{d}x'_j}{\mathrm{d}t} = f'\left(x'_j, z_j, w\right) \le 0, \\
& \frac{\mathrm{d}z_j}{\mathrm{d}t} = u\left(x'_j, z_j\right), \\
\text{total production:} \quad & y = \sum_{i=1}^{N_1} x_i + \sum_{j=1}^{N_2} x'_j,
\end{aligned}
\tag{2.6}
$$

where $N_1 + N_2 = N$.

Again, we assume the feedback control circuit is well-designed at single cell-level so each individual cell can maintain a robust X concentration at a constant value μ. However, the circuit regulation only robustly operates when cells are in normal metabolic state and are producing the target chemical. In the heterogeneous population perturbed by the environmental disturbance w, We can expect that each cell with the 'producing' phenotype has a stable and robust production despite w, i.e., $x_i(\infty) = \mu$. Yet, the concentration of X in 'non-producing' cells only has decreasing

dynamics where $f'\left(x'_j, z_j, w\right) \leq 0$, so there won't be a stable concentration of X unless $x'_j(\infty) = 0$. As a result, the population-level production cannot maintain a robust concentration to this environmental disturbance w that causes heterogeneous phenotypes, i.e., $y(\infty) \neq N\mu$.

To obtain a more qualitative understanding, we use the same example circuit with an integral feedback controller in the previous section for demonstration, shown in Figure 2.5B. The upper panel presents the circuit in the ith 'producing' cell, where the disturbance w perturbs the production rate of X, denoted as $\alpha(w)$. We can derive the dynamics of the ith 'producing' cell:

$$
\begin{aligned}
\frac{dx_i}{dt} &= f\left(x_i, z_i, w\right) = \frac{\alpha(w)}{z_i} - x_i, \\
\frac{dz_i}{dt} &= u\left(x_i, z_i\right) = \frac{1}{\mu}x_i z_i - z_i.
\end{aligned}
\tag{2.7}
$$

At steady state, we can solve $\frac{dx_i}{dt} = 0$, $\frac{dz_i}{dt} = 0$ and obtain a stable solution:

$$
\begin{aligned}
x_i(\infty) &= \mu, \\
z_i(\infty) &= \frac{\alpha(w)}{\mu},
\end{aligned}
\tag{2.8}
$$

which is consistent with the result of a homogeneous population from equation (2.4). The integral controller ensures that the concentration of X converges to the desired constant value μ in each 'producing' cell.

On the other hand, the lower panel in Figure 2.5B is the circuit in the jth 'non-producing' cell. Since the production rate of X becomes zero, the integral controller fails to operate. The dynamics of the 'non-producing' cell becomes

$$
\begin{aligned}
\frac{dx'_j}{dt} &= f'\left(x'_j, z_j, w\right) = -x'_j \leq 0, \\
\frac{dz_j}{dt} &= u\left(x'_j, z_j\right) = \frac{1}{\mu}x'_j z_j - z_j.
\end{aligned}
\tag{2.9}
$$

The stable solution at steady state becomes

$$
\begin{aligned}
x'_j(\infty) &= 0, \\
z_j(\infty) &= 0.
\end{aligned}
\tag{2.10}
$$

Therefore, the total population production only depends on the 'producing' phenotype and the steady state of y after the disturbance becomes

$$
y(\infty) = \sum_{i=1}^{N_1} \mu + \sum_{j=1}^{N_2} 0 = N_1 \mu.
\tag{2.11}
$$

Compared to the condition before the disturbance where all cells exhibit the 'producing' phenotype, we can find the error in the population-level production as

$$\text{error} = \frac{|N_1\mu - N\mu|}{N\mu} = \frac{N_2}{N}. \tag{2.12}$$

Equation (2.12) shows that with only the single cell-level control circuit, if more cells are perturbed to enter the 'non-producing' phenotype, the population-level production will be lowered, leading to a larger error that is proportional to the 'non-producing' cell density N_2.

Simulation in Figure 2.5C illustrates that 'producing' cells adapt to the disturbance and converge to the desired level of X concentration with the single cell-level control circuit, but the population cannot maintain a robust overall production due to the loss of function in 'non-producing' cells. Therefore, single cell-level design fails to achieve robust population-level expression to uncertainties and disturbances from the environment that lead to heterogeneous phenotypes in a cell population.

2.3 Population-level control circuit design

To overcome the loss in the population-level production due to the appearance of 'non-producing' phenotypes, proper coordination among cells is needed. We apply cell-cell signaling systems in a population for coordination and adopt the idea of 'division-of-labor' from natural multicellular systems, and propose population-level design principles of control circuits. Therefore, heterogeneous phenotypes in a synthetic cell population can communicate and cooperatively fulfill an overall chemical production and even more complicated functions in a robust manner.

Cell-cell signaling system

Cell-cell signaling systems are common in natural organisms, for example, bacterial quorum sensing (Fuqua, Winans, and Greenberg, 1994; Miller and Bassler, 2001), pheromones communication of fungi (S. C. Lee et al., 2010), and morphogen in tissue development (Tabata and Takei, 2004). These signaling systems have also been widely used in synthetic microbial consortia or artificial multicellular tissues (Scott and Hasty, 2016; Hennig et al., 2018; Tian et al., 2019; McCarty and Ledesma-Amaro, 2019).

One major cell-cell signaling system in bacterial populations is quorum sensing (Swift et al., 1996; Miller and Bassler, 2001). Quorum sensing molecules are usually small and diffusible molecules synthesized and secreted by cells, and they
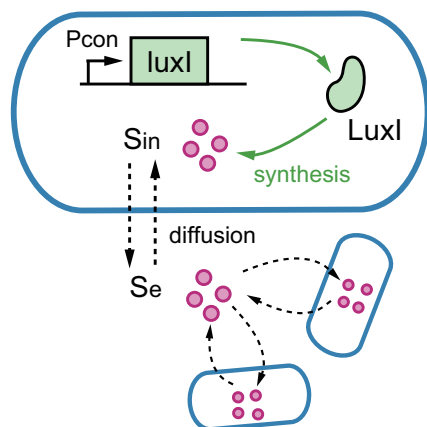
Figure 2.6: Schematic diagram of a quorum sensing signaling system.The signaling molecule AHL are synthesized by the enzyme LuxI and diffuse freely across the membrane.

quickly accumulate in the environment forming a global signal for cell-cell communication. In a well-mixed environment, the concentration of quorum sensing signaling molecules depends on the synthesis rate and total population density, so it can measure the population-level expression. When signaling molecules are detected by bacteria cells, downstream gene expression machinery can be activated as a respond to the global signal of the population-level measurement. Therefore, in synthetic circuits, quorum sensing systems can be utilized as the sending-receiving module to realize population-level feedback control.

To understand how quorum sensing molecules can be used as a population-level measurement in a quantitative manner, we first explore the synthesis and diffusion dynamics of quorum sensing signaling molecules in a homogeneous bacterial population using a mathematical model. We consider the LuxI-AHL molecule as an example. The luxI gene codes for an acyl-homoserine lactone (AHL), which is a quorum sensing molecule first identified in *Vibrio fischeri* (Fuqua, Winans, and Greenberg, 1994). Similar systems of AHL molecules have been characterized in other Gram-negative bacteria, and used in synthetic microbial populations. In the schematic diagram in Figure 2.6, we consider a constitutive expression of luxI so cells can constantly produce the signaling molecule AHL. LuxI is an enzyme that synthesizes the signaling molecule AHL. S_{in} represents the signaling molecule inside a single cell and S_e represents the extracellular signaling molecule. Assume there are N cells in the well-mixed environment and the external dilution rate of the signaling molecule is d. We can develop an ODE model of LuxI and AHL

concentrations:

$$\text{enzyme LuxI:} \qquad \frac{\mathrm{d}I}{\mathrm{d}t} = \alpha - \gamma I,$$

$$\text{intracellular AHL:} \quad \frac{\mathrm{d}S_{in}}{\mathrm{d}t} = \beta I - DS_{in} + DS_e, \qquad (2.13)$$

$$\text{external AHL:} \qquad \frac{\mathrm{d}S_e}{\mathrm{d}t} = N(DS_{in} - DS_e) - dS_e.$$

Parameters α and β are production rates of LuxI and AHL. γ is the self-degradation and dilution rate of LuxI due to cell growth. D is the diffusion rate of AHL across cell membranes. At steady state, we solve for $\frac{\mathrm{d}S_{in}}{\mathrm{d}t}, \frac{\mathrm{d}S_e}{\mathrm{d}t} = 0$, and obtain

$$S_{in} = \frac{\beta I}{D} + S_e,$$

$$Se = \frac{ND}{ND + d} S_{in}. \qquad (2.14)$$

Since quorum sensing signaling molecules diffuse quickly, we assume the diffusion across cell membranes with rate D is much larger than the intracellular transcription and translation and external dilution rates, i.e., $D \gg d, \beta, \alpha, \gamma$. We can derive the quasi-steady state solution of signaling molecule concentrations:

$$S_{in} \approx S_e. \qquad (2.15)$$

Equation (2.15) shows that fast diffusing signaling molecules have the same intracellular and extracellular concentrations at quasi-steady state. Applying the quasi-steady state solution in equation (2.15) to equation (2.13), we can derive

$$\frac{\mathrm{d}I}{\mathrm{d}t} = \alpha - \gamma I,$$

$$\frac{\mathrm{d}(NS_{in} + S_e)}{\mathrm{d}t} = N\beta I - dS_e. \qquad (2.16)$$

At steady state, equation (2.16) is set to zero, and we obtain

$$I = \frac{\alpha}{\gamma},$$

$$S_{in} \approx S_e = N\frac{\beta I}{d} = N\frac{\beta \alpha}{\gamma d}. \qquad (2.17)$$

The steady state solution shows that the concentration of the fast diffusing signaling molecule depends on the synthesis rate β as well as single cell-level expression of the enzyme I and the total population density N. Therefore, the signaling molecule concentration can be considered as a measurement of the total gene expression in a cell population. Note that we can approximate intracellular and extracellular signaling molecule concentration to be the same with the fast diffusion assumption, and we will use S to represent the signaling molecule in the following sections.

Coordination in heterogeneous population

Now we propose a population-level circuit design for the same desired function (control objective) in section 2.2. As shown in Figure 2.7A, the circuit utilizes a cell-cell signaling system as the feedback controller to regulate the population-level production of a target chemical X. We suggest that the signaling molecule S can directly measure the total production of X in the population and coordinate the response of heterogeneous phenotypes to robustly adapt to environmental disturbances.

In the heterogeneous population, all cells can secrete and sense the signaling molecule S. The signaling molecule S is synthesized based on the target chemical production of X and further regulates X dynamics in the closed loop. According to the quasi-steady state analysis in equation (2.15), we assume that both intracellular and extracellular signaling molecules have the same concentration s. We model the X dynamics in the ith cell exhibiting the 'producing' phenotype by a function $g\left(x_i, s, w\right)$, and the X dynamics in the jth cell exhibiting the 'non-producing' phenotype by a function $g'\left(x'_j, s, w\right)$, where w represents an environmental disturbance w. Since 'non-producing' cells do not produce X, we have $g'\left(x'_j, s, w\right) \leq 0$ to describe the self-degradation and dilution of X. The dynamics of the heterogeneous population are modeled with ODEs:

$$
\begin{aligned}
\text{producing cells:} \quad & \frac{\mathrm{d}x_i}{\mathrm{d}t} = g\left(x_i, s, w\right), \\
\text{non-producing cells:} \quad & \frac{\mathrm{d}x'_j}{\mathrm{d}t} = g'\left(x'_j, s, w\right) \leq 0, \\
\text{global signal:} \quad & \frac{\mathrm{d}s}{\mathrm{d}t} = \sum_{i=1}^{N_1} v\left(x_i, s\right) + \sum_{j=1}^{N_2} v\left(x'_j, s\right) - ds, \\
\text{total production:} \quad & y = \sum_{i=1}^{N_1} x_i + \sum_{j=1}^{N_2} x'_j,
\end{aligned}
\tag{2.18}
$$

where $N_1 + N_2 = N$.

The term $v\left(x, s\right)$ describes the intracellular dynamics of S that depends on X in each individual cell. The parameter d is self-degradation and external dilution of S in the environment. Self-degradation of most signaling molecules is rather small, so d is often approximated as the external dilution rate in the environment. In environments without external dilution, the signaling molecule often accumulates to a high concentration. In lab experiments, the external dilution rate can be tuned by varying the flow rate of culture media (Burmeister and Grünberger, 2020).
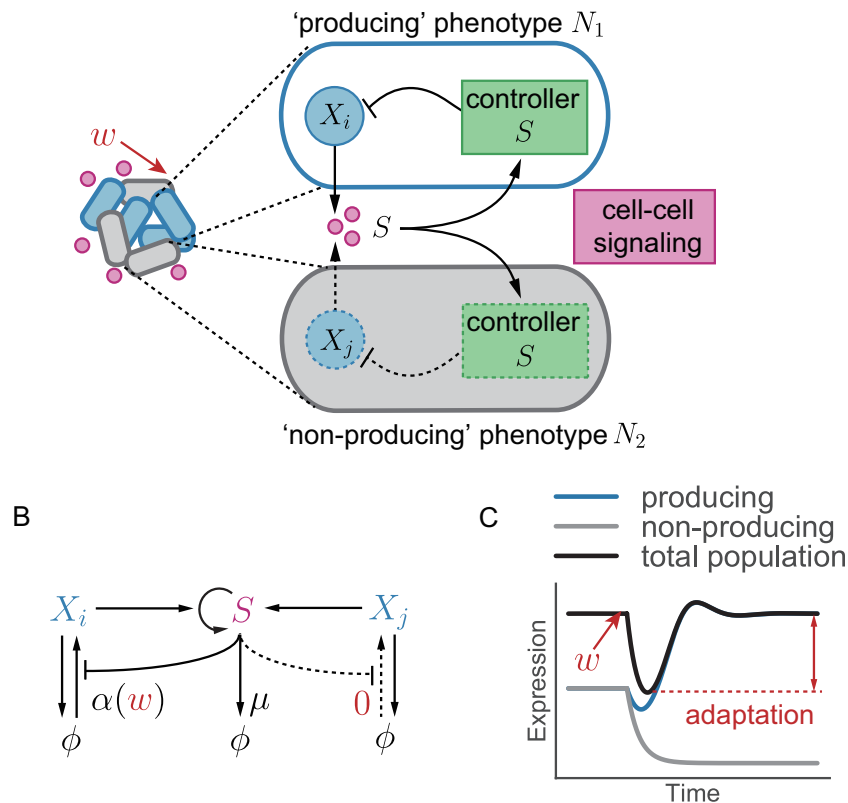
Figure 2.7: Population-level circuit design in a heterogeneous cell population. (A) Schematic diagram of two emerging phenotypes after a cell population is perturbed by an environmental disturbance w. Dashed lines in the 'non-producing' cell represents the circuit regulation is not properly functional due to cell's metabolic state change under stress. The cell-cell signaling system includes a quorum sensing signaling molecule S. (B) An example circuit of gene regulation that implements integral feedback control on X concentration at population-level. The left half is regulation in the ith 'producing' cell and the right half is regulation in the jth 'non-producing' cell. The middle represnts the global signal S in the environment. (C) The simulation of two phenotypes' production and the total population-level production of X after a perturbation from a step disturbance w.

The regulation between S and X depends on specific control mechanisms. Here, we consider the same example of the integral controller as in the single cell-level design in section 2.2, except that the feedback control species is no longer an intracellular chemical Z, but the signaling molecule S. The circuit schematic is shown in Figure 2.7B, where the self-activating signaling molecule S down-regulates X production and X activates S synthesis.

The environmental disturbance w perturbs the production rate of X in the 'producing' phenotype, denoted by $\alpha(w)$, while cells exhibiting 'non-producing' phenotype stop the production completely. The intracellular species X has self-degradation and dilution due to cell growth and division. Then we can define X dynamics in 'producing' and 'non-producing' cells:

$$
\begin{aligned}
\text{producing cells:} \quad & \frac{\mathrm{d}x_i}{\mathrm{d}t} = \frac{\alpha(w)}{s} - x_i, \\
\text{non-producing cells:} \quad & \frac{\mathrm{d}x'_j}{\mathrm{d}t} = -x'_j \leq 0.
\end{aligned}
\tag{2.19}
$$

The synthesis of S depends on the activation by X and its self-activation in all cells. We assume that there is an external dilution of S in the environments with a constant rate μ. Then the dynamics of S becomes

$$
\text{global signal:} \frac{\mathrm{d}s}{\mathrm{d}t} = \sum_{i=1}^{N_1} x_i s + \sum_{j=1}^{N_2} x'_j s - \mu s.
\tag{2.20}
$$

Now we evaluate the population-level response to the disturbance w and show whether the total population-level expression can robustly adapt. By setting $\frac{\mathrm{d}x_i}{\mathrm{d}t}, \frac{\mathrm{d}x'_j}{\mathrm{d}t}, \frac{\mathrm{d}s}{\mathrm{d}t} = 0$, we can obtain stable steady-state solutions:

$$
\begin{aligned}
\text{producing cells:} \quad & x_i(\infty) = \frac{\mu}{N_1}, \\
\text{non-producing cells:} \quad & x'_j(\infty) = 0, \\
\text{global signal:} \quad & s(\infty) = \frac{N_1 \alpha(w)}{\mu}.
\end{aligned}
\tag{2.21}
$$

Moreover, we have

$$
\text{total production:} \quad y(\infty) = \sum_{i=1}^{N_1} \frac{\mu}{N_1} + \sum_{j=1}^{N_2} 0 = \mu.
\tag{2.22}
$$

It shows that the population-level production always converges to the constant value μ despite the disturbance w. In contrast to the single cell-level design, the population-level production at steady state does not depend on fractions of cells that enter the 'non-producing' phenotype. In other words, the total concentration y robustly adapts to the disturbance while forming a heterogeneous population.

The simulation in Figure 2.7C also shows that 'producing' cells can compensate for the loss in the population-level production caused by 'non-producing' cells. When 'non-producing' cells stop producing X, the global signaling molecule S

has a lower overall synthesis rate. The transient decrease in S concentration will further stimulate the production of X in the 'producing' phenotype. As a result, the overall population-level expression can robustly adapt to the disturbance, even though each individual cell's expression is highly heterogeneous and not robust to the disturbance.

Robustness at population-level

Population-level robustness discussed here is different from robustness to intracellular noises and uncertainties, as often considered in single cell-level studies. The context is based on the population's heterogeneous response to environmental disturbances with distinct phenotypes. Such heterogeneity is an emergent behavior in a group of cells. In contrast to realizing robust gene expression in all individual cells, coordinating behaviors of phenotypes may be more essential and beneficial, as commonly seen in natural multicellular systems. For example, robust growth of a microbial consortium is maintained with cooperating phenotypes (Balaban et al., 2004; Holland et al., 2014); homeostasis in tissues depends on interactions among differentiated subpopulations (Nakada, Levi, and Morrison, 2011; Satija and Shalek, 2014). Thus, population-level robustness is a new and critical property of synthetic multicellular systems that requires novel control circuit design strategies.

Analysis in previous sections reveals an essential feature of population-level robustness that emerges from a collection of cells. We find in a cell population, not all cells need to be homogeneously adaptive to disturbances and uncertainties and maintain a robust gene expression. Instead, the heterogeneity can be harnessed to facilitate the population's adaptation with proper coordination among phenotypes. The stable and robust emergent behavior arises at the population-level even single cells may become unstable or fragile. The idea collides with distributed control in networks, yet design principles for implementable synthetic circuits are lacking.

We conclude that cell-cell communication is a critical component to achieve population-level robustness from a simple theoretical study of quorum sensing systems in bacteria. Cell-cell signaling molecules function as the sending-receiving module, which provides a precise measurement of the overall population expression and can actuate required regulations in cells of different phenotypes. Therefore, cells are no longer controlled individually but are coordinated at population-level. Similar tools of diffusible signaling systems have also been engineered in yeast and mammalian cells (Youk and Lim, 2014; Y. Ma et al., 2020).

The analysis also suggests that cell-cell communication can improve the circuit's performance by dividing the control labor. Single cell-level control circuits often depend on transcription and translation of a large amount of components in individual cells. Such synthetic circuits may impose a major metabolic burden on the host cell, which may fail to thrive (Del Vecchio, Dy, and Qian, 2016). With population-level control mediated by cell-cell signaling, the burden is divided among the population.

Moreover, in synthetic consortia consist of multiple cell populations, robust functionalities depend on stable coexistence. Interactions among cell populations play a crucial role in maintaining their growth and survival in diverse conditions, often through the formation of synergistic population-level structures, balanced metabolic feeding, removal of toxins and mitigation of stress (S. Zhang et al., 2018). Cell-cell signaling can help fulfilling complicated interactions among populations via quorum sensing, growth factors, nutrients and toxins, etc (Brenner, Karig, et al., 2007; Kong et al., 2018).

2.4 Population control of density-dependent functionalities

Many complex functionalities in multicellular systems depend on the population density, phenotype fractions and relative ratios between cell populations. Population density-dependent functions often involves cell growth, death and metabolic processes that may be perturbed by fluctuations in environments. Thus, building synthetic microbial consortia or artificial tissues requires efforts of population-level design of robust control circuits.

In the following sections, we will present examples of synthetic circuits that are designed with population-level feedback control circuits using cell-cell signaling systems to regulate population density-dependent functionalities.

Population density control

To achieve a robust population density, we design a sequestration-based integral feedback control circuit at population-level by coupling genes regulating cell growth and death with quorum sensing systems [1]. The circuit design in shown in Figure 2.8A.

The population density feedback control circuit consists of a sensor, a comparator and an actuator. The sensor is fulfilled by the quorum sensing system. Each cell produces and secretes a signaling molecule AHL that is synthesized by the enzyme LuxI with a constant rate, so the concentration of AHL measures the population

---

[1]*A version of this section has been published (Ren, Baetica, et al., 2017).*
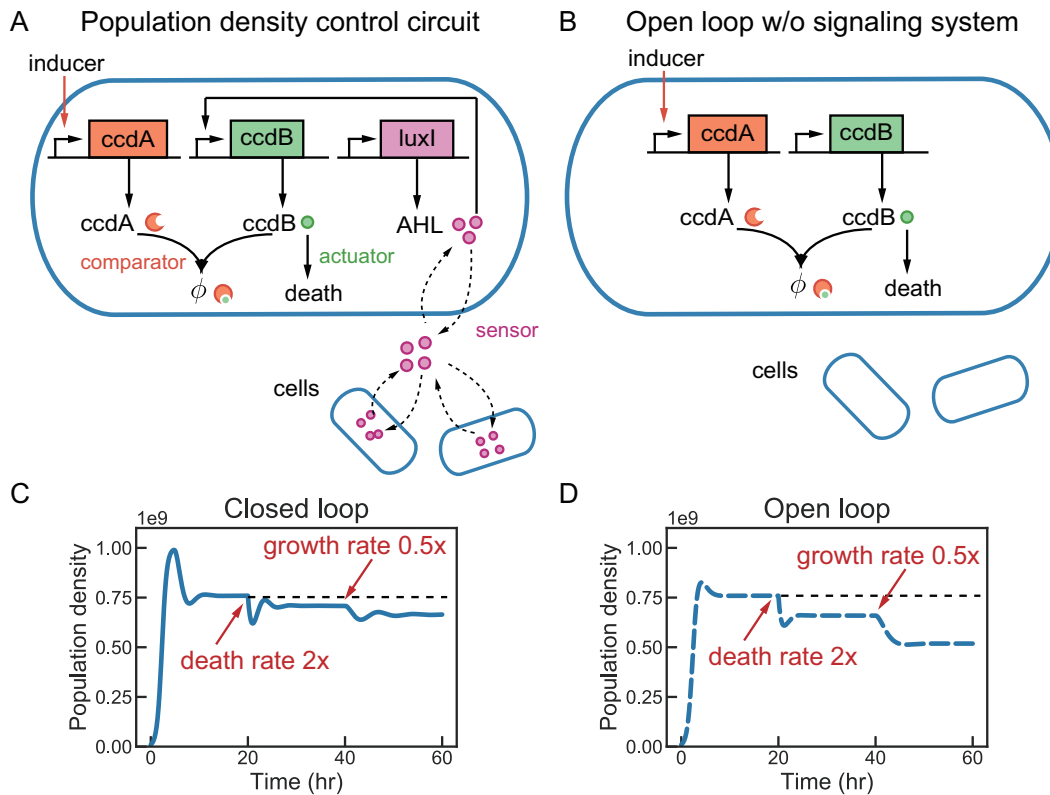
Figure 2.8: Schematic diagram and simulation of population density control. (A) The control circuit implementation of a toxin-antitoxin (ccdB-ccdA) pair and the Lux-AHL quorum sensing system. (B) The open loop circuit implementation of only a toxin-antitoxin (ccdB-ccdA) pair without any feedback control. (C)(D) Simulations of population density dynamics with the circuits in (A)(B). There is a step disturbance in cells' death rate at 20hr and in cells' growth rate at 40hr.

density in a proportional manner. The comparator is realized by chemical species that can compute for the error between the current population density and the desired value (reference). We consider a pair of sequestering proteins: the toxin ccdB and the antitoxin ccdA, where one protein sequester the other and inhibits its function. Sequestration has been proposed to function as an integral controller, also known as 'antithetic controller' (Briat, Gupta, and Khammash, 2016), and experiments have shown that such circuits achieve robust gene expressions in *Escherichia coli* (Aoki et al., 2019). Finally, the output of comparator is used to actuate cell growth or death to modulate the population density. The actuator depends on essential genes that regulate cell growth or death. In this circuit, the toxin protein ccdB kills the cell by poisoning the DNA gyrase complex (You et al., 2004).

In the closed loop circuit, AHL molecules activate the production of the toxin

ccdB, forming a negative feedback at population-level. The reference of population density is set by an external induction of the antitoxin ccdA. When the population density is smaller than the reference level, fewer AHL molecules are secreted and accumulate in the environment, alleviating cell death by reducing ccdB production. Eventually, more cells survive and grow to a higher density as desired. Inducing more ccdA can set a higher reference and tune the desired population density. In Figure 2.8B, we also illustrate the open loop circuit without the feedback controller by AHL-mediated signaling system. Cells are expected to growth or die based on its own expression of the toxin ccdB and the antitoxin ccdA under induction.

We derive a deterministic ODE model of a homogeneous population in a well-mixed environment with following assumptions:

- Cell growth follows logistic kinetics with growth rate k_N and carrying capacity $N_{\max}$. Cell death is proportional to the toxin concentration with rate d_N.

- Activation of the toxin ccdB by AHL molecules is governed by a Hill function with dissociation constant K_S and Hill coefficient $n = 2$. The toxin production rate is β_T.

- The antitoxin ccdA is produced under an external induction with a tunable rate β_A.

- Sequestration between ccdB and ccdA is sufficiently strong with a large rate γ.

- All intracellular species decay with first-order kinetics due to cell growth and division, where the decay rate is determined by cell growth rate.

- The total AHL production in the population is proportional to the population density with rate β_S.

- AHL concentration reaches quasi-steady state by fast diffusion. AHL decays with an external dilution in the environment with rate d_S.

We can obtain the model:

$$\text{population density:} \quad \frac{dN}{dt} = k_N \left(1 - \frac{N}{N_{\max}}\right) N - d_N T N,$$

$$\text{toxin ccdB:} \quad \frac{dT}{dt} = \beta_T \frac{S^2}{K_S^2 + S^2} - \gamma T A - dT,$$

$$\text{antitoxin ccdA:} \quad \frac{dA}{dt} = \beta_A - \gamma T A - dA,$$

$$\text{signal AHL:} \quad \frac{dS}{dt} = \beta_S N - d_S S,$$

$$(2.23)$$

where $d = k_N \left(1 - \frac{N}{N_{\max}}\right)$.

According to the assumption of large sequestration rate where $\gamma \gg d$, we can derive the quasi-steady state of ccdB and ccdA concentration by setting $\frac{dT}{dt} = 0$, $\frac{dA}{dt} = 0$:

$$T \approx \frac{\beta_T}{\gamma A} \frac{S^2}{K_S^2 + S^2}, \quad A \approx \frac{\beta_A}{\gamma T}. \tag{2.24}$$

We can further derive AHL concentration from equation (2.24):

$$S \approx \sqrt{\frac{\beta_A}{\beta_T - \beta_A}} K_S. \tag{2.25}$$

The steady state of AHL concentration is solved by setting $\frac{dS}{dt} = 0$:

$$S = \frac{\beta_S}{d_S} N. \tag{2.26}$$

According to equations (2.25) and (2.26), we can obtain the steady state solution of population density:

$$N \approx \sqrt{\frac{\beta_A}{\beta_T - \beta_A}} \frac{K_S d_S}{\beta_S}, \tag{2.27}$$

which is not dependent on the cell growth rate k_N, death rate d_N or carrying capacity $N_{\max}$. It suggests that when the cell growth condition is perturbed by environmental disturbances, such as changes in nutrients, antibiotics and temperature that cause variations in the growth/death rates or carrying capacity, the steady state population density will not be affected.

Note that the robust population density result is derived with the assumption of a strong sequestration rate γ and a small dilution rate d. In fact, the robust cell population density is approximately achieved by an integral feedback in the circuit when the leakiness from the dilution caused by cell growth is negligible. We can

derive the controller dynamics of the difference between the toxin and the antitoxin concentration $\Delta_{TA} = T - A$ by subtracting $\frac{dA}{dt}$ from $\frac{dT}{dt}$. Assuming dilution d is negligible, i.e., $d \ll \beta_T, \beta_A$, we have

$$\begin{aligned}
\frac{d\Delta_{TA}}{dt} &= \beta_T \frac{S^2}{K_S^2 + S^2} - \beta_A - d\Delta_{TA} \\
&\approx \beta_T \frac{S^2}{K_S^2 + S^2} - \beta_A.
\end{aligned} \tag{2.28}$$

Furthermore, we can find the time integral of $\frac{d\Delta_{TA}}{dt}$:

$$\Delta_{TA}(t') \approx \beta_T \int_0^{t'} \left(\frac{S^2(t)}{K_S^2 + S^2(t)} - \frac{\beta_A}{\beta_T} \right) dt. \tag{2.29}$$

It means that the difference between the toxin and antitoxin concentration is proportional to the integral of the error between $\frac{S^2(t)}{K_S^2 + S^2(t)}$ and $\frac{\beta_A}{\beta_T}$, so called the integral controller. In other words, the left-hand side of equation (2.29) converges to steady state only when the integrand becomes zero, leading to the same result as in equation (2.25). Therefore, at steady state, the AHL concentration S is steered to a lumped parameter that is independent of cell growth and death rates or the carrying capacity. Then based on the proportional relationship between population density and AHL concentration, the population density N converges to a constant level despite uncertainties and disturbances to cell growth and death conditions, which explains the direct solution of steady state population density N in equation (2.27).

The population-level controller is not exactly integral controller due to leakiness from dilution, which we neglect above by assuming $d \ll \beta_T, \beta_A$. With the leakiness in consideration, the population density cannot achieve perfect adaptation to disturbances, but is ensured with a small error compared to the open loop. To demonstrate the robustness performance of the control circuit, we simulate for the population growth dynamics with the closed loop circuit as well as the open loop circuit, as illustrated in Figure 2.8A,B. We introduce step disturbances on both cell death rate d_N and growth rate k_N to the population. Compared to the open loop, the closed loop achieves adaptation to disturbance of 2-fold change of growth and death rates with a small error, as shown in simulations in Figure 2.8C,D.

According to equation (2.27), the population density reference can be set by the production rate of the antitoxin ccdA, represented by the parameter β_A. In circuit implementation, the production rate can be tuned by an external induction on an
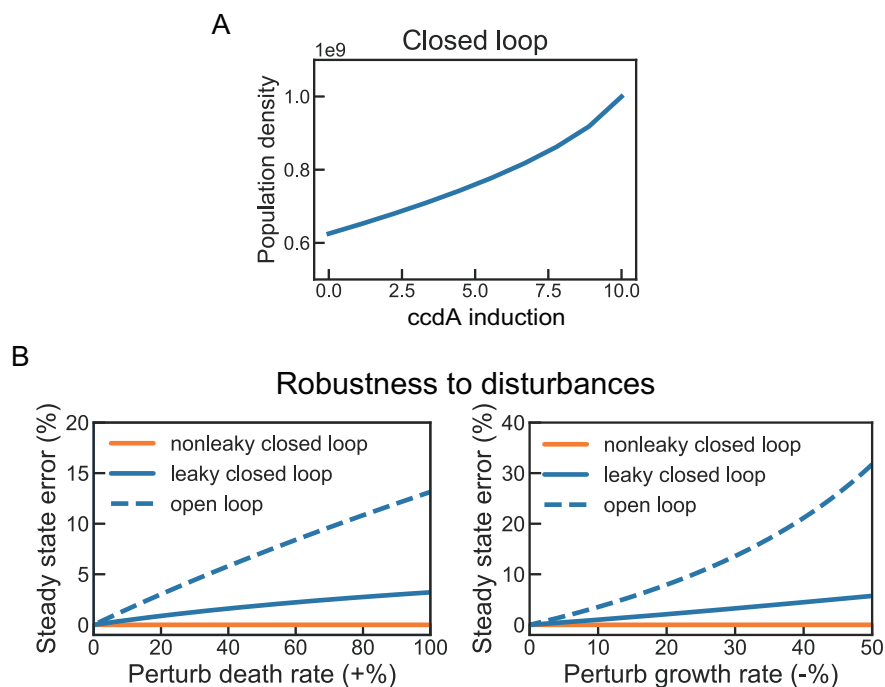
Figure 2.9: Tunability and robustness performance of the population density control circuit. (A) Tunable population density by inducing the antitoxin ccdA expression in the closed loop control circuit. (B) Steady state errors in population density when the population is perturbed by a step disturbance in cell death rate and growth rate. 0% represents no perturbation, +100% represents doubling the rate and −50% represents halving the rate.

inducible promoter. Increasing β_A while ensuring $\beta_A < \beta_T$ should lead to a higher population density, which is also shown by simulation results in Figure 2.9A.

We also compare the robustness performance of non-leaky closed loop, leaky closed loop and open loop circuits under the same step disturbance to cell growth and death rates by measuring the steady state error in population density. It is shown in Figure 2.9B that even though the population density controller has leakiness and cannot achieve zero steady state error as the non-leaky controller, it ensures a much smaller error compared with the open loop. The leakiness is caused by dilution of intracellular species when cells grow and divide, so it is unavoidable for this kind of integral controller implementations (Del Vecchio, Dy, and Qian, 2016). More discussion of leaky integral controllers can be found in theoretical studies (Qian and Del Vecchio, 2018).

Population fraction control

Circuits with bistable gene expressions are widely observed to exhibit distinct cellular states, e.g., the lac operon in *Escherichia coli* (Ozbudak et al., 2004), the bacteriophage λ switch (Ptashne et al., 1980; Ptashne, 1992), the MAPK cascade (Ferrell and Machleder, 1998), etc. Synthetic circuits have been implemented to realize bistability in single cells with general design principles including a positive feedback or mutually inhibiting genes (Becskei, Séraphin, and Serrano, 2001; Wilhelm, 2009; Isaacs et al., 2003; D. Chen and Arkin, 2012; Gardner, Cantor, and Collins, 2000; Kramer et al., 2004; Ajo-Franklin et al., 2007). However, these bistable circuits constructed at single cell-level are not sufficient for robust fraction control to heterogeneous disturbances. When some cells are perturbed and fail to exhibit bistablity, other unperturbed cells can hardly respond or adapt by switching cellular states (Burrill et al., 2012).

In this section, we propose a population-level circuit design that achieves robust and tunable population fraction using cell-cell signaling mediated feedback control.

The population fraction control circuit schematic is illustrated in Figure 2.10A. The circuit includes a self-activating transcription factor tagged with a fluorescence reporter Citrine. The transcription factor activates an enzyme iAAH that catalyzes the synthesis of a signaling molecule auxin from its precursor. Auxin is a diffusible signaling molecule (W. Ma et al., 2009), functioning as the sensor of the population-level expression of Citrine. Both the transcription factor and iAAH are tagged with an auxin inducible degradase AID, where the induced degradation by auxin functions as the actuator of the controller. The auxin is also diluted externally with a tunable flow rate in the environment.

Cells exhibit bistable states from the positive feedback loop of the self-activating transcription factor, where ON and OFF states correspond to high and low concentrations of the transcription factor, as well as the reporter Citrine. When cells are in ON state, more auxin molecules are produced, leading to a stronger degradation of the transcription factor and iAAH and negatively regulating ON cell state fraction in the population. The regulated state transition can be described by a simple switch model, as demonstrated in Figure 2.10B. Since auxin concentration depends on all cells' states, it can be regarded as a measurement of the population fraction of cells exhibiting ON and OFF state in the sensor arm. In the actuator arm, the population fraction is determined by the relative switching rates between ON and OFF states, which are under the regulation of auxin. Therefore, by varying auxin synthesis rate
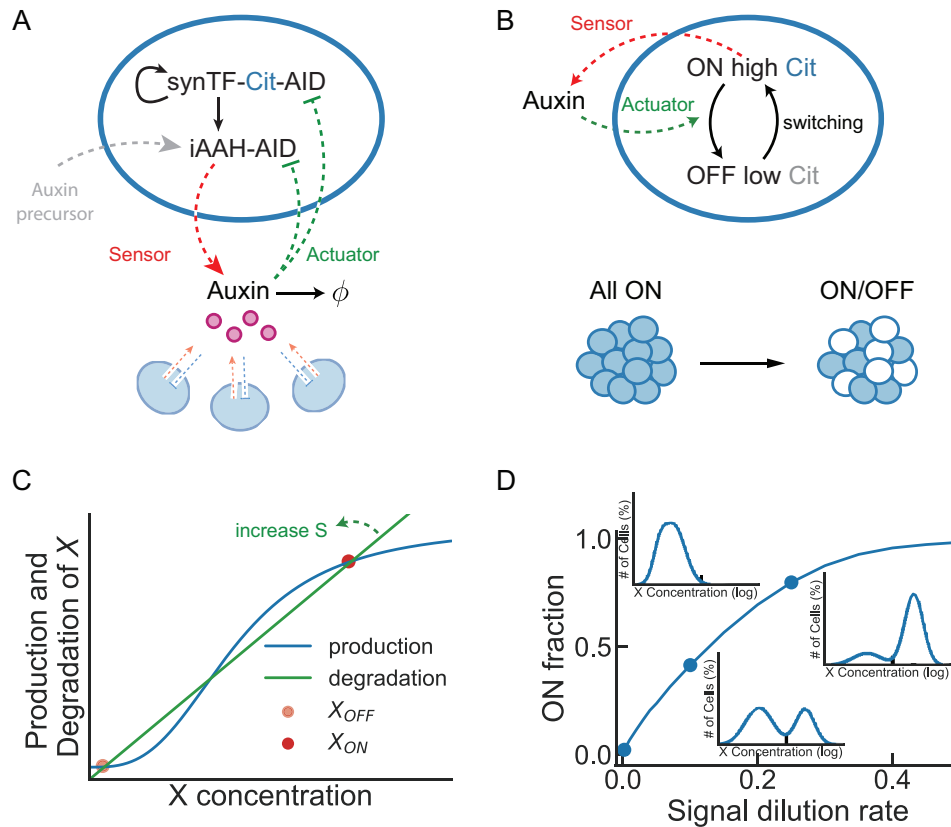
Figure 2.10: Schematic diagram and simulation of population fraction control. (A) The control circuit implementation of a self-activating transcription factor with an inducible degradation tag and a signaling molecule auxin. (B) The simplified ON/OFF switch circuit with a feedback regulation by auxin. (C) Steady states of the bistable switch circuit determined by the production and degradation of X. The slope of the green line is determined by auxin concentration S, representing the degradation rate of X. (D) Simulation results of the steady state population fraction tuned by a range of the dilution rate d_S of auxin. The distributions of X concentration correspond to different ON cell fractions (blue dots) on the curve.

or the external dilution rate, the population fraction can be tuned.

To understand the tunable bistable states, we first introduce an ODE model of biomolecular reactions and study the fundamental features of the actuator arm of the circuit. Since the reporter Citrine is assumed to be proportional to the concentration of the transcription factor, we do not distinguish Citrine and the transcription factor, and will use the same variable X to represent their concentrations in the model. The concentration of iAAH is denoted by H and auxin concentration is denoted by S. We assume:

- The kinetics of activation by the transcription factor follows the Hill-type function with dissociate constant K_X and coefficient n.

- Auxin induced degradation follows the Hill-type function with dissociate constant K_S, coefficient n_S and degradation rate γ.

- There are basal production of the transcription factor and iAAH with rates α_X, α_H, and activated production with rates β_X, β_H.

- Intracellular species have self-degradation and dilution of first-order kinetics with rate d.

The dynamics of the transcription factor and iAAH are modeled by

$$\text{TF (Citrine):} \quad \frac{dX}{dt} = \alpha_X + \beta_X \frac{X^n}{K_X^n + X^n} - \gamma \frac{S^{n_S}}{K_S^{n_S} + S^{n_S}} X - dX,$$
$$\text{iAAH:} \quad \frac{dH}{dt} = \alpha_H + \beta_H \frac{X^n}{K_X^n + X^n} - \gamma \frac{S^{n_S}}{K_S^{n_S} + S^{n_S}} H - dH. \tag{2.30}$$

For a simpler analysis, if we assume that the transcription factor activates itself and iAAH with the same production rate and leakiness, i.e., $\alpha_X = \alpha_H := \alpha, \beta_X = \beta_H := \beta$, we can find that the transcription factor and iAAH have the same dynamics:

$$\text{TF (Citrine):} \quad \frac{dX}{dt} = f_+(X) - f_-(S)X,$$
$$\text{iAAH:} \quad \frac{dH}{dt} = f_+(X) - f_-(S)H, \tag{2.31}$$

where $f_+(X)$ is the production rate dependent on the activation by the transcription factor, and $f_-(S)$ is the degradation rate involving the induced degradation by auxin:

$$\text{production rate:} \quad f_+(X) = \alpha + \beta \frac{X^n}{K_X^n + X^n},$$
$$\text{degradation rate:} \quad f_-(S) = \gamma \frac{S^{n_S}}{K_S^{n_S} + S^{n_S}} + d. \tag{2.32}$$

According to equations (2.31) and (2.32), we can find the steady state solutions of X given a fixed auxin concentration by looking for the intersection of $f_+(X)$ and $f_-(S)X$. It is shown in Figure 2.10C that there are three solutions with two stable states corresponding to ON and OFF states, and one unstable intermediate state. It means that deterministically cells converge to either ON or OFF state based on their initial conditions. Auxin concentration determines the degradation rate $f_-(S)$ and establishes the barrier between stable ON and OFF states. When there are more

auxin molecules in the environment, cells are more likely to switch to OFF state because of the degradation of X, leading to a lower ON population fraction.

Now we model the sensor arm to study the dynamics of auxin. We assume the synthesis of auxin is linearly dependent on the enzyme iAAH concentration with rate β_S, given the precursor is abundant. Consider there are N cells in the population secreting auxin and auxin is diluted externally in the environment with rate d_S. The ODE model of the total auxin concentration is:

$$\text{auxin:} \quad \frac{dS}{dt} = \sum^{N} \beta_S H - d_S S. \tag{2.33}$$

Equations (2.30) and (2.33) describe the closed loop circuit in ODEs. By changing the external dilution rate d_S of auxin, we are able to tune the concentration of S and therefore obtain different population fractions of ON and OFF states. To test the tunability, we vary d_S values and run a stochastic simulation of 1000 cells for X expression distribution, and compute for the ON state population fraction at steady state. As shown in Figure 2.10D, increasing the dilution rate d_S leads to a higher ON state cell fraction in a wide regime.

To further demonstrate how the population-level controller regulates cell state switching and tunes the population fraction, we develop a population-level ODE model. Consider there are N_{ON} ON state cells that have steady states of transcription factor and iAAH with concentrations X_{ON}, H_{ON}, and $N_{OFF} = N - N_{ON}$ OFF state cells have steady states X_{OFF}, H_{OFF}. We can derive the steady state of total auxin concentration according to equation (2.33):

$$
\begin{aligned}
S &= \sum^{N} \beta_S H / d_S \\
&= \frac{\beta_S}{d_S} \left(N_{ON} H_{ON} + N_{OFF} H_{OFF} \right) \\
&= \frac{N \beta_S}{d_S} \left(H_{OFF} + (H_{ON} - H_{OFF}) \frac{N_{ON}}{N} \right).
\end{aligned} \tag{2.34}
$$

Consider the control objective y is the ON cell fraction $\frac{N_{ON}}{N}$. Equation (2.34) shows that the auxin concentration S is proportional to y and the proportion depends on the total population density N, the synthesis rate β_S and the dilution rate d_S of auxin. Therefore, the signaling molecule auxin functions as a proportional feedback control species at population-level.

Now we test the adaptation response of the population-level control circuit mediated by the signaling molecule auxin under disturbances. Consider a heterogeneous
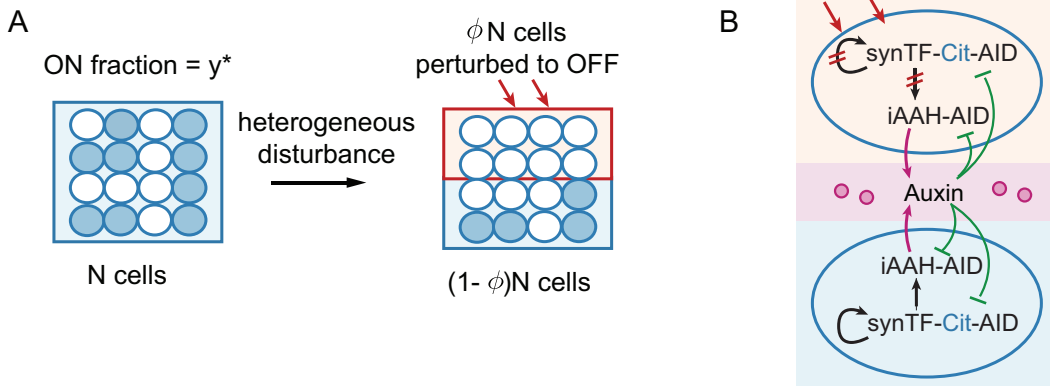
Figure 2.11: Schematic diagram of a heterogeneous disturbance in population fraction control. (A) Illustration of the disturbance that perturbs a fraction of ϕN cells in the population. Cells in ON and OFF states are shown in white and blue circle. Cells in the red box are perturbed to OFF state. (B) A detailed illustration of the disturbance mechanism. Cells that are perturbed fail to express the transcription factor and iAAH (upper cell).

disturbance in the environment that breaks the expression of the transcription factor and iAAH, leading to an emerging phenotype with only OFF state. Figure 2.11A illustrates the heterogeneous disturbance that only hits partial of the population. In a population of N cells, the initial population fraction of ON cells is y^*. A subpopulation of ϕN $(0 < \phi < 1)$ cells are perturbed to OFF state, while the other cells are not perturbed. In perturbed cells, the transcription factor and iAAH are no longer expressed, eventually cells stay in the OFF state, as shown in Figure 2.11B.

Without cell-cell signaling via auxin (open loop), we can find the ON cell fraction of the overall population after the disturbance becomes

$$y_{ol} = \frac{(1-\phi)Ny^*}{N} = (1-\phi)y^*, \tag{2.35}$$

leading to an error

$$e_{ol} = \frac{|(1-\phi)y^* - y^*|}{y^*} = \phi. \tag{2.36}$$

The open loop result shows that there is no adaptation to the disturbance in the population fraction and the steady state error is direcly determined by the fraction of perturbed cells that are turned to OFF state, denoted by ϕ.

With the population-level control circuit proposed above, we expect that more unperturbed cells can switch to ON state and maintain a robust level of overall ON cell fraction in the population, since the signaling molecule auxin can measure the change of the overall population fraction and actuate state switching in other
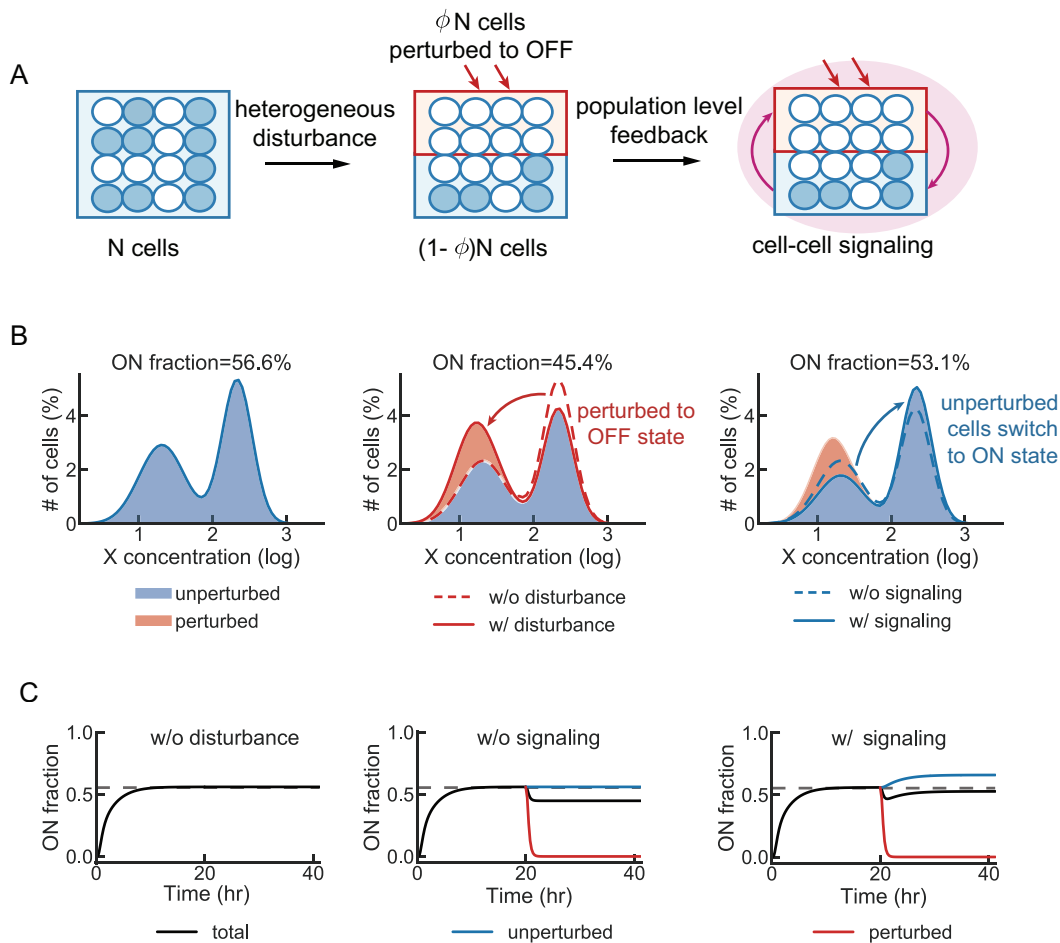
Figure 2.12: Simulation of response to a heterogeneous disturbance in population fraction control. (A) Illustration of the perturbation and adaptation process in the population. (B) Simulated *X* concentration distributions. Left panel shows a bimodal stationary distribution without the disturbance. Middle panel shows a perturbed distribution without the population fraction control circuit. Right panel shows the adapted distribution with the control circuit. Dashed curves and arrows demonstrate how cells switching between states affect the distribution change. (C) Simulated time trajectories of ON cell fraction in the total population, unperturbed and perturbed subpopulations corresponding to the three scenarios.

unperturbed cells. To test that, we simulate the evolution of the distribution of *X* expression and demonstrate how unperturbed cells compensate for perturbed cells. Figure 2.12A shows the simulation results of the perturbation and adaptation process.

Figure 2.12B (left) is the population distribution of *X* expression at steady state without disturbance. The bimodal distribution shows two peaks of high/low *X* expression (ON/OFF state), and we can compute the ON fraction $y_* = 56.6\%$.

Figure 2.12C (left) is the corresponding time trajectory of ON fraction starting from all OFF state cells initially at time zero. When a fraction of 20% population are perturbed to OFF state, we can observe from the simulation in Figure 2.12B (middle) that the distribution of ON state peak shrinks and adds to the OFF state peak, leading to an error of 20% in overall ON fraction in the population as calculated in equation (2.36). Simulation of time trajectory shown in Figure 2.12C (middle) also demonstrates that without the signaling system via auxin, the ON fraction of the perturbed subpopulation decreases to zero while the unperturbed subpopulation maintain their initial ON fraction. With the population-level controller by auxin mediated feedback, the distribution of OFF state peak moves to ON state peak since a fraction of unperturbed subpopulation switch to ON state, as shown in Figure 2.12B (right). The time trajectory in Figure 2.12C (right) shows how unperturbed subpopulation compensate for the breakdown in perturbed subpopulation to maintain a robust overall ON fraction in the population.

Heterogeneous disturbances are common in environments. Strong disturbances may significantly interfere with cellular dynamics and cause a large fraction of cells under stress, resulting in a large perturbation in population-level behaviors (Veening, Smits, and Kuipers, 2008; Kussell and Leibler, 2005). It is also known as a survival strategy for cell populations to exhibit phenotypes with low metabolism and slow growth in fluctuating environments, which may also affect other desired functionalities in synthetic cell populations (Balaban et al., 2004; Fraser and Kaern, 2009; Ackermann, 2015). Therefore, we expect the population-level control circuit to achieve robust control of desired functionalities under diverse environmental disturbances that may lead to phenotypes with broken or even failed regulation.

We further test the robustness performance of the population fraction control circuit to disturbances with varying amplitude (Figure 2.13A) in a large range of perturbed population fraction (Figure 2.13C) and compared the closed loop steady state error in ON fraction with open loop results (Figure 2.13B, D).

When the disturbance causes a larger perturbation to the expression of X with a lower production rate as shown in Figure 2.13A, the potential well for the ON state becomes shallower, allowing perturbed cells to switch to the OFF state more easily. Thus a larger amplitude in perturbing X production rate leads to a larger error in population ON fraction, as shown in the simulation in Figure 2.13B. When the disturbance is large enough to fully turn off perturbed cells, which is the scenario considered in Figure 2.11, the error of the closed loop is kept at a constant value. Compared to the
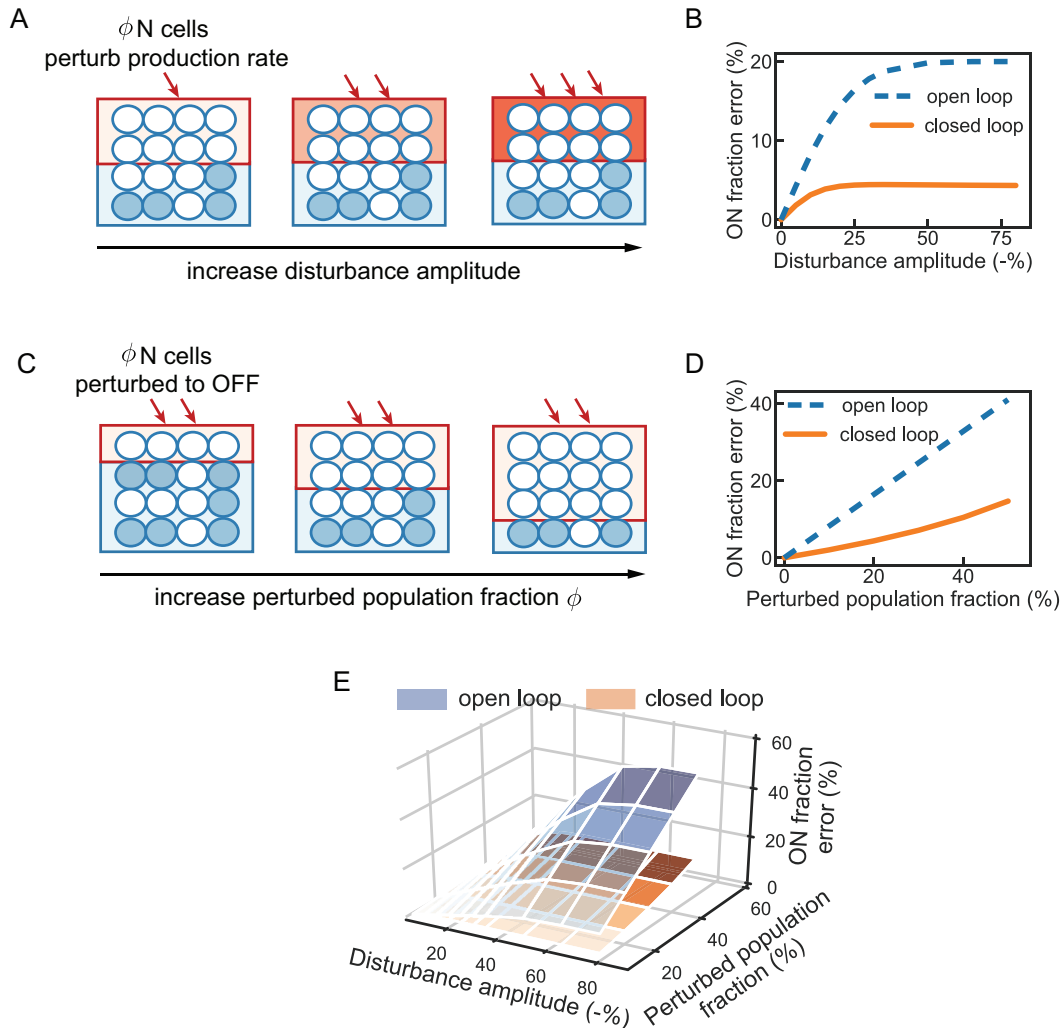
Figure 2.13: Robustness performance of the population fraction control circuit. (A) Illustration of a disturbance with an increasing amplitude. A fixed fraction of cells in the red box are perturbed with an increasing disturbance in X production rate from left (light red) to right (dark red). (C) Illustration of a disturbance with an increasing fraction of perturbed cells. An increasing fraction of cells in the red box are perturbed with a fixed disturbance in X production rate from left (small red box) to right (large red box). (B)(D)(E) Simulations of ON fraction error at steady state of the open loop circuit without the signaling feedback and the closed loop circuit with the signaling feedback.

open loop where the ON fraction error saturates at the value equal to the perturbed population fraction ϕ, the closed loop ensures a much smaller error. On the other hand, we quantify the steady state error of ON fraction given an increasing fraction of perturbed cells. The simulation in Figure 2.13D shows that when perturbed cells are fully turned off, the error increases along the perturbed population fraction ϕ but

is much smaller than the open loop error. An integrated robustness performance is characterized in Figure 2.13E, indicating the population fraction control circuit is able to significantly reduce the error in ON cell fraction compared to no signaling feedback between the perturbed and the unperturbed subpopulations.

Two populations ratio control

Engineering synthetic microbial consortia relieves the loading effect and burden in individual cells by division of labor (Roell et al., 2019; Sabra et al., 2010). Recent studies have started building circuits in consortia of multiple cell types instead of a single cell type for more complex functionalities. For example, a predator prey system with two cell strains (Balagaddé et al., 2008), a two strain system for programmed pattern formation (Basu et al., 2005), and a two strain population-level oscillator (Y. Chen et al., 2015). When implementing circuits at the population-level across multiple cell strains, maintaining a stable population fraction of all cell strains is challenging. Without population-level control, the ratio between cell types merely depends on their initial fractions, resource in environments and corresponding growth rates, which can be constantly varying with cellular noise and environmental disturbances. In addition to achieving stable and robust coexistence of different cell types, the ratio between the cell types might require tuning for the best performance of the consortium.

Here, we present a population-level control circuit that robustly tunes the population ratio between two cell types in a consortium [2]. The closed loop system includes two orthogonal cell-cell signaling systems via quorum sensing signals. The quorum sensing signals function as the sensor of cell population density of both cell types. Both cell types have a sequestering pair of toxin-antitoxin proteins, which is the comparator and actuator.

As shown in Figure 2.14A, we consider two different cell types of N_1 and N_2 cells in a well-mixed culture. Cell type I constitutively produces a signaling molecule Lux-AHL, where the concentration of Lux-AHL is considered as a proportional measurement of cell number N_1. Lux-AHL activates the production of a toxin protein ccdB in cell type I, forming a negative feedback loop regulating its own population density. Cell type II produces another orthogonal signaling molecule Cin-AHL under an external induction that activates toxin ccdB in cell type II, self-regulating its density. Cell type I can also sense Cin-AHL and produce an

---

[2]*A version of this section has been published as (Ren, Baetica, et al., 2017).*
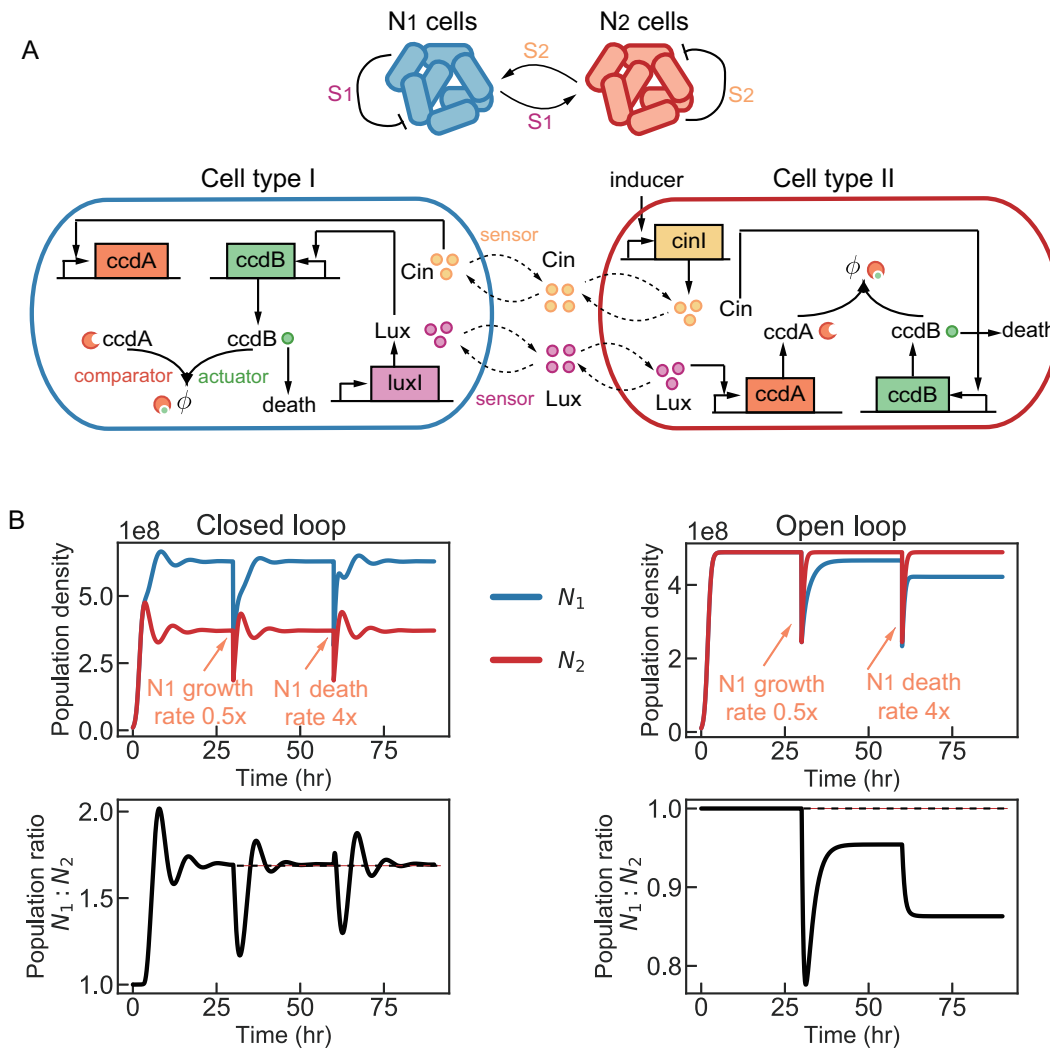
Figure 2.14: Schematic diagram and simulation of two populations ratio control. (A) The control circuit implementation of toxin-antitoxin (ccdB-ccdA) pairs and the Lux-AHL, Cin-AHL quorum sensing systems in two cell types. The upper diagram illustrates concept of the control circuit with self-killing and mutual-rescuing mechanisms to control population density ratio. (B) Simulations of population density dynamics of two cell types with the closed loop circuit in (A) and the open loop circuit without the quorum sensing system. There is a step disturbance in cell type I cells' growth rate at 30hr and in death rate at 60hr.

antitoxin protein ccdA by Cin-AHL's activation, where ccdA can rescue cell type I by sequestering more toxin ccdB. Similarly, Lux-AHL activates ccdA production in cell type II to inhibit cell death.

Both cell types actuate cell death and rescuing reactions by sensing signaling molecules from their own and the other cell type. The desired ratio between cell

Parameters	Description
k_{N_1}, k_{N_2}	Population growth rate of cell type I and II
$N_{\max}$	Carrying capacity
d_{N_1}, d_{N_2}	Population death rate by toxin of cell type I and II
α_T, α_A	Basal production rate of toxin ccdB and antitoxin ccdA
β_T, β_A	Activated production rate of toxin ccdB and antitoxin ccdA by AHL
γ	Sequestration rate of toxin ccdB and antitoxin ccdA
d_1, d_2	Dilution rate of intracellular species in cell type I and II
K_{S_1}, K_{S_2}	Dissociation coefficient of Lux-AHL and Cin-AHL activation
β_{S_1}, β_{S_2}	Production rate of Lux-AHL and Cin-AHL
d_S	External dilution of AHL

Table 2.1: Parameters of the two populations ratio control model.

types (reference) can be set by tuning the synthesis rates of two AHLs, for example, the external induction of Cin-AHL. When the ratio between cell type I and II ($N_1 : N_2$) is perturbed to a higher value than the desired ratio, more Lux-AHL will be synthesized and released, leading to more toxin ccdB production in cell type I. On the other hand, fewer Cin-AHL molecules are secreted in the environment, resulting in a reduced production of antitoxin ccdA in cell type I. Both pathways cause more cell type I cells dead. Meanwhile, the increase in Lux-AHL concentration and the decrease in Cin-AHL concentration can rescue more cell type II cells. As a result, the ratio between cell type I and II is down-regulated until it reaches the desired value and adapts to the perturbation.

We develop an ODE model to describe both cell growth/death dynamics and intracellular gene expression dynamics of two cell types in a well-mixed culture. We assume:

- Both cell types share the same resource in the environment for growth and the growth is characterized by Lokta-Volterra model.

- Both cell types have the same production rates of the toxin ccdB and the toxin ccdA.

- The two quorum sensing AHLs are orthogonal.

The model of cell type I is:

population density: $\quad \dfrac{dN_1}{dt} = k_{N_1}\left(1 - \dfrac{N_1 + N_2}{N_{\max}}\right)N_1 - d_{N_1}T_1 N_1,$

toxin ccdB: $\quad \dfrac{dT_1}{dt} = \alpha_T + \beta_T \dfrac{S_1^2}{K_{S_1}^2 + S_1^2} - \gamma T_1 A_1 - d_1 T_1,$

antitoxin ccdA: $\quad \dfrac{dA_1}{dt} = \alpha_A + \beta_A \dfrac{S_2^2}{K_{S_2}^2 + S_2^2} - \gamma T_1 A_1 - d_1 A_1,$

signal Lux-AHL: $\quad \dfrac{dS_1}{dt} = \beta_{S_1} N_1 - d_S S_1,$
$$(2.37)$$

where $d_1 = k_{N_1}\left(1 - \frac{N_1 + N_2}{N_{\max}}\right)$. Parameters are listed in Table 2.1.

The model of cell type II is:

population density: $\quad \dfrac{dN_2}{dt} = k_{N_2}\left(1 - \dfrac{N_1 + N_2}{N_{\max}}\right)N_2 - d_{N_2}T_2 N_2,$

toxin ccdB: $\quad \dfrac{dT_2}{dt} = \alpha_T + \beta_T \dfrac{S_2^2}{K_{S_2}^2 + S_2^2} - \gamma T_2 A_2 - d_2 T_2,$

antitoxin ccdA: $\quad \dfrac{dA_2}{dt} = \alpha_A + \beta_A \dfrac{S_1^2}{K_{S_1}^2 + S_1^2} - \gamma T_2 A_2 - d_2 A_2,$

signal Cin-AHL: $\quad \dfrac{dS_2}{dt} = \beta_{S_2} N_2 - d_S S_2,$
$$(2.38)$$

where $d_2 = k_{N_2}\left(1 - \frac{N_1 + N_2}{N_{\max}}\right)$.

Assuming the sequestration between ccdB and ccdA is strong with fast rate $\gamma \gg d_1, d_2$, we can derive the quasi-steady state of ccdB and ccdA in cell type I by setting $\frac{dT_1}{dt} = 0$, $\frac{dA_1}{dt} = 0$:

$$T_1 A_1 \approx \frac{\alpha_T}{\gamma} + \frac{\beta_T}{\gamma}\frac{S_1^2}{K_{S_1}^2 + S_1^2} = \frac{\alpha_A}{\gamma} + \frac{\beta_A}{\gamma}\frac{S_2^2}{K_{S_2}^2 + S_2^2}. \tag{2.39}$$

We can further derive from equation (2.24):

$$\beta_T \frac{S_1^2}{K_{S_1}^2 + S_1^2} - \beta_A \frac{S_2^2}{K_{S_2}^2 + S_2^2} \approx \alpha_A - \alpha_T. \tag{2.40}$$

Similarly, we solve for the quasi-steady state of ccdB and ccdA in cell type II:

$$\beta_A \frac{S_1^2}{K_{S_1}^2 + S_1^2} - \beta_T \frac{S_2^2}{K_{S_2}^2 + S_2^2} \approx \alpha_T - \alpha_A. \tag{2.41}$$

From equations (2.40) and (2.41), we can obtain

$$\frac{S_1^2}{K_{S_1}^2 + S_1^2} = \frac{S_2^2}{K_{S_2}^2 + S_2^2} \approx \frac{\alpha_A - \alpha_T}{\beta_T - \beta_A}. \tag{2.42}$$

Given the steady state of AHL concentration when $\frac{dS_1}{dt} = 0$, $\frac{dS_2}{dt} = 0$, we have

$$S_1 = \frac{\beta_{S_1}}{d_S} N_1, \; S_2 = \frac{\beta_{S_2}}{d_S} N_2. \tag{2.43}$$

Combining equations (2.42) and (2.43), we can solve for the population ratio between cell type I and II:

$$r_{12} = \frac{N_1}{N_2} = \frac{\beta_{S_2}}{\beta_{S_1}} \frac{S_1}{S_2} \approx \frac{\beta_{S_2}}{\beta_{S_1}} \frac{K_{S_1}}{K_{S_2}}, \tag{2.44}$$

which is not dependent on the population growth rates k_{N_1}, k_{N_2}, death rates d_{N_1}, d_{N_1} or carrying capacity $N_{\max}$. From the theoretical solution, we can expect that fluctuations in the environment that perturb the growth condition of cell populations will not affect the steady state ratio with the feedback control circuit.

In fact, the population ratio control circuit includes an approximated integral feedback. We can define the controller dynamics by the concentration difference between toxins and antitoxins in two cell types: $\Delta_{TA} = (T_1 - A_1) - (T_2 - A_2)$. Assuming dilution rates d_1, d_2 are negligible, i.e., $d_1, d_2 \ll \beta_T, \beta_A$, we can derive the controller dynamics:

$$\frac{d\Delta_{TA}}{dt} \approx \beta_T \frac{S_1^2}{K_{S_1}^2 + S_1^2} - \beta_A \frac{S_2^2}{K_{S_2}^2 + S_2^2} - \beta_T \frac{S_2^2}{K_{S_2}^2 + S_2^2} + \beta_A \frac{S_1^2}{K_{S_1}^2 + S_1^2}. \tag{2.45}$$

Furthermore, we can find the time integral of $\frac{d\Delta_{TA}}{dt}$:

$$\Delta_{TA}(t') \approx (\beta_T + \beta_A) \int_0^{t'} \left(\frac{S_1^2(t)}{K_{S_1}^2 + S_1^2(t)} - \frac{S_2^2(t)}{K_{S_2}^2 + S_2^2(t)} \right) dt. \tag{2.46}$$

It means the difference between toxin and antitoxin concentrations in two cell types is proportional to the integral of the error between two signaling molecule activation strengths $\frac{S_1^2}{K_{S_1}^2 + S_1^2}$ and $\frac{S_2^2}{K_{S_2}^2 + S_2^2}$. In other words, the left-hand side of equation (2.46) converges to steady state only when the integrand becomes zero, requiring steering two AHL concentrations S_1, S_2 to values that are independent of cell growth rates, death rates and carrying capacity. Then based on the proportional relationship between population density and AHL concentration, the population fraction ratio r_{12} converges to a constant level that depends on AHL synthesis rates β_{S_1} and
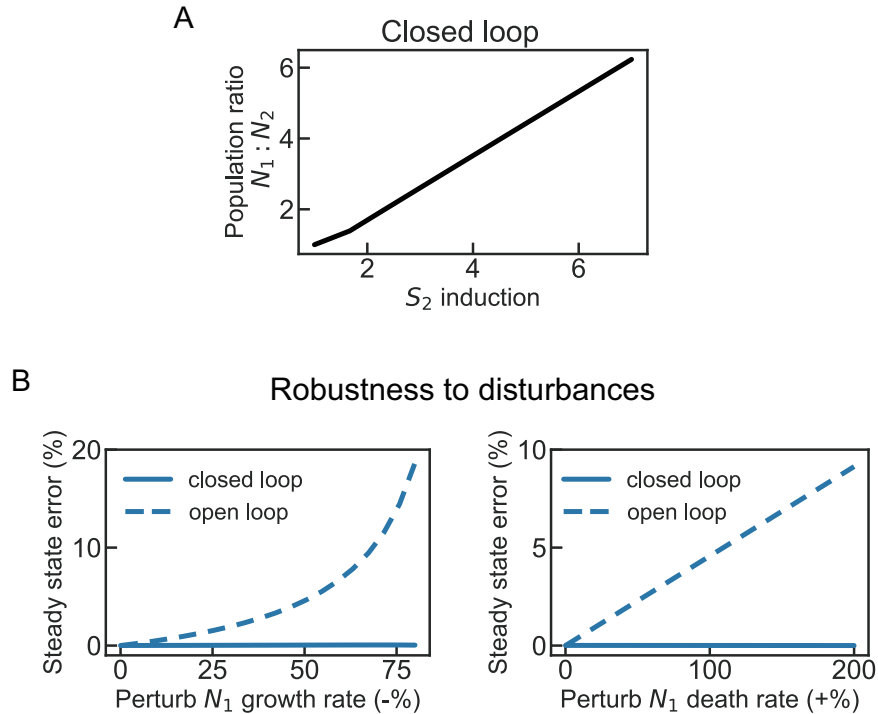
Figure 2.15: Tunability and robustness performance of the two populations ratio control circuit. (A) Tunable population density ratio by inducing the Cin-AHL (S_2) synthesis rate in cell type II. (B) Steady state errors in population density ratio when cell type I population is perturbed by a step disturbance in cell growth rate and death rate. 0% represents no perturbation.

β_{S_2}, despite uncertainties and disturbances in population growth conditions. The integral controller ensures robust population ratio between two cell types, which is also consistent with the steady state solution of r_{12} in equation (2.44).

To demonstrate the population ratio controller maintains a robust ratio between two cell types, we simulate for population growth dynamics with closed loop circuit under step disturbances to cell type I. We also compared the results with open loop circuit that does not includes the quorum sensing systems of Lux-AHL or Cin-AHL molecules. When cell type I cells are perturbed with lower growth rate k_{N_1} or higher death rate d_{N_1}, the population density N_1 decreases to a lower level in the open loop circuit, leading to a large error in population ratio, as shown in Figure 2.14B (right). However, in the closed loop with AHL mediated regulation, the ratio between cell type I and II robustly adapts to the disturbances, as shown in Figure 2.14B (left).

According to equation (2.44), the population ratio can be tuned by AHL synthesis rates β_{S_1} and β_{S_2}. With an external induction of Cin-AHL production in cell type II,

we can set a higher ratio by increasing β_{S_2}, which is demonstrated by simulation in Figure 2.15A. We also compare the robustness performance of closed loop and open loop circuits under a wide range of disturbances to cell growth and death by measuring the steady state error of population ratio, shown in Figure 2.15B. The simulation results suggest that the population ratio control circuit ensures robust adaptation to environmental disturbances to population growth conditions, and improves robust ratio control significantly than the open loop.

2.5 Principle I: Signal integral feedback control

Population-level control circuits via cell-cell signaling systems have been shown to improve robustness in maintaining the overall population production, population density, fraction and relative ratio between cell types in Section 2.2 and 2.3. Next we explore general design principles and implementable regulation networks that utilize cell-cell signaling molecules as a population-level feedback controller for robust population-level behaviors.

Integral feedback control is commonly used in engineering to achieve a robust setpoint output without error (Aström and Murray, 2010). In biology, integral feedback can be realized by biomolecular reactions for robust perfect adaptation in gene expression (Briat, Gupta, and Khammash, 2016; Xiao and Doyle, 2018; Olsman et al., 2019). Integral feedback ofen requires a chemical species to measure the deviation in the expression output and actuate gene regulation for adaptation when the cell is perturbed. However, to measure population-level expression, any chemical species associated within single cells is not a good fit. In addition, the dilution of intracellular chemical species from cell growth and division is an inevitable source of leakiness for many integral controllers in growing cells (Qian and Del Vecchio, 2018). Implementing integral control in intracellular circuits also faces practical challenges, such as inducing burden to host cells by large transcription and translation reactions (Del Vecchio, Dy, and Qian, 2016), constraints on relative chemical abundance at single cell-level (Ang and McMillen, 2013), etc.

Meanwhile, cell-cell signaling molecules can sense the whole population's expression as a global measurement and regulate downstream intracellular gene expression. Fast and diffusible signaling molecules are particularly a good fit for integral chemical species since they are not diluted by cell growth and division, and its concentration can be tuned by external dilution from the environment. Diverse manipulation approaches of signaling molecules in the environment can also provides flexible

while controlled behaviors in cell populations. Therefore, we propose a population-level design principle using the signaling molecule as the control variable of an integral feedback, so called signal integral feedback control.

Regulation network structures

Signal integral feedback depends on dynamics of the signaling molecule S. Here, we show biological designs with different mechanisms including regulation of the synthesis, degradation and external dilution of the signaling molecule, illustrated in Figure 2.16.

We consider the control goal is to maintain a robust expression of a target gene X in a population. We define the total expression of X in a population of N cells as the sum of X concentration in single cells, denoted by y. To make sure the system is stable with the signal integral feedback control circuit, we focus on regulation networks that form a negative feedback between X and S in the closed loop. According to the analysis of intracellular and extracellular concentrations of fast diffusible signaling molecules in equations (2.13-2.17), we use the same variable for signaling molecule concentration. In this section, we will use capital letters to indicate chemical species, lower case letters to denote the corresponding concentration, and subscript i to denote the concentration in the ith cell. For example, species S has concentration s, and the total expression $y = \sum_{i=1}^{N} x_i$.

Saturated enzymatic degradation of signaling molecules

Signaling molecules can be actively degraded by enzymes. For example, Aiia is an enzyme found in bacteria that degrades quorum sensing molecules AHL (S. J. Lee et al., 2002), and Bar1 protease can degrade a mating pheromone α-factor in yeast cells (Youk and Lim, 2014). In most signaling systems, signaling molecules have a much higher concentration than intracellular enzymes, which leads to a saturation in signaling molecules' degradation.

We assume in the closed loop, the signaling molecule S is synthesized by X and degraded by an constitutive enzyme E, and there is no external dilution in the environment, as shown in Figure 2.16A. The enzymatic degradation is modeled using Michaelis-Menten kinetics with dissociation constant K. The dynamics of S can be described as

$$\frac{\mathrm{d}s}{\mathrm{d}t} = \sum_{i=1}^{N} \left(x_i - \frac{s}{K+s} e_i \right), \tag{2.47}$$
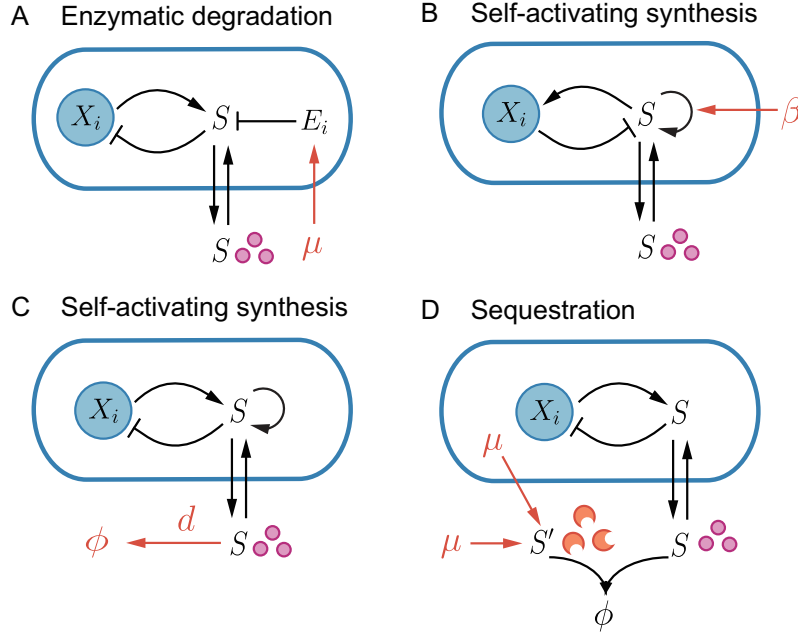
Figure 2.16: Circuit designs of signal integral feedback control. (A) A circuit schematic based on enzymatic degradation. There is an external induction μ on the enzyme expression to tune the robust average expression of X in the population. (B)(C) Circuit schematics based on self-activating signaling molecules. The average expression of X can be tuned by varying the synthesis rate β of the signaling molecule. The total expression of X can be tuned by manipulating the external dilution rate of the signaling molecule. (D) A circuit schematic based on sequestration of signaling molecule pairs. The average or expression of X can be tuned by inducing S' synthesis rate or adding S' externally.

where e_i is a constant concentration of the enzyme E in the ith cell. We can set the enzyme concentration $e_i = \mu$ by an external induction of enzyme expression. When S saturates, i.e., $K, e_i \ll s$, the enzymatic degradation can be approximated by e_i since $\frac{s}{K+s} \approx 1$. We can obtain

$$\frac{\mathrm{d}s}{\mathrm{d}t} \approx \sum_{i=1}^{N} (x_i - e_i) = N\left(\frac{y}{N} - \mu\right). \tag{2.48}$$

The controller described by equation (2.48) indicates that the average population expression $\frac{y}{N}$ is robustly set by the enzyme concentration μ. To tune the population average expression, we can vary the enzyme production with inducible promoters and obtain different enzyme concentrations.

The Michaelis-Menten model of enzymatic degradation is derived from reactions:

$$\emptyset \xrightarrow{X} S + E_i \underset{k_-}{\overset{k_+}{\rightleftharpoons}} ES_i \rightarrow E_i \tag{2.49}$$

with an ODE model:

$$
\begin{aligned}
\frac{\mathrm{d}s}{\mathrm{d}t} &= x_i - k_+ s e_i + k_- [es]_i, \\
\frac{\mathrm{d}e_i}{\mathrm{d}t} &= -k_+ s e_i + k_- [es]_i + [es]_i, \\
\frac{\mathrm{d}[es]_i}{\mathrm{d}t} &= k_+ s e_i - k_- [es]_i - [es]_i.
\end{aligned}
\tag{2.50}
$$

We assume the binding and unbinding process between the signaling molecule S and the enzyme E is much faster than the synthesis and degradation process. Given the enzyme conservation law, i.e., $e_i + [es]_i = e_{total}$, we can derive the quasi-steady state of S where $\frac{\mathrm{d}s}{\mathrm{d}t} = 0$:

$$
\begin{aligned}
k_+ s e_i &\approx k_- [es]_i, \\
k_+ (e_{total} - [es]_i) s &\approx k_- [es]_i, \\
[es]_i &\approx \frac{k_+ e_{total} s}{k_- + k_+ s} = \frac{s}{K + s} e_{total},
\end{aligned}
\tag{2.51}
$$

where $K = \frac{k_-}{k_+}$ is the dissociation constant.

At the slow timescale where S is synthesized by X by N cells and ES_i degrades, we denote the total signaling molecule concentration by $s_{total} = s + \sum_{i=1}^{N} [es]_i$ and obtain:

$$
\frac{\mathrm{d}s_{total}}{\mathrm{d}t} = \sum_{i=1}^{N} (x_i - [es]_i) = \sum_{i=1}^{N} \left(x_i - \frac{s}{K + s} e_{total} \right),
\tag{2.52}
$$

which is rewritten in equation (2.47).

Self-activating synthesis of signaling molecules

Many signaling molecules are found to activate their own synthesis through a positive feedback in nature, such as bacterial quorum sensing molecules AHL, AI-2, and AIP (Miller and Bassler, 2001).

As shown in Figure 2.16B, we assume the self-activating signaling molecule S is degraded or sequestered by X in the close loop, and there is no external dilution. We model the self-activation with Michaelis-Menten kinetics with dissociation constant K, and assume S concentration is within the linear regime, i.e., $s \ll K$. The degradation or sequestration is modeled with mass action kinetics. Then the dynamics of S becomes

$$
\frac{\mathrm{d}s}{\mathrm{d}t} = \sum_{i=1}^{N} \left(\beta \frac{s}{K + s} - x_i s \right).
\tag{2.53}
$$

Given the assumption $s \ll K$, we can approximate the self-activation with linear kinetics since $\frac{s}{K+s} \approx \frac{s}{K}$, and obtain

$$\frac{\mathrm{d}s}{\mathrm{d}t} \approx \sum_{i=1}^{N} \left(\beta \frac{s}{K} - x_i s \right) = -N \left(\frac{y}{N} - \frac{\beta}{K} \right) s. \tag{2.54}$$

The stable steady state is achieved when $\frac{y}{N} - \frac{\beta}{K} = 0$ given $N > 0$, implying that the average population expression $\frac{y}{N}$ converges to a constant $\frac{\beta}{K}$ despite disturbances in X expression. To tune the desired average expression, we can vary the parameter β, representing the synthesis rate of the signaling molecule. For example, we can externally induce the the synthase's expression of the signaling molecule.

Another regulation network structure includes X catalyzing the synthesis of the self-activating signaling molecule S. There is an external dilution of S at a constant rate d, as shown in Figure 2.16C. Then the dynamics of S becomes

$$\frac{\mathrm{d}s}{\mathrm{d}t} = \sum_{i=1}^{N} x_i \frac{s}{K+s} - ds. \tag{2.55}$$

Again, we assume $s \ll K$ so the self-activation operates in the linear regime. We can derive

$$\frac{\mathrm{d}s}{\mathrm{d}t} \approx \sum_{i=1}^{N} x_i \frac{s}{K} - ds = (y - Kd) \frac{s}{K}. \tag{2.56}$$

This network structure sets a robust total population expression y at concentration level Kd, despite disturbances in X expression or population density N. The external dilution rate d can be varied to tune the total expression linearly.

Note that S concentration needs to satisfy the linear regime assumption in its activation to derive the integral feedback in these regulation networks. Therefore, we require that S has a small concentration, i.e., $s \ll K$. This assumption suggests that the feedback control only guarantees robust set-point output with low population density or fast dilution in the environment.

Sequestration of signaling pairs

An integral feedback can be realized through sequestration of chemical species (Briat, Gupta, and Khammash, 2016; Aoki et al., 2019). In multicellular systems, we find sequestering chemical pairs also function as signals, e.g., quorum sensing molecules and antibodies (Grandclément et al., 2016), antibiotics and interceptors

(Sabnis et al., 2018), and growth factors and their inhibitors (Belair, Le, and Murphy, 2014).

We denote the signaling molecule pair by S and S', with concentrations s and s'. In sequestration-based regulation networks, the variable $\Delta s = s - s'$ functions as the integral variable.

As shown in Figure 2.16D, S synthesis is catalyzed by X and S' is constitutively produced by cells or added from an external input. The dynamics of the signaling pair are modeled by

$$\frac{ds}{dt} = \sum_{i=1}^{N} x_i - \gamma s s',$$
$$\frac{ds'}{dt} = \sum_{i=1}^{N} \mu - \gamma s s', \text{ or } \frac{ds'}{dt} = \mu - \gamma s s'. \tag{2.57}$$

For both cases, we can derive

$$\frac{d\Delta s}{dt} = N\left(\frac{y}{N} - \mu\right), \text{ or } \frac{d\Delta s}{dt} = y - \mu. \tag{2.58}$$

Then the average expression $\frac{y}{N}$ or the total expression y can be set to a robust concentration μ when the anti-signal is produced by cells or added with constant rate.

Population expression control

Following the design principles of signal integral feedback control, we propose a synthetic circuit that controls an average gene expression in an *Escherichia coli* population as an example. We test if the signal integral circuit can achieve perfect adaptation to disturbances that lead to 'low-producing' or even 'non-producing' phenotypes in a heterogeneous population. To demonstrate the conclusion in Section 2.2 and 2.3 that intracellular regulation fails in heterogeneous populations, we also present an intracellular integral circuit for comparison.

In this example, the desired population-level expression is a fluorescent protein GFP concentration, which can be seen as a reporter of any gene expression of interests. The signal integral circuit shown in Figure 2.17A is designed based on the network structure of saturated enzymatic degradation presented in Figure 2.16A. In the closed loop circuit, GFP is sensed by a quorum sensing signal AHL and AHL molecules activate a transcription factor TetR that represses GFP and AHL synthase LuxI. The enzyme Aiia degrades AHL and its concentration can be tuned
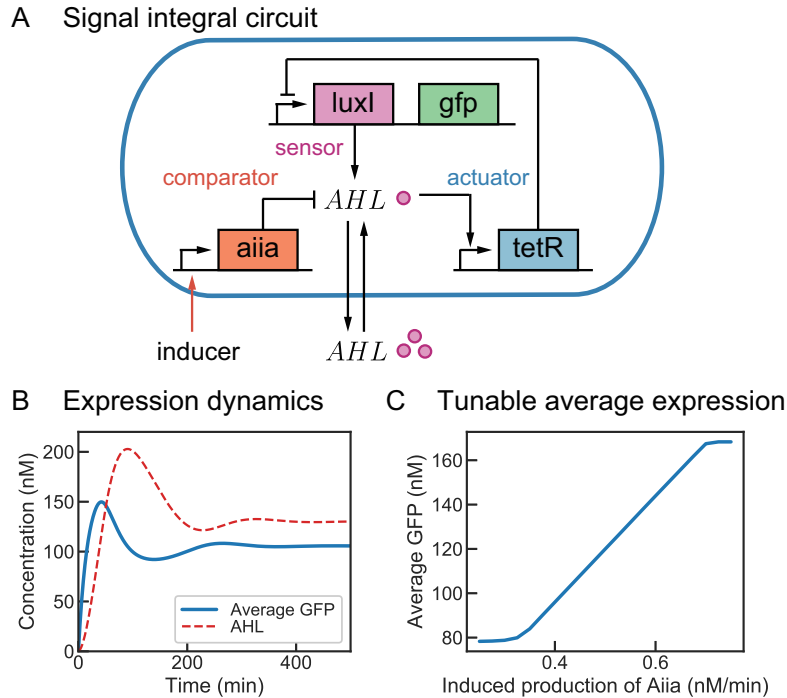
Figure 2.17: Schematic diagram and simulation of a signal integral circuit for population expression control. (A) The control circuit implementation of signal integral feedback based on enzymatic degradation mechanism. (B) Simulations of population-level average expression of GFP and AHL dynamics. (C) Simulations of steady state average GFP concentration under a range of Aiia induction.

through an inducible expression. With a higher expression of Aiia, more AHL molecules are degraded and GFP reaches a lower concentration accordingly. Thus the induction level of Aiia can set the desired population-level expression. Since AHL is a diffusible molecule secreted by all cells and quickly gets well-mixed in the environment, AHL concentration is considered as the signal integral control variable that globally measures the population-level expression of GFP.

We build an ODE model of the signal integral circuit in a population of N cells with following assumptions:

- AHL production rate is proportional to its synthase LuxI concentration.

- AHL concentration is larger than Aiia concentration and the dissociation constant K_{SE} of Michaelis-Menten kinetics of enzymatic degradation, so AHL degradation is saturated by Aiia.

- There is no external dilution of AHL in the environment.

Parameters	Description
α_X, β_X	Basal and repressed production rate of GFP by TetR
α_I, β_I	Basal and repressed production rate of LuxI by TetR
K_T	Dissociation constant of TetR repression
α_E	Inducible production rate of Aiia
α_T, β_T	Basal and activated production rate of TetR by Lux-AHL
K_S	Dissociation constant of Lux-AHL activation
d	Dilution rate of intracellular species
β_S	Synthesis rate of Lux-AHL
γ	Degradation rate of Lux-AHL by Aiia

Table 2.2: Parameters of the signal integral circuit model for population expression control.

- The binding reactions of AHL and its receptor LuxR are neglected given a constitutive expression of LuxR, so AHL-mediated activating production depends on AHL concentration.

- Activating and repressing production rates are modeled by Hill-type functions.

The dynamics of the closed loop circuit is modeled using ODEs with parameters are listed in Table 2.2:

$$
\begin{aligned}
\text{GFP:} \quad & \frac{dX}{dt} = \alpha_X + \beta_X \frac{K_T^2}{K_T^2 + T^2} - dX, \\
\text{LuxI:} \quad & \frac{dI}{dt} = \alpha_I + \beta_I \frac{K_T^2}{K_T^2 + T^2} - dI, \\
\text{Aiia:} \quad & \frac{dE}{dt} = \alpha_E - dE, \\
\text{TetR:} \quad & \frac{dT}{dt} = \alpha_T + \beta_T \frac{S^2}{K_S^2 + S^2} - dT, \\
\text{Lux-AHL:} \quad & \frac{dS}{dt} = \sum^N (\beta_S I - \gamma E), \\
\text{total GFP:} \quad & y = \sum^N X.
\end{aligned}
\tag{2.59}
$$

In the simulation shown in Figure 2.17B and C, we demonstrate that the average GFP expression in the population is regulated by AHL and reaches a stable steady state. Moreover, the steady state concentration of GFP can be tuned by the induction level of Aiia expression in a wide range.

Note that in equation (2.60), the degradation of AHL saturates by the enzyme concentration Aiia since AHL concentration is much higher than Aiia concentration and

A Signal integral circuit under disturbance

'producing' phenotype N_1

B Population level response
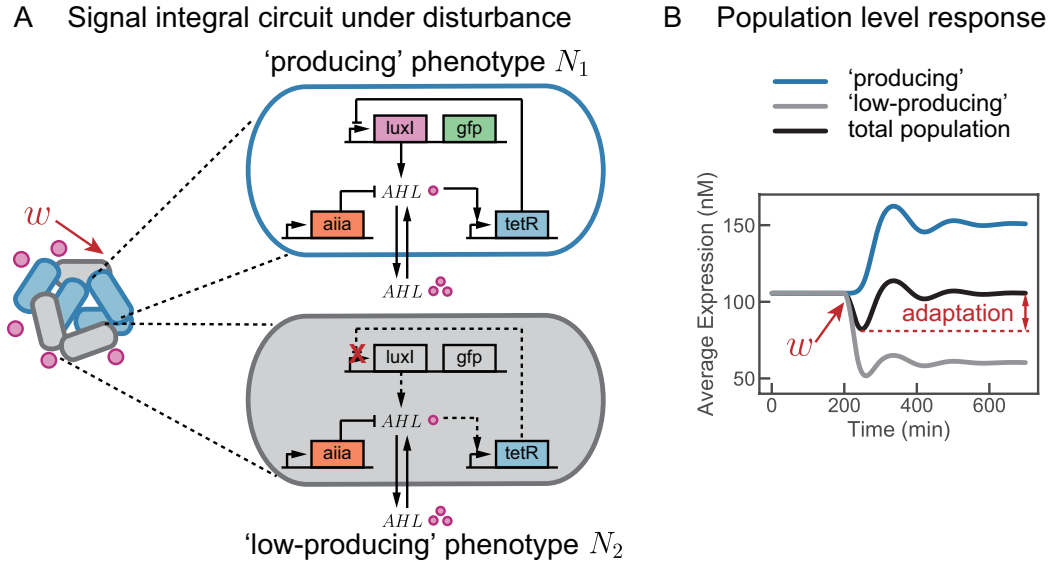
Figure 2.18: Schematic diagram and simulation of the signal integral circuit in a heterogeneous population. (A) Schematic diagram of two phenotypes when the population is perturbed by an environmental disturbance. Dashed lines represent loss of function or regulation in 'low-producing' cells. (B) Simulation of average GFP expression in two phenotypes and the total population. The overall population-level expression shows adaptation to the disturbance.

the dissociation constant K_{SE} of enzymatic kinetics, which is the key assumption for this signal integral control circuit. Small fluctuations in cellular expression of Aiia or AHL usually won't break the assumption, yet large environmental disturbances might have an big effect if critical production of these molecules is shut down. More generally, we can derive AHL dynamics from different degradation kinetics under different assumptions:

$$
\begin{aligned}
\text{if } S \gg K_{SE}: \quad & \frac{\mathrm{d}S}{\mathrm{d}t} \approx \sum_{}^{N} (\beta_S I - \gamma E), \\
\text{if } S \ll K_{SE}: \quad & \frac{\mathrm{d}S}{\mathrm{d}t} \approx \sum_{}^{N} \left(\beta_S I - \frac{\gamma}{K_{SE}} E S \right).
\end{aligned}
\tag{2.60}
$$

Now we evaluate the average GFP expression in the population regulated by the signal integral circuit under large environmental disturbances. We assume the population exhibit emerging phenotypes due to the environmental disturbance. There appear N_1 'producing' cells and N_2 'low-producing' cells that fail to produce the required concentration of GFP, as illustrated in Figure 2.18A. When the disturbance is strong where cells are under critical stress, the 'low-producing' phenotype becomes 'non-producing' and cells stop expressing GFP at all. Without proper control, the

average GFP concentration in the population will be perturbed to a lower level by these 'low-producing' or 'non-producing' cells.

We simulate the response of 'producing', 'low-producing' phenotypes and the total population to the disturbance, shown in Figure 2.18B. After hit by the disturbance, the emerging 'low-producing' cells have a decreasing GFP expression, meanwhile the 'producing' phenotype increase their expression. Therefore, the total population can adapt to the disturbance and maintain a robust average GFP concentration. In this example, we conclude that the global AHL molecules can coordinate heterogeneous response in different phenotypes. Even though 'low-producing' cells undergo severe perturbations in their expression, the disturbance and required control action are divided among all cells. Thus, the population-level control circuit ensures robust adaptation when a fraction of the population are strongly perturbed.

On the other hand, we also propose an intracellular integral circuit for comparison. As illustrated in Figure 2.19A, the circuit utilizes a transcription factor AraC as the control species. AraC is tagged to be actively degraded by a protease ClpXP which has a tunable concentration for various set-point values. The main difference from the signal integral circuit is that we replace the quorum sensing system with an intracellular transcription factor with enzymatic degradation. There is also a dilution in AraC concentration due to cell growth and division. We build ODE models to study the intracellular circuit's dynamics. Parameters can be found in Table 2.3. Similarly, we assume the degradation of AraC is saturated by the protease ClpXP given a high concentration of AraC in cells to satisfy the constraint of an integral controller.

The ODE model of the intracelluar integral circuit in a population of N cells is:

$$
\begin{aligned}
\text{GFP:} \quad & \frac{\mathrm{d}X}{\mathrm{d}t} = \alpha_X + \beta_X \frac{K_T^2}{K_T^2 + T^2} - dX, \\[2ex]
\text{AraC:} \quad & \frac{\mathrm{d}C}{\mathrm{d}t} = \alpha_C + \beta_C \frac{K_T^2}{K_T^2 + T^2} - \gamma P - dC, \\[2ex]
\text{ClpXP:} \quad & \frac{\mathrm{d}P}{\mathrm{d}t} = \alpha_P - dP, \\[2ex]
\text{TetR:} \quad & \frac{\mathrm{d}T}{\mathrm{d}t} = \alpha_T + \beta_T \frac{C^2}{K_C^2 + C^2} - dT, \\[2ex]
\text{total GFP:} \quad & y = \sum^{N} X.
\end{aligned}
\tag{2.61}
$$

Note that the circuit only includes an approximate integral feedback because of
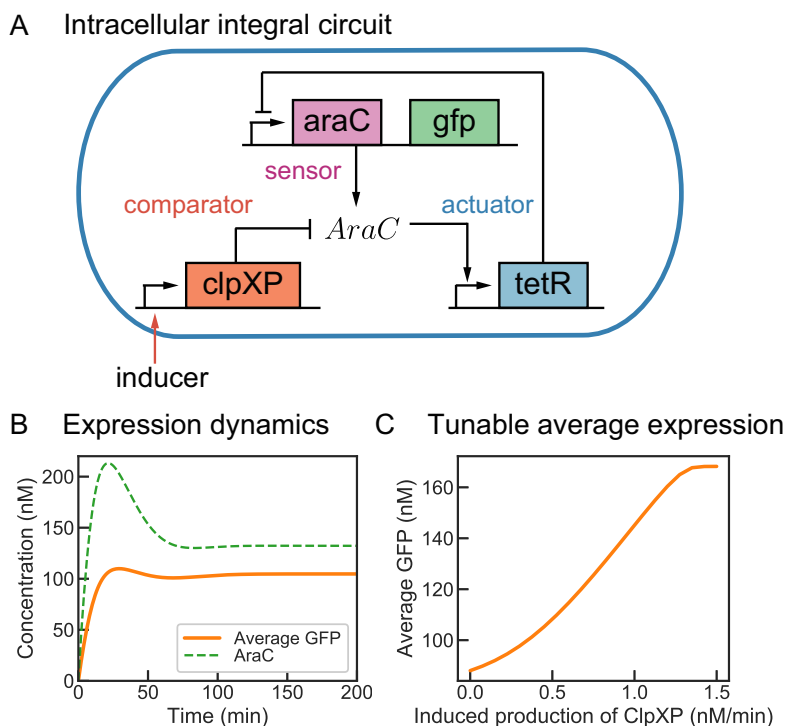
Figure 2.19: Schematic diagram and simulation of a intracellular integral circuit for population expression control. (A) The control circuit implementation of intracellular integral feedback based on enzymatic degradation mechanism. (B) Simulations of population-level average expression of GFP and AraC dynamics. (C) Simulations of steady state average GFP concentration under a range of ClpXP induction.

the dilution of intracellular species, as discussed in Section 2.3. For example, AraC dilution leads to a leaky memory of the error information. In simulation, we find similar dynamics of GFP expression under control of the intracelluar integral feedback circuit, as shown in Figure 2.19B. The induction expression of ClpXP can set the desired concentration of GFP in the population, as shown in Figure 2.19C.

Then we consider the same environmental disturbance that leads to 'producing' and 'low-producing' phenotypes in the population, as illustrated in Figure 2.20A. We demonstrate with simulations in Figure 2.20B that the intracellular circuit cannot adapt, resulting in a large error in the population average expression. The 'low-producing' phenotype fails to express enough GFP as required, while the 'producing' phenotype cannot respond to other cells' dysfunctional performance. In fact, in 'low-producing' cells, the intracellular integral control circuit no longer operates as expected because low production of GFP as well as AraC breaks the key assumption that AraC is abundant to function as an integral controller. The dynamics of

Parameters	Description
α_X, β_X	Basal and repressed production rate of GFP by TetR
α_C, β_C	Basal and repressed production rate of AraC by TetR
K_T	Dissociation constant of TetR repression
α_P	Inducible production rate of ClpXP
α_T, β_T	Basal and activated production rate of TetR by AraC
K_C	Dissociation constant of AraC activation
d	Dilution rate of intracellular species
γ	Degradation rate of AraC by ClpXP

Table 2.3: Parameters of the intracellular integral circuit model for population expression control.
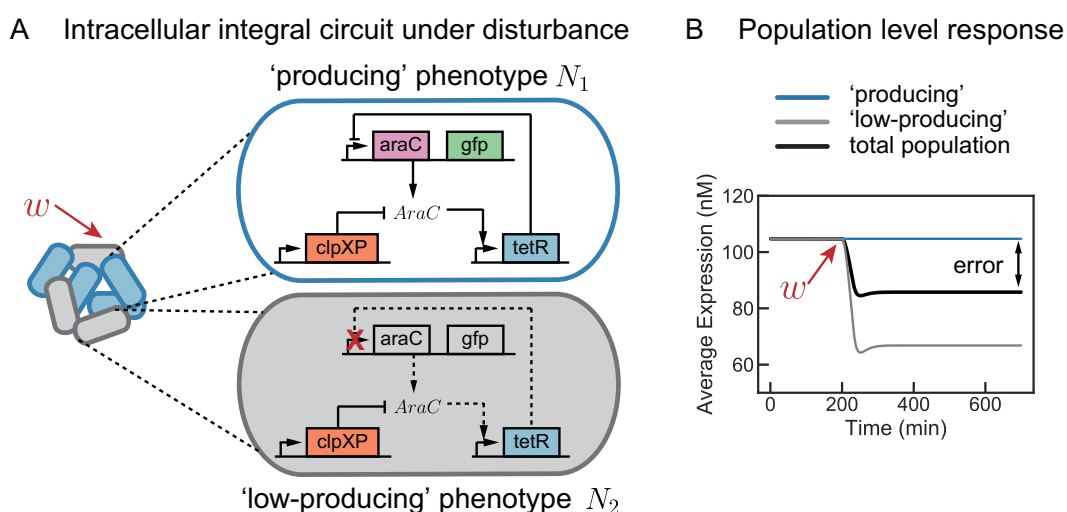
Figure 2.20: Schematic diagram and simulation of the intracellular integral circuit in a heterogeneous population. (A) Schematic diagram of two phenotypes when the population is perturbed by an environmental disturbance. Dashed lines represent loss of function or regulation in 'low-producing' cells. (B) Simulation of average GFP expression in two phenotypes and the total population. The overall population-level expression shows no adaptation to the disturbance.

AraC cannot be approximated with saturated degradation as in equation (2.61), but becomes

$$\text{AraC:} \quad \frac{\mathrm{d}C}{\mathrm{d}t} = \eta\left(\alpha_C + \beta_C \frac{K_T^2}{K_T^2 + T^2}\right) - \frac{\gamma}{K_{CP}}PC - dC, \qquad (2.62)$$

where $0 \le \eta < 1$ represents the disturbance amplitude in production. The degradation of AraC is proportional to both the protease ClpXP concentration and itself. The parameter K_{CP} describes the dissociation constant of Michaelis-Menten kinetics of enzymatic degradation.

A   Disturbance causes a lower production

B   Disturbance causes a larger fraction of 'non-producing' cells
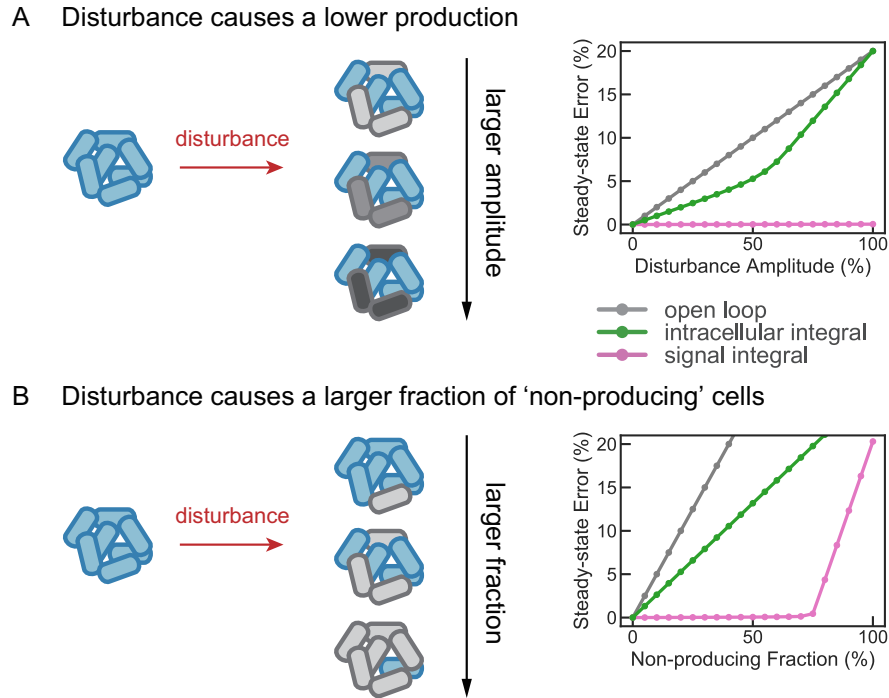
Figure 2.21: Robustness performance of signal and intracellular integral circuits. (A) Illustration of a disturbance with an increasing amplitude and simulations of steady state error in average GFP expression with three circuits. A fixed fraction of cells are perturbed with an increasing disturbance in GFP expression from upper (light grey) to lower (dark grey). (B) Illustration of a disturbance with an increasing fraction of perturbed cells and simulations of steady state error in average GFP expression with three circuits. An increasing fraction of cells are perturbed with a fixed disturbance in GFP expression from upper (fewer grey cells) to lower (more grey cells).

To understand the limit of robustness performance in a heterogeneous population with signal integral and intracellular integral control circuits, we further test if a larger disturbance or a higher fraction of the 'low-producing' phenotype will break the integral circuits. We show the error in the population-level GFP expression at steady state under a wide range of disturbance amplitude and 'low-producing' phenotype fraction in Figure 2.21. Open loop corresponds to the circuit without feedback regulation of GFP expression. We find that for a fixed fraction of the 'low-producing' phenotype, the intracellular circuit has a small error when the disturbance is relatively weak, mainly caused by the leakiness from dilution. When the disturbance becomes strong, the integral controller fully breaks and causes a larger error. The breaking point corresponds to the disturbance amplitude where the intracellular controller no longer satisfies its constraint on the relative abundance of

AraC and ClpXP. Meanwhile, the signal integral circuit achieves perfect adaptation with zero error to a large range of disturbance amplitude, since large disturbances to single cells may appear to be small disturbances at population-level. Moreover, when the disturbance perturbs more cells to exhibit the 'non-producing' phenotype, the population GFP expression error increases linearly with intracellular integral circuit. In contrast, the signal integral circuit can tolerate a higher fraction of 'non-producing' cells in the population before most cells become dysfunctional.

The failure of the intracellular integral controller in this example suggests a common challenge in synthetic control circuit design. Like the desired process that needs to be controlled, the controller may also be perturbed by disturbances. When controllers fail, there is no proper regulation to maintain robust behaviors in cells. Compared to population-level control circuits, single cell-level control circuit such as the intracellular integral controller that aims to regulate individual cells are more likely to fail under severe environmental disturbances. Without coordination in the population, cells are disconnected, making each one of them equally fragile to disturbances.

2.6   Principle II: Bistable state switching feedback control

In this chapter, we introduce a novel population-level design of robust control circuits based on heterogeneous cell state switching behaviors [3].

Besides integral feedback control, high gain feedback has been shown to improve robustness in control theory (Aström and Murray, 2010). The inclusion of ultrasensitive modules in synthetic circuits has been recently demonstrated to improve robust gene expression as a high gain feedback mechanism (Samaniego and Franco, 2017; Cuba Samaniego and Franco, 2018). However, a challenge posed by ultrasensitive mechanisms is that they may require transcription and translation of a large amount of components, imposing a major metabolic burden on the host cell (Del Vecchio, Dy, and Qian, 2016). A possible route to mitigate the burden imposed by high gain controllers is the reliance on heterogeneous cellular states. Heterogeneity in gene expression is common in natural microbial populations, and often leads to diverse population phenotypes (Kaern et al., 2005). Importantly, heterogeneity in gene expression has been described as a strategy of 'division-of-labor' to relieve burden in single cells (West and Cooper, 2016). Furthermore, heterogeneous populations better adapt to environmental disturbances, by taking advantage of changes in phe-

---

[3] *A version of this section has appeared in (Ren, Samaniego, et al., 2020).*
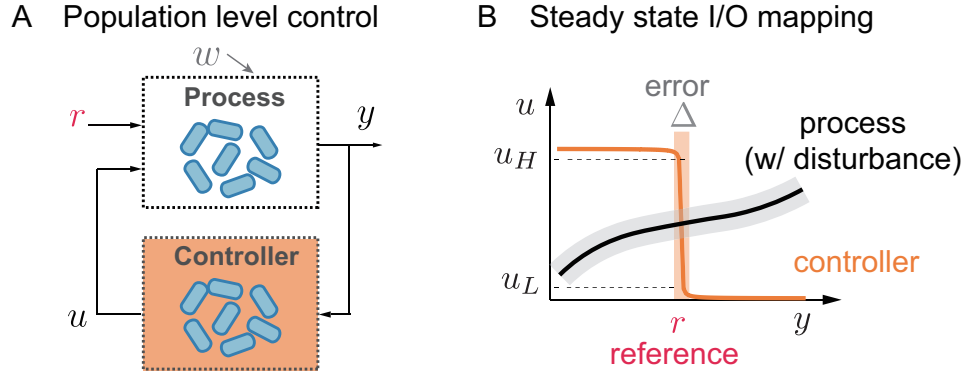
Figure 2.22: Schematic diagram of ultrasensitive feedback control. (A) A closed-loop diagram with an ultrasensitive feedback controller at population-level. (B) The steady state input-output mapping of the controller and the process. The steady state of output y is determined by the intersection of input-output mappings of the controller and the process and converges to the reference r. u_L and u_H denote the low and high level of control input u, and Δ demonstrates the steady state error of output y when the process is perturbed.

notypical ratios and switching between distinct cellular states (Balaban et al., 2004; Thattai and Van Oudenaarden, 2004).

Ultrasensitive controller at population-level

We show a schematic diagram of an ultrasensitive controller and a process interconnected in a feedback loop in a cell population in Figure 2.22A. The process represents population-level behaviors that require tight control with disturbances, uncertainties and noises, for example, target gene expression or chemical production. The controller can be considered as an integration of control circuits in all cells that can sense the population-level output and actuate regulation. We use r to represent the reference that sets the desired output of the closed loop system, and w for disturbances and uncertainties. The output y of the process is the input to the controller and the controller produces u as an output to actuate the process. We define the steady state input-output mappings of the process and the controller:

$$\begin{aligned} \text{process:} \quad & y = f\left(u, r, w\right), \\ \text{controller:} \quad & u = g\left(y\right). \end{aligned} \tag{2.63}$$

As shown in Figure 2.22B, when the controller is ultrasensitive, the input-output mapping of the controller exhibits a sharp transition. Input-output mappings of the controller (orange line) and the process (black line) intersect at the equilibrium of the closed loop system. As long as the equilibrium is stable and lies in the

A   Single cell switch dynamics
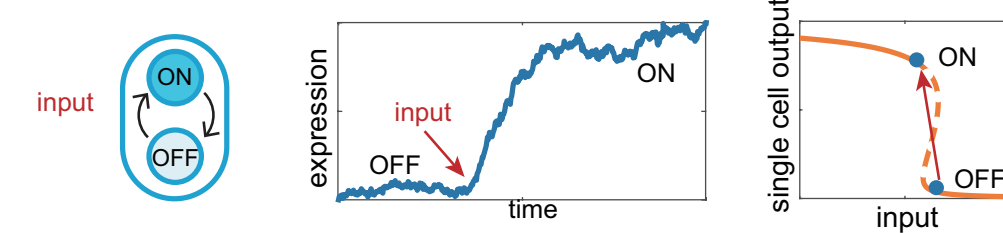
B   Population cell dynamics of multiple switches
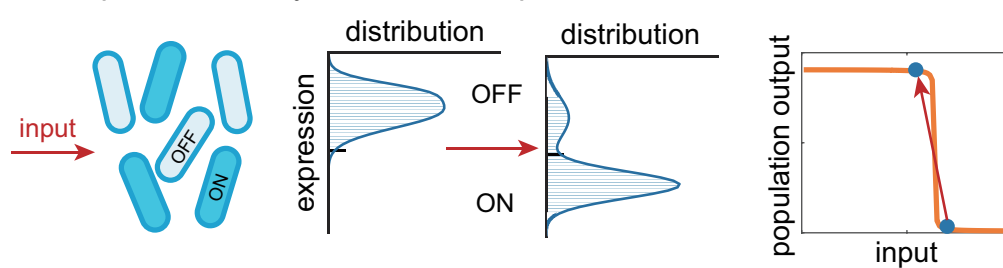
Figure 2.23: Schematic diagram of cells switching states in a population. (A) A single cell switch with bistable ON/OFF state. The state switching dynamics (middle) stimulated by an input corresponds to the transition between two stable states in the input-output mapping (right). (B) A population of cells with the switch circuit. The transition in expression distribution in the population (middle) stimulated by an input corresponds to the transition between two stable states in the input-output mapping at population-level (right).

ultrasensitve regime, the output y defined by the intersection always converges to a neighborhood of the transition threshold, even when the process is uncertain or perturbed by disturbances (gray area). The ability to tune the threshold externally is analogous to setting the reference of the desired output.

Ultrasensitivity can be viewed as a 'high-gain' mechanism that makes it possible to achieve quasi-integral behavior (Cuba Samaniego and Franco, 2018). An important advantage of the concept of ultrasensitive controller is that it points to the individual roles of reference (threshold of the controller) and gain (slope of the controller) in a biological context. Yet it may require large production rates of transcription and translation, and cells become burdened and stressed as a consequence. Therefore, it is important to find biological designs that achieve ultransensitive input-output functions without relying on drastic up-regulation of gene expression in individual cells.

We notice that a bistable switch circuit enables ON/OFF states with high/low gene expression in single cells, as shown in Figure 2.23A. The hysteresis can generate a

sharp switch in its input-output mapping. With a small stimulating input, a single cell can switch from ON to OFF state or vice versa. In a population operating as multiple single cells in parallel illustrated in Figure 2.23B, we can consider there are multiple bistable switches in parallel. Cells may exhibit a bimodal distribution in expression due to random initial conditions and stochastic switching dynamics, and the small input turning cells into ON or OFF state will reshape the distribution. As a result, the population-level gene expression by exploiting the sum of heterogeneous states of individual cells is also sharply tuned by the small input. Therefore, when characterizing the input-output mapping at population-level, we expect to obtain an ultrasensitive response.

As illustrated in Figure 2.22B, it is important that the closed loop steady state lies in the neighborhood of the ultrasensitive region and is stable when combining the process and the controller. Comparing the single cell and population-level input-output mappings in Figure 2.23, we notice that each single cell only has two stable ON/OFF states out of the ultrasensitive regime and one unstable intermediate state in the ultrasensitive regime. Yet it is possible to stabilize the total population-level output in the ultrasensitive regime. Even when single cells exhibit oscillatory expression, the total population-level expression can average out the fluctuation and achieve a stable output.

In addition to the ultrasensitive response in the controller, it is necessary to design a mechanism to sense the total output, to coordinate switches in individual cells in a closed loop system. We suggest that cell-cell signaling systems can be used to close the loop between the population-level process and the controller. Cell-cell signaling molecules are secreted by all cells, forming a global measurement of population-level output and further activating downstream gene expression in cells. With this approach, bistable switch circuits mediated by cell-cell signaling systems can be used as an ultrasensitive feedback controller at population-level.

Regulation network structures

Bistable genetic switch usually requires direct or indirect positive feedback loops, such as self-activation and mutual inhibition (Gardner, Cantor, and Collins, 2000; Ajo-Franklin et al., 2007; Y. Chen et al., 2015). Here, we show biological designs with different bistable switch mechanisms to realize ultrasensitive feedback control of population-level gene expression.

We consider the control goal is to maintain a robust expression of a target gene Y in a

population. In a population of N cells, the concentration of Y in the ith cell is denoted by y_i. We define the total expression in the population as the sum of individual cells, denoted by y, where $y = \sum_{i=1}^{N} y_i$. In this section, we will use capital letters to indicate chemical species, lower case letters to denote the corresponding concentration, and the subscript i to denote the species or corresponding concentration in the ith cell. According to the analysis of intracellular and extracellular concentrations of fast diffusible signaling molecules in equations (2.13)-(2.17), we use the same variable S for the signaling molecule, and s for its concentration.

Self-activation with signal induced degradation

Self-activating genes that trigger their own expression can generate bistability through an auto-feedback (Ajo-Franklin et al., 2007; Hermsen, Erickson, and Hwa, 2011). We propose that a self-activator combined with signaling molecules that induce its degradation can form a closed loop system with population-level ultra-sensitive control. The circuit schematic is shown in Figure 2.24A.

In the ith cell, the self-activating transcription factor X_i also activates expression of the target gene Y_i and the signaling molecule S. The signaling molecule S measures the target gene expression across the population and can induce the degradation of X_i to negatively regulate Y_i expression. We list the chemical reactions in the population, for $i = 1, 2, ..., N$:

$$
\begin{array}{llll}
\text{basal production:} & \emptyset \xrightarrow{\alpha} X_i, & \text{self-activation:} & \emptyset \xrightarrow{\theta u_i} X_i, \\
\text{induced degradation:} & X_i + S \xrightarrow{\gamma} S, & \text{cellular dilution:} & X_i \xrightarrow{\delta} \emptyset, \\
\text{target production:} & \emptyset \xrightarrow{\rho u_i} Y_i, & \text{cellular dilution:} & Y_i \xrightarrow{\delta} \emptyset, \\
\text{signal production:} & \emptyset \xrightarrow{\sum \rho u_i} S, & \text{external dilution:} & S \xrightarrow{\delta} \emptyset,
\end{array}
\tag{2.64}
$$
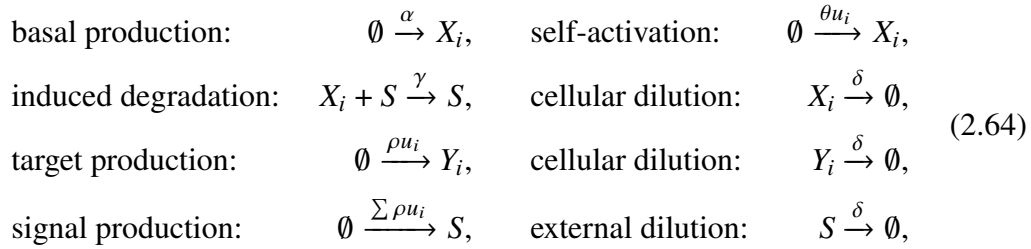
where $u_i = \frac{x_i^n}{K_x^n + x_i^n}$. This results in an ODE model:

$$
\begin{array}{ll}
\text{transcription factor:} & \dfrac{\mathrm{d}x_i}{\mathrm{d}t} = \alpha + \theta \dfrac{x_i^n}{K_x^n + x_i^n} - \gamma x_i s - \delta x_i, \\[3mm]
\text{target gene:} & \dfrac{\mathrm{d}y_i}{\mathrm{d}t} = \rho \dfrac{x_i^n}{K_x^n + x_i^n} - \delta y_i, \\[3mm]
\text{signaling molecule:} & \dfrac{\mathrm{d}s}{\mathrm{d}t} = \sum_{i=1}^{N} \rho \dfrac{x_i^n}{K_x^n + x_i^n} - \delta s, \\[3mm]
\text{total target gene:} & \dfrac{\mathrm{d}y}{\mathrm{d}t} = \sum_{i=1}^{N} \dfrac{\mathrm{d}y_i}{\mathrm{d}t} = \sum_{i=1}^{N} \rho \dfrac{x_i^n}{K_x^n + x_i^n} - \delta y.
\end{array}
\tag{2.65}
$$

A Circuit of self-activation + signal induced degradation

B Bistable states of X_i

C Single cell I/O mapping

D Population I/O mapping
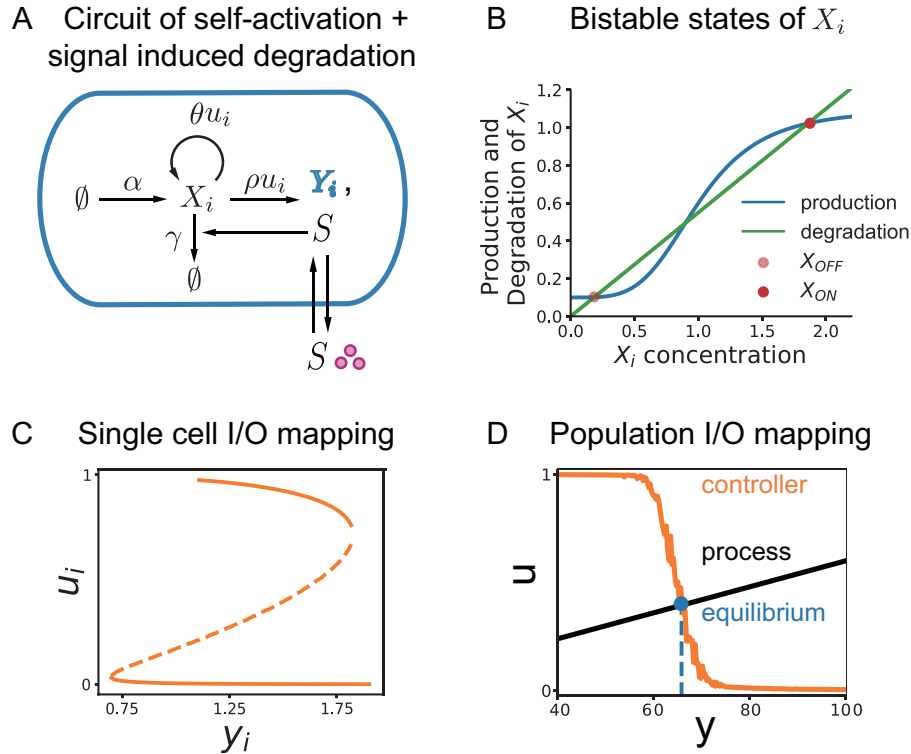
Figure 2.24: Schematic diagram of an ultrasensitive circuit of self-activation and signal induced degradation. (A) A circuit design based on a self-activating species that is induced by the signaling molecule to degrade. (B) The production and degradation curves that determine two stable states and one unstable state of X_i expression in a single cell. (C) The hysteresis in the single cell-level input-output mapping of the bistable switch. (D) The population-level input-output mappings of bistable switches in parallel (controller) and the target expression (process).

We demonstrate in Figure 2.24B that each single cell has two stable states in X_i expression given a fixed input of signaling molecule concentration s. In the closed loop, when the total target gene expression Y is perturbed, the signaling molecule concentration changes accordingly and alters the slope of the degradation curve. Therefore, cells switch to a different set of ON/OFF states in X_i expression with different potentials, leading to a new expression distribution to adapt to the disturbance in the target gene expression dynamics.

We first explore the input-output mapping of a single bistable switch. Note that u_i describes the Michaelis-Menten kinetics of Y_i production from X_i activation, and can be considered as the single cell-level controller output to actuate the expression process. We plot the steady state input-output mapping of a single bistable switch (y_i versus u_i) in Figure 2.24C, and the mapping shows hysteresis with an unstable

intermediate state.

Next, we define the population-level controller output to the population-level process:

$$u = \sum_{i=1}^{N} \frac{x_i^n}{K_x^n + x_i^n} = \sum_{i=1}^{N} u_i. \tag{2.66}$$

Based on a stochastic simulation of $N = 100$ cells, we plot the steady state input-output mapping of multiple bistable switches in parallel at population-level (y versus u) in Figure 2.24D. The mapping colored in orange exhibits a graded response of the population-level controller with an ultrasensitive regime in the target gene expression y.

To figure out the population-level expression in the closed loop, we need to find the intersection of input-output mappings of both the controller and the process. According to equation (2.65), we can obtain the steady state solution of the total target gene expression y by setting $\frac{dy}{dt} = 0$. By applying equation (2.66), we find a linear input-output mapping of the population-level process:

$$y = \frac{\rho}{\delta} u. \tag{2.67}$$

As shown in Figure 2.24D, the intersection of input-output mappings lies in the ultrasensitive region. Therefore, the population-level ultrasensitive controller ensures a small derivation in the desired expression of the target gene when there are disturbances and uncertainties in process dynamics.

Self-activation with sequestration and signal activation

Recent work has shown that sequestration with positive feedback is also sufficient to generate bistability despite the prevalence of cooperativity (Buchler and Cross, 2009; D. Chen and Arkin, 2012). We propose that a sequestration based bistable switch that consists of a self-activator and an anti-activator can be coupled with a signaling system for ultrasensitive feedback control. The circuit schematic is shown in Figure 2.25A.

In the ith cell, the self-activating transcription factor X_i also activates expression of the target gene Y_i and the sensing signaling molecule S. The signaling molecule S measures the target gene expression across the population and can activate an anti-activator Z_i that sequesters with the self-activator X_i. The sequestration provides nonlinear dynamics in X_i and Z_i, thus it generates bistable states without requiring cooperativity of in the self-activator, as shown in Figure 2.25B. We assume that

A   Circuit of self-activation with sequestration + signal activation

B   Bistable states of X_i

C   Single cell I/O mapping

D   Population I/O mapping
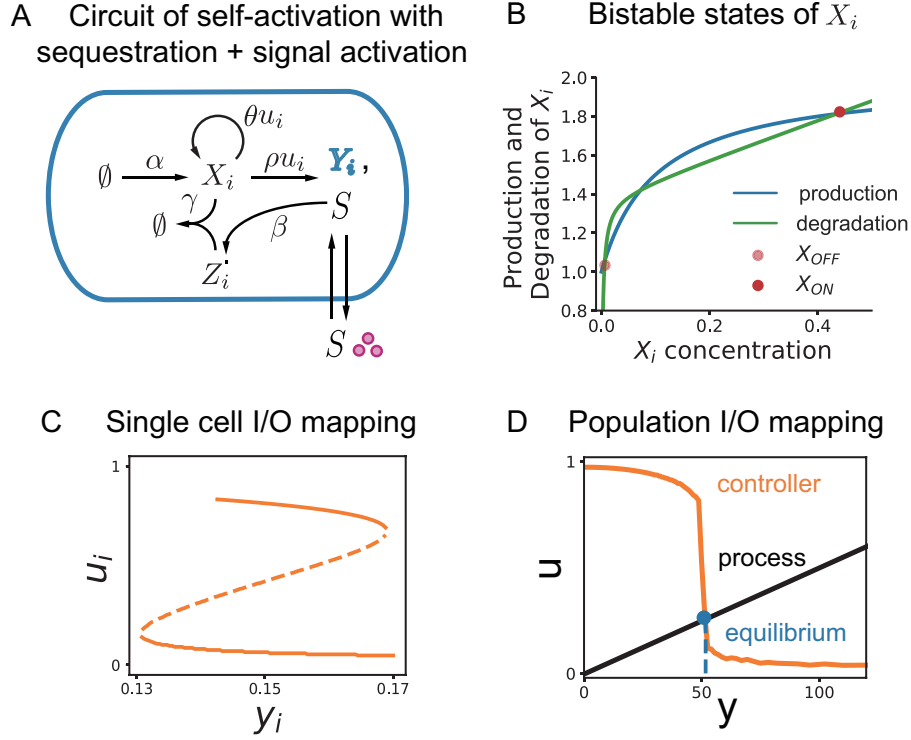
Figure 2.25: Schematic diagram of ultrasensitive circuit of self-activation with sequestration and signal activation. (A) A circuit design based on a self-activating species with a sequestering pair coupled with the signaling molecules. (B) The production and degradation curves that determine two stable states and one unstable state of X_i expression in a single cell. (C) The hysteresis in the single cell-level input-output mapping of the bistable switch. (D) The population-level input-output mappings of bistable switches in parallel (controller) and the target expression (process).

the sequestration is strong and the complex is stable enough to ignore the reverse reaction. We list the chemical reactions in the population, for $i = 1, 2, ..., N$:

$$\text{basal production:} \quad \emptyset \xrightarrow{\alpha} X_i, \qquad \text{self-activation:} \quad \emptyset \xrightarrow{\theta u_i} X_i,$$

$$\text{sequestration:} \quad X_i + Z_i \xrightarrow{\gamma} \emptyset, \qquad \text{cellular dilution:} \quad X_i \xrightarrow{\delta} \emptyset,$$

$$\text{anti-activator production:} \quad \emptyset \xrightarrow{\beta \frac{s^2}{K_s^2 + s^2}} Z_i, \qquad \text{cellular dilution:} \quad Z_i \xrightarrow{\delta} \emptyset,$$

$$\text{target production:} \quad \emptyset \xrightarrow{\rho u_i} Y_i, \qquad \text{cellular dilution:} \quad Y_i \xrightarrow{\delta} \emptyset,$$

$$\text{signal production:} \quad \emptyset \xrightarrow{\sum \rho u_i} S, \qquad \text{external dilution:} \quad S \xrightarrow{\delta} \emptyset,$$

$$\tag{2.68}$$
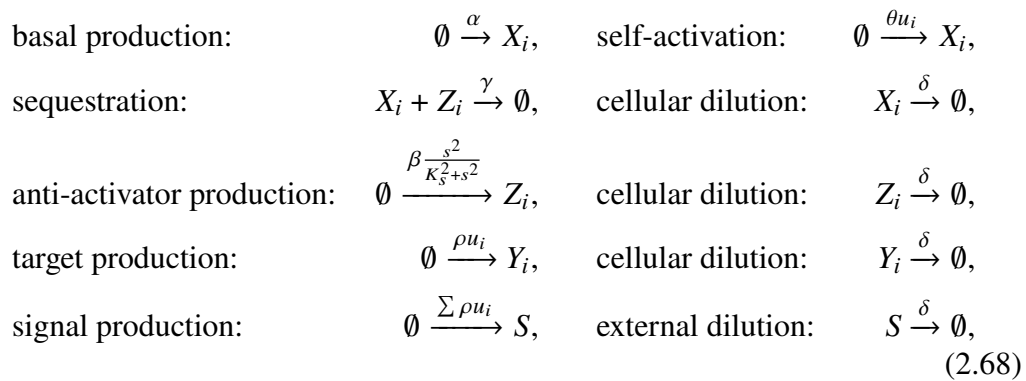
where $u_i = \frac{x_i}{K_x + x_i}$. This results in an ODE model:

$$
\begin{aligned}
\text{self-activator:} \quad & \frac{\mathrm{d}x_i}{\mathrm{d}t} = \alpha + \theta \frac{x_i}{K_x + x_i} - \gamma x_i z_i - \delta x_i, \\
\text{anti-activator:} \quad & \frac{\mathrm{d}z_i}{\mathrm{d}t} = \beta \frac{s^2}{K_s^2 + s^2} - \gamma x_i z_i - \delta z_i, \\
\text{target gene:} \quad & \frac{\mathrm{d}y_i}{\mathrm{d}t} = \rho \frac{x_i}{K_x + x_i} - \delta y_i, \\
\text{signaling molecule:} \quad & \frac{\mathrm{d}s}{\mathrm{d}t} = \sum_{i=1}^{N} \rho \frac{x_i}{K_x + x_i} - \delta s, \\
\text{total target gene:} \quad & \frac{\mathrm{d}y}{\mathrm{d}t} = \sum_{i=1}^{N} \frac{\mathrm{d}y_i}{\mathrm{d}t} = \sum_{i=1}^{N} \rho \frac{x_i}{K_x^n + x_i} - \delta y.
\end{aligned}
\tag{2.69}
$$

Similarly to equations (2.66) and (2.67), we define the population-level controller output u as the sum of single cell-level output u_i, and find the linear input-output mapping of the population-level process:

$$
\begin{aligned}
u &= \sum_{i=1}^{N} \frac{x_i}{K_x + x_i} = \sum_{i=1}^{N} u_i, \\
y &= \frac{\rho}{\delta} u.
\end{aligned}
\tag{2.70}
$$

We plot steady state input-output mapping of the controller at single cell-level (y_i versus u_i) in Figure 2.25C, and find that it exhibits hysteresis. Meanwhile, the population-level mappings show ultrasensitivity in the controller response, leading to a robust closed loop steady state of population-level expression y.

Mutual inhibition with signal inhibition

The toggle switch is a well-characterized bistable circuit that involves mutual inhibition of two species (Gardner, Cantor, and Collins, 2000). We couple the signaling molecule dynamics with the mutual inhibition species and demonstrate that the population-level controller exhibits an ultrasensitive response. The circuit is illustrated in Figure 2.26A.

In the ith cell, transcription factors X_i and Z_i inhibit each other's expression. X_i also inhibits the target gene Y_i and the sensing signaling molecule S. The signaling molecule S measures the target gene expression across the population and can inhibit Z_i. The mutual inhibition generates bistable states: high X_i and low Z_i concentration or low X_i and high Z_i concentration. We list the chemical reactions in the population,

A   Circuit of mutual inhibition
     + signal inhibition

B   Bistable states of X_i

C   Single cell I/O mapping

D   Population I/O mapping
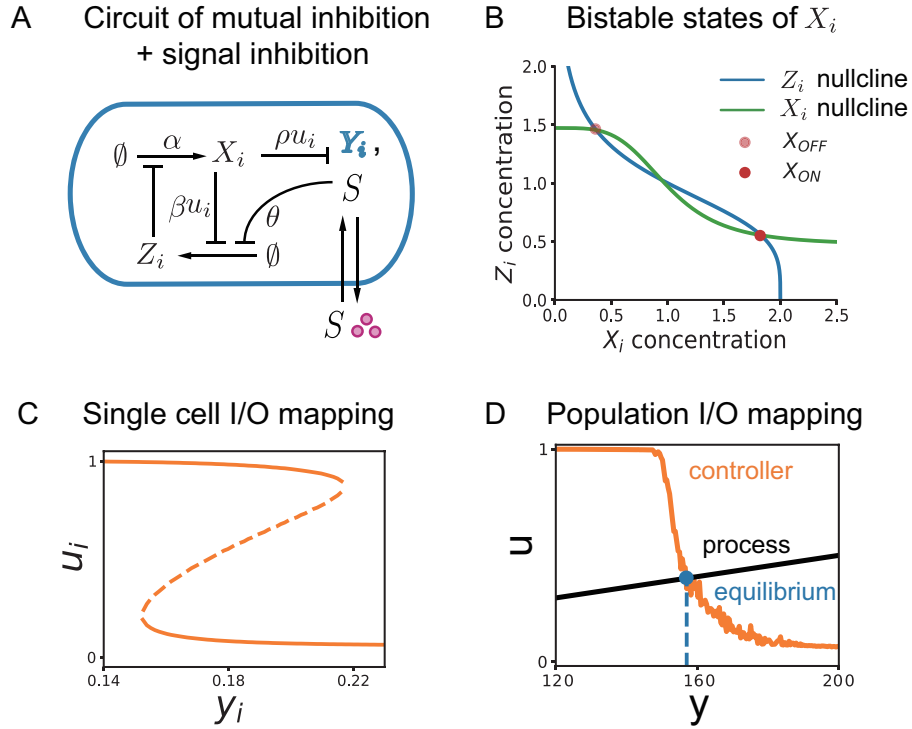
Figure 2.26: Schematic diagram of ultrasensitive circuit of mutual inhibiton and signal inhibition. (A) A circuit design based on a mutual inhibiting species and signaling molecules. (B) The nullclines of X_i and Z_i that determine two stable states and one unstable state of expression in a single cell. (C) The hysteresis in the single cell-level input-output mapping of the bistable switch. (D) The population-level input-output mappings of bistable switches in parallel (controller) and the target expression (process).

for $i = 1, 2, ..., N$:

X_i production: $\emptyset \xrightarrow{\alpha \frac{K_z^n}{K_z^n + z_i^n}} X_i$,   cellular dilution: $X_i \xrightarrow{\delta} \emptyset$,

Z_i production: $\emptyset \xrightarrow{\beta u_i} Z_i$, $\emptyset \xrightarrow{\theta \frac{K_s^2}{K_s^2 + s^2}} Z_i$,   cellular dilution: $Z_i \xrightarrow{\delta} \emptyset$,

target production: $\emptyset \xrightarrow{\rho u_i} Y_i$,   cellular dilution: $Y_i \xrightarrow{\delta} \emptyset$,

signal production: $\emptyset \xrightarrow{\sum \rho u_i} S$,   external dilution: $S \xrightarrow{\delta} \emptyset$,

$$(2.71)$$
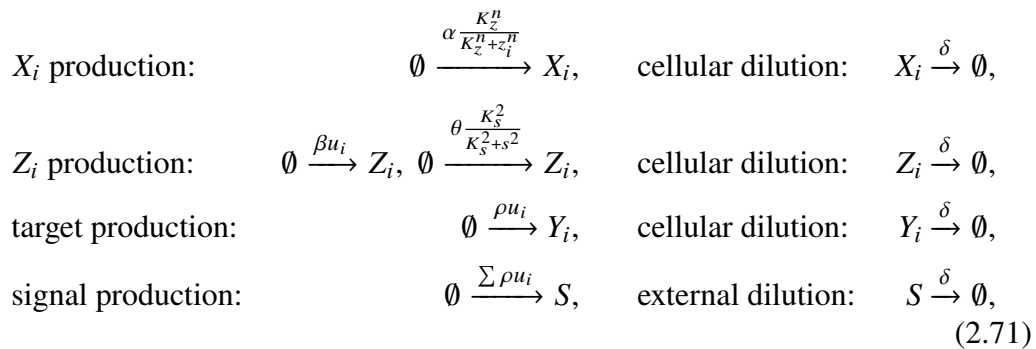
where $u_i = \frac{K_x^n}{K_x^n + x_i^n}$. This results in an ODE model:

$$
\begin{aligned}
\text{inhibitor } X_i: \quad & \frac{dx_i}{dt} = \alpha \frac{K_z^n}{K_z^n + z_i^n} - \delta x_i, \\[1em]
\text{inhibitor } Z_i: \quad & \frac{dz_i}{dt} = \beta \frac{K_x^n}{K_x^n + x_i^n} + \theta \frac{K_s^2}{K_s^2 + s^2} - \delta z_i, \\[1em]
\text{target gene:} \quad & \frac{dy_i}{dt} = \rho \frac{K_x^n}{K_x^n + x_i^n} - \delta y_i, \\[1em]
\text{signaling molecule:} \quad & \frac{ds}{dt} = \sum_{i=1}^{N} \rho \frac{K_x^n}{K_x^n + x_i^n} - \delta s, \\[1em]
\text{total target gene:} \quad & \frac{dy}{dt} = \sum_{i=1}^{N} \frac{dy_i}{dt} = \sum_{i=1}^{N} \rho \frac{K_x^n}{K_x^n + x_i^n} - \delta y.
\end{aligned}
\tag{2.72}
$$

We plot nullclines of X_i and Z_i given a fixed signaling molecule concentration in Figure 2.25B. Intersections of nullclines determine two stable states corresponding to (X_{ON}, Z_{OFF}) and (X_{OFF}, Z_{ON}) with distinct gene expression.

Similarly to equations (2.66) and (2.67), we define the population-level controller output u as the sum of single cell-level output u_i, and find the linear input-output mapping of the population-level process:

$$
\begin{aligned}
u &= \sum_{i=1}^{N} \frac{K_x^n}{K_x^n + x_i^n} = \sum_{i=1}^{N} u_i, \\[1em]
y &= \frac{\rho}{\delta} u.
\end{aligned}
\tag{2.73}
$$

We plot steady state input-output mapping of the controller at single cell-level (y_i versus u_i) in Figure 2.26C, and find that it exhibits hysteresis. Meanwhile, the population-level mappings show ultrasensitivity in the controller response, leading to a robust closed loop steady state of population-level expression y.

Population dosage control

Following the design principles of bistable switch-based feedback, we propose a synthetic circuit for robust dosage control in an *Escherichia coli* population as an example. Potential applications of engineered populations include releasing a constant amount of drugs into the gut or producing a certain level of metabolites for balanced fluxes in biochemical production, where the global dosage needs to be tightly controlled (Venayak et al., 2015; Charbonneau et al., 2020)..

For simplicity, we consider the desired population-level output is the concentration of the quorum sensing signal AHL. As shown in Figure 2.27A, we adopt the

A Population level ultrasensitive feedback   B Sigma factor-based implementation
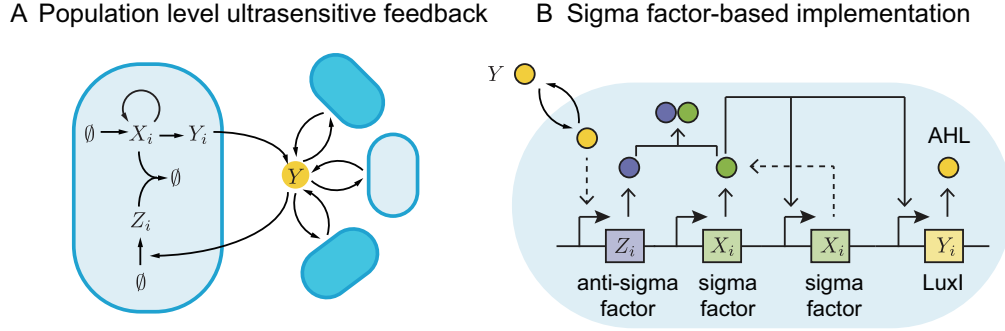

Figure 2.27: Schematic diagram of an ultrasensitive circuit for population dosage control. (A) The full circuit design with bistable switches and quorum sensing across the population. (B) A synthetic circuit implementation using sigma and anti-sigma factors and quorum sensing molecules Lux-AHL.

sequestration-based switch and link the output Y to the activation of Z_i, forming a negative feedback loop. A synthetic circuit implementation is also proposed in Figure 2.27B. We suggest that a sigma factor activates itself and an enzyme LuxI that catalyzes the synthesis of a quorum sensing signaling molecule AHL. The signaling molecule diffuses across cell membranes and activates an anti-sigma factor that can sequester the sigma factor and form an inactive complex. There is another inducible production of the sigma factor, which can be used to set references by external inducers.

We assume the AHL concentration is proportional to the concentration of the enzyme LuxI. Assuming the AHL concentration reaches quasi-steady state with fast diffusion, we do not specify the intracellular and extracellular concentrations. We also assume that AHL molecules activate the anti-sigma factor following a Hill-type kinetics. Then we write down the model of the closed loop of N cells, for $i = 1 : N$:

$$\text{sigma factor:} \qquad \frac{\mathrm{d}x_i}{\mathrm{d}t} = \alpha + \theta \frac{x_i}{x_i + K} - \gamma x_i z_i - \delta x_i,$$

$$\text{anti-sigma factor:} \quad \frac{\mathrm{d}z_i}{\mathrm{d}t} = \beta \frac{y^2}{y^2 + K_y^2} - \gamma x_i z_i - \delta z_i, \qquad (2.74)$$

$$\text{target AHL:} \qquad \frac{\mathrm{d}y}{\mathrm{d}t} = \sum_{i=1}^{N} \rho \frac{x_i}{x_i + K} - \delta_y y.$$

We first test if the population-level output y can achieve the desired dosage concentration by tracking different references. The references are set by the external induction of X production, represented by the parameter α in the model. We set three different references by increasing values of α. We run a stochastic simu-
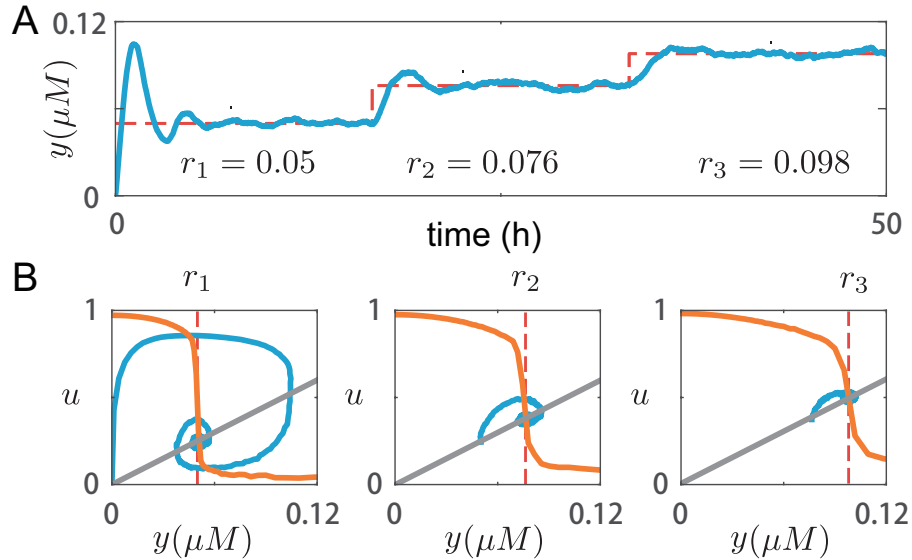
Figure 2.28: Simulation of reference tracking for population dosage control. (A) The population-level output tracking three different references in the closed-loop system. (B) Tracking trajectories (blue line) that converge towards the equilibrium determined by the intersection of the controller's input-output mapping (orange line) and the process's (gray line) input-output mapping.

lation of $N = 100$ cells in parallel and plot the time trajectory in Figure 2.28A. The population-level output y (blue line) closely tracks each reference (dashed red line). Figure 2.28B shows input-output mappings of the population-level process and the controller under corresponding reference. The process (gray line) shows a linear input-output mapping and the controller (orange line) exhibits an ultrasensitive input-output response. The threshold of the controller's input-output map is moved towards the right when α is set with a larger value. We find that the closed-loop trajectory of y (blue line) indeed converges to the intersection of input-output mappings of the process and the controller. The equilibrium determined by the intersection falls in the neighborhood of the threshold, which is consistent with the previous analysis of the controller.

Next, we test if the closed loop system can adapt to disturbances in the process dynamics via the ultrasensitive controller. We consider step disturbances that perturb the production rate ρ and degradation and dilution rate δ_y of Y. In Figure 2.29A, the time trajectory shows that the population-level output can adapt to disturbances with very small errors. It is more clear in Figure 2.29B that the ultrasensitive controller ensures the output y to converge to the same concentration even with large changes in the process due to disturbances. The gray lines in the middle and
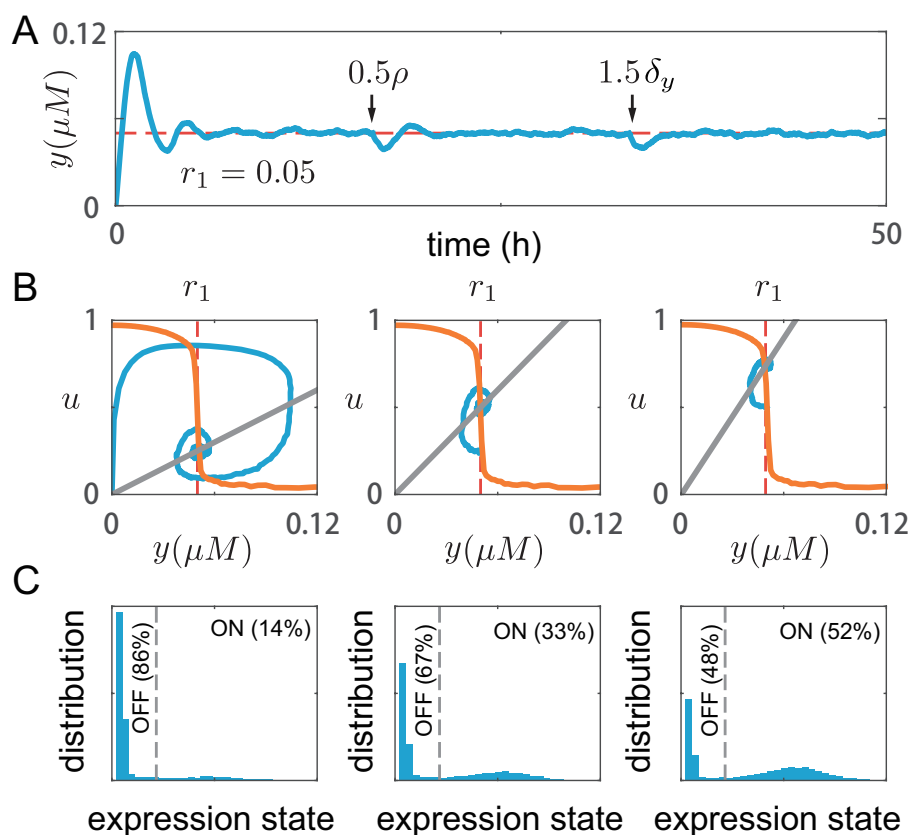
Figure 2.29: Simulation of disturbance rejection for population dosage control. (A) The adaptation of the closed-loop system when the process undergoes disturbances of a decreased production rate ρ and a increased of degradation and dilution rate ϕ. (B) Input-output mappings of the controller and the process. All intersections are within the ultrasensitive regime, so the trajectories all converge to the same output determined by the threshold. (C) The target expression distributions corresponding to three conditions. The adaptation is achieved at population-level by changing the phenotypical ratio of cells in ON and OFF states.

right panels illustrate how the process is disturbed with a smaller ρ and a larger δ_y, compared to the left panel. Moreover, if we look at the expression state distribution for each condition in Figure 2.29C, more cells switch to ON state to adapt to the disturbance, indicating the ON/OFF ratio change fulfills the ultrasensitive feedback at population-level.

In summary, with the sequestration-based bistable switch circuit and quorum sensing system, the population-level secretion of AHL molecules robustly tracks references that are set externally and adapts to disturbances in AHL production and dilution dynamics. In this circuit, we consider the quorum sensing signal AHL concentration as the target population output. More generally, any species dosage of interest can

be controlled by signal mediated bistable switch circuits proposed in Section 2.6.

Emergent population-level ultrasensitivity

From numerical analysis of potential circuit designs shown in Figure 2.24-2.26, we notice that at population-level, the input-output mappings of bistable switch circuits show emergent properties compared to single cell-level.

First, while individual switches only present two stable states (ON and OFF states) and one unstable state (intermediate state), the total population output exhibits a graded response to the input where all outputs admit a stable level. The output of multiple switches is considered as the sum of all single switches' states. Therefore, whenever a single bistable switch changes its state, the total output admits a new stable equilibrium. When the numbers of single switches in ON states and OFF states are not restricted, the total output can reach a larger range of stable equilibrium. As a result, in a population that consists of millions of cells, the extreme large number of bistable switches in parallel enables a smooth and graded response with stable outputs.

Second, multiple switches also generate an ultrasensitive input-output mapping at population-level. The ultrasensitivity emerges from the sharp transition in single switches,leading to a sharp transition between ON/OFF population ratio. To better understand how transition rates between ON and OFF states effect the ultrasensitive response, we consider a simple population-level model of multiple switches:

$$
\begin{aligned}
\text{ON cell population:} \quad & \frac{\mathrm{d}N_{on}}{\mathrm{d}t} = -f_+(y)N_{on} + f_-(y)N_{off}, \\
\text{OFF cell population:} \quad & \frac{\mathrm{d}N_{off}}{\mathrm{d}t} = -f_-(y)N_{off} + f_+(y)N_{on},
\end{aligned}
\tag{2.75}
$$

where $N = N_{on} + N_{off}$. Functions f_+ and f_- are transition rates from ON to OFF and vice versa that depend on the concentration of the target expression via signal molecules. Given a fixed y, we can solve for the population ratio of ON and OFF cells at steady state:

$$
\begin{aligned}
\text{ON cell ratio:} \quad & r_{on}(y) = \frac{N_{on}}{N} = \frac{f_-(y)}{f_+(y) + f_-(y)}, \\
\text{OFF cell ratio:} \quad & r_{off}(y) = \frac{N_{off}}{N} = \frac{f_+(y)}{f_+(y) + f_-(y)}.
\end{aligned}
\tag{2.76}
$$

We assume a bistable switch at ON state generates an output u_{on}, and at OFF state it generates an output u_{off}. Then we can derive the population-level control output
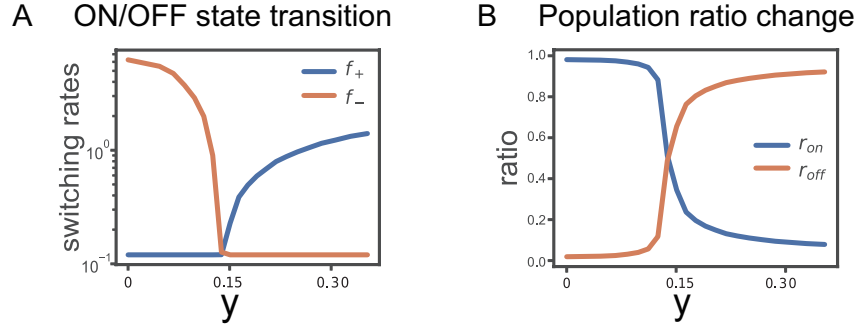
Figure 2.30: Simulation of ultrasensitive state transition rates and ratio change. (A) Simulation results of transition rates f_+ and f_- that depend on the population-level expression y. (B) Simulation results of the ON and OFF cell ratios r_{on} and r_{off} that depend on the population-level expression y.

u as the sum of single control outputs:

$$\begin{aligned} u &= N_{on}u_{on} + N_{off}u_{off} \\ &= \frac{f_-(y)u_{on} + f_+(y)u_{off}}{f_+(y) + f_-(y)}N. \end{aligned}$$

(2.77)

It shows that the population-level output u of bistable switches not only depends on the single cell-level outputs u_{on}, u_{off}, but also transition rates between states. We can find out in single cell-level input-output mappings that the outputs at either ON state or OFF state are not very sensible to s and have rather flat curves compared to the intermediate transition. Meanwhile, transition rates $f_-(y), f_+(y)$ can be very sensitive to y in bistable switches. In Figure 2.30A, we plot how transition rates depend on y from simulations of the sequestration-based switch circuit presented in Figure 2.25. Both transition rates show a sharp change when y is in the ultrasensitive regime, which explains why the population-level output u exhibits an ultrasensitive response.

We can also rewrite equation (2.77) with population ratios r_{on} and r_{off}:

$$u = \left(r_{on}(y)u_{on} + r_{off}(y)u_{off}\right)N.$$

(2.78)

It suggests that an ultrasensitive controller can be achieved by sharp population ratio changes. In other words, if $r_{on}(y), r_{off}(y)$ is ultrasensitive to y, the output u becomes ultrasensitive, which only appears at population-level. We show in Figure 2.30B that simulations of the ON and OFF population ratios indeed exhibit sharp changes. Such emergent properties further explains why bistable switch circuits can be used for ultrasensitive control at population-level.

Here, we demonstrate emergent ultrasensitivity with computations, yet more theoretical work is needed to understand what conditions guarantee an ultrasensitive response at population-level. We emphasize that heterogeneity at population-level means uniform gene expression is not needed in all cells, and state switching behaviors result in 'division of labor' and reduce burden in single cells. Follow-up work will examine specifically how our strategy can improve colony survival by burden reduction, resilience to stress, and stress-related mutations.

2.7 Layered control circuit design

Robust behaviors of cell populations depend on regulation across single cell-level to population-level since uncertainties and disturbances arise from diverse sources. Cells face uncertainties and disturbances from fluctuating environments externally, internal perturbations such as noises or stochasticity in cellular expression, and mutations that cause evolutionary perturbations. Developing design principles for robust behaviors in cell populations requires specifying what uncertainties and disturbances are non-trivial to cell population systems. Noises and stochasticity in gene expressions are usually small and local perturbations, yet all individual cells may undergo these perturbations and require fast adaptation at single cell-level. Meanwhile, adaptation to environmental disturbances and stress depends on collective response from all cells to reduce the impact and relieve the burden in a population.

In natural cell populations, many critical functions are under control of both intracellular and intercellular processes in face of diverse perturbations in cellular dynamics and from environments. For example, circadian clocks maintain robust rhythms by both intracellular regulation of core loop and secondary loops, and cell-cell interactions via intercellular signals (Hogenesch and Herzog, 2011). Robust progression through the cell cycle also has been shown to be driven by bistable switches promoted by cell-cell contact and mitogenic signaling globally (Stallaert et al., 2019).

These observations suggest that layered control of single cell-level and population-level can improve robustness to various uncertainties and disturbances. As illustrated in Figure 2.31A, the single cell-level feedback controller determines each individual cell's adaptive response to cellular noises and stochastic fluctuations w_i fast and accurately. The population-level feedback controller coordinates heterogeneous phenotypes in face of environmental disturbances w. Therefore in synthetic circuit
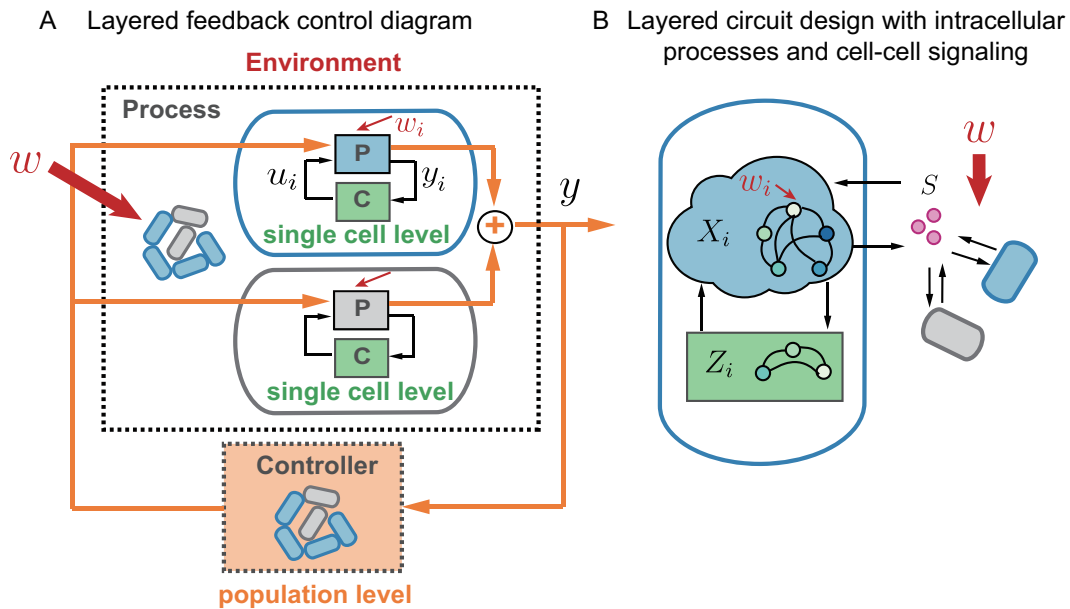
Figure 2.31: Schematic diagram of layered feedback control. (A) Block diagram of a layered feedback control system in a cell population. Each single cell has a local and intracellular feedback controller (balck arrows) and all cells are coordinated as a population-level feedback control system (orange arrows). (B) Circuit design of a layered feedback controller using intracellular gene regulation with control species Z and cell-cell signaling molecules S.

design, controllers via both intracellular processes and cell-cell signaling systems form the layered feedback, as shown in Figure 2.31B.

In Section 2.2 and 2.3, we introduced single cell-level control and population-level control separately, and demonstrated how cell populations with these control circuits adapt to environmental disturbances. Here, we show that by combining single cell-level and population-level controllers, cell populations with such layer structured control circuits exhibit more robust behaviors with higher fitness.

Population dosage and cellular expression control

We consider the population dosage control problem proposed in Section 2.6. The bistable switch circuit mediated by signaling molecules performs as an ultrasensitive population-level controller and maintains a robust overall dosage of the target chemical. The population-level controller enables robust adaptation to environmental disturbances that perturb the target chemical production. In extreme cases when severe stress occurs to some cells and turns off the cellular expression, signaling molecules can coordinate other cells to switch to ON state to maintain a constant
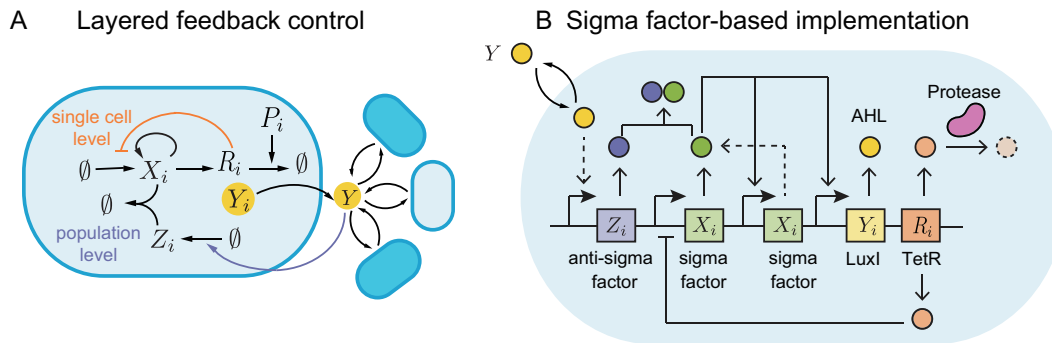
Figure 2.32: Schematic diagram of a layered feedback circuit for population dosage and cellular expression control. (A) The full circuit design with a bistable switching based feedback with signaling molecules at population-level and a single cell-level feedback using enzymatic degradation mechanism. (B) A synthetic circuit implementation using sigma and anti-sigma factors, quorum sensing molecules Lux-AHL and a protease.

overall dosage.

However, the population-level controller only guarantees robust overall dosage by inducing over-expression in other cells. It may be detrimental to these cells since higher expression without regulation can cause much burden and become disadvantageous to their fitness. Thus, a single cell-level controller can set a reasonable high expression level for ON state cells when coupled with the population-level control circuit. In addition, cellular gene expression can be noisy and stochastic, resulting in small but constant local perturbations to all cells. single cell-level controller can provide a fast and accurate response that adapts to these intracellular perturbations without the going through the population-level feedback with global response.

Here, we add a single cell-level integral feedback controller to the bistable switch-based population-level control circuit. As illustrated in Figure 2.32A, besides the sequestering pair X_i, Z_i and the signaling molecule Y that fulfills a feedback control at population-level, there is an intracellular feedback loop. A transcription factor R_i is activated by X_i and further represses X_i production, forming a negative feedback. R_i is actively degraded by a constitutive protease P_i. When the cell exhibits ON state with high X_i concentration, R_i is also at high concentration so the degradation of R_i is saturated by the protease. With saturated degradation, R_i performs as an approximate integral controller that steers X_i concentration to a constant value in ON cells despite cellular noises. Therefore, the population-level controller ensures robust overall dosage while the single cell-level controller guarantees robust expression in

ON cells. A implementation of the layered feedback control circuit is shown in Figure 2.31B.

We model the layered circuit in a population of N cells by ODEs, for $i = 1, 2, ..., N$:

$$\text{sigma factor:} \quad \frac{\mathrm{d}x_i}{\mathrm{d}t} = \alpha\frac{r_i^2}{r_i^2 + K_r^2} + \theta\frac{x_i}{x_i + K} - \gamma x_i z_i - \delta x_i,$$

$$\text{anti-sigma factor:} \quad \frac{\mathrm{d}z_i}{\mathrm{d}t} = \beta\frac{y^2}{y^2 + K_y^2} - \gamma x_i z_i - \delta z_i,$$

$$\text{repressor TetR:} \quad \frac{\mathrm{d}r_i}{\mathrm{d}t} = \phi\frac{x_i}{x_i + K} - \eta\frac{r_i}{r_i + K_{rp}}p_i - \delta r_i,$$

$$\text{target AHL:} \quad \frac{\mathrm{d}y}{\mathrm{d}t} = \sum_{i=1}^{N}\rho\frac{x_i}{x_i + K} - \delta_y y,$$

(2.79)

where p_i represents the protease concentration. We assume the protease has a constant concentration. Note that we use Michaelis-Menten kinetics with dissociation rate K_{rp} to describe the degradation of TetR in a more general condition. When cells are in ON state and express a high concentration of TetR, i.e., $r_i \gg K_{rp}$, we can approximate TetR dynamics with saturated degradation:

$$\text{TetR in ON cells:} \quad \frac{\mathrm{d}r_i}{\mathrm{d}t} = \phi\frac{x_i}{x_i + K} - \eta p_i - \delta r_i. \tag{2.80}$$

We can further find that equation (2.80) implies an approximate integral controller on x_i when δ is negligible:

$$r_i(t') \approx \rho \int_0^{t'}\left(\frac{x_i(t)}{x_i(t) + K} - \frac{\eta}{\phi}p_i\right)\mathrm{d}t. \tag{2.81}$$

It suggests that in ON state cells, X_i concentration is expected to converge to a constant set-point value determined by η, ϕ and p_i instead of over-expression.

Now we test the robustness performance of the layered feedback control circuit in face of both cellular noises and severe environmental disturbances. We consider intracellular species have fluctuating dilution rate δ in all cells, meanwhile a partial cell population are stressed to stay in OFF state without normal production of X_i nor target chemical Y by an environmental disturbance. We first simulate $N = 100$ cells dynamics with only population-level controller, and show population-level output Y concentration, single cell trajectories of X_i concentration and corresponding distribution of expression state in Figure 2.33. At time 20h, we induce a small perturbation in all cells' dilution rate δ. Even though the total population output is almost not affected, single trajectories show an increase in X_i concentration in all

Figure 2.33: Simulation of the population-level feedback circuit under diverse disturbances. (A) The adaptation of population-level expression when the process undergoes disturbances of a decreased dilution rate δ and a 50% fraction of cells being turned to OFF state. (B) Single cell trajectories of expression. (C) The target expression distributions corresponding to three conditions. The adaptation is achieved at population-level by changing the phenotypical ratio of cells in ON and OFF states and over-expression in ON cells.

cells, leading to a ON peak with higher X expression in the distribution. At time 40h, we turn off 50% of the population by setting their production rate $\theta = 0$ to mimic an environmental stress. Single trajectories show an increase in both ON state cell fraction and X_i concentration so that the population-level output y can maintain a robust concentration. With population-level control, only the total output y is robust yet single cells become more fragile with over-expression.

With the layered feedback control, we show in Figure 2.34 that the population-level output y can adapt to disturbances while the cell's intracellular expression has a robust ON state. Figure 2.34B and C demonstrate that the ON state cells always exhibit a constant expression level of X concentration with a smaller variance under
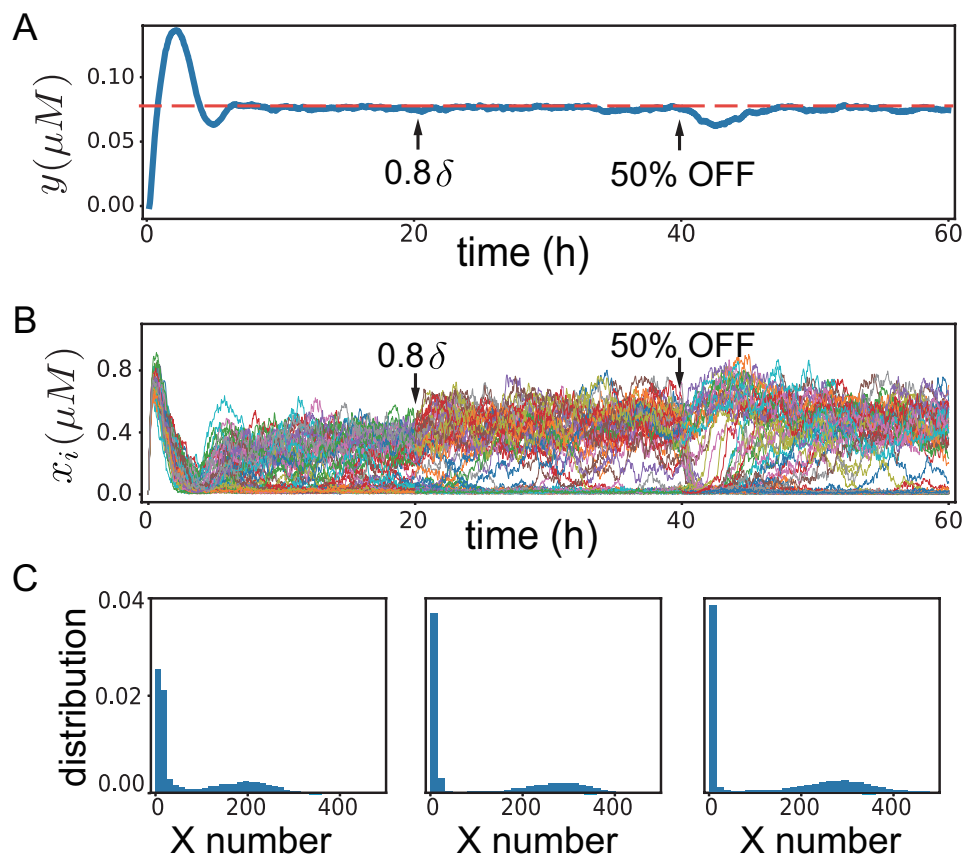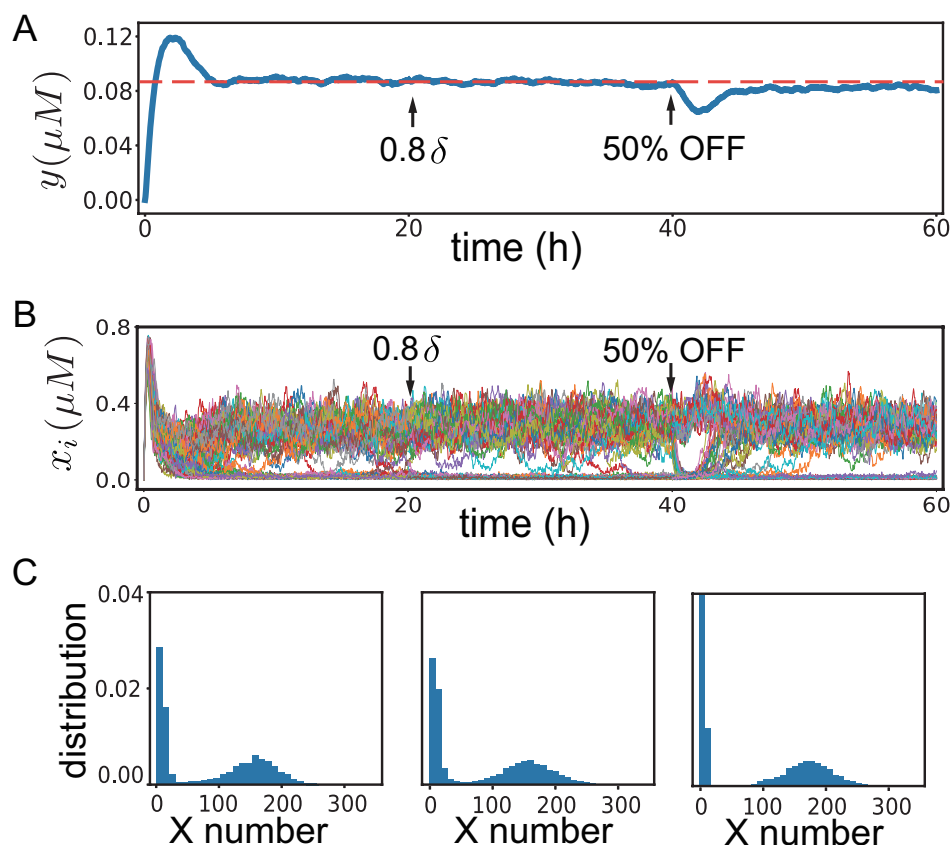
Figure 2.34: Simulation of the layered feedback circuit under diverse disturbances. (A) The adaptation of population-level expression when the process undergoes disturbances of a decreased dilution rate δ and a 50% fraction of cells being turned to OFF state. (B) Single cell trajectories of expression. (C) The target expression distributions corresponding to three conditions. The adaptation is achieved at population-level by changing the phenotypical ratio of cells in ON and OFF states without over-expression in ON cells.

perturbations from intracellular noises and stochasticity or the environmental stress. Compared to only population-level control, the layered control structure are more robust to diverse disturbances and uncertainties at both single cell and population-level. It also helps avoiding over-expression in single cells. For example, when a strong environmental disturbance turns off 50% of the total population, the rest of the population adapts by switching more likely to ON state instead of producing higher concentration of X.

2.8 Discussion

In this chapter, we discuss design principles of synthetic circuits ensuring robust behaviors in cell populations. We emphasize that cell populations may face a wide

range of perturbations, including internal noises and stochasticity in gene expression and fluctuating environments and stress. Therefore, circuit design at single cell-level and population-level need to be carefully considered based on target functions and main sources of perturbations. We demonstrate that population-level control mediated by cell-cell signaling systems ensures more robust behaviors in heterogeneous populations compared to single cell-level control circuits. Specifically, we propose two population-level design principles that utilize cell-cell signaling molecules to achieve integral feedback or ultrasensitive feedback for robustness.

We notice that population-level robustness does not require single cell's robustness mechanism, and can even emerge from instability and fragility of single cells. The opposite is also true that single cell-level robustness cannot guarantee population-level robustness or may instead cause disadvantage in fitness and survival of the population. These observations from modeling and simulation of circuit examples agree with 'robust yet fragile' properties of many natural biological systems (Stelling et al., 2004), suggesting that multiple layers of controllers with distributed contribution to robustness may become a general design principle. We illustrate the concept of layered control of both single cell-level and population-level feedback in the population dosage control example, and show an improvement in adapting to local and internal perturbations as well as environmental stress.

In general, design of robust behaviors in cell populations faces theoretical challenges. Tradeoffs often exist where the controlled system is robust to some perturbations but fragile to others. Adding more layers of control may help improving the tradeoffs, but also leads to higher complexity, increased sources of perturbations and cost. We argue that future investigations should involve understanding of how layered control structures across single cell-level to population-level can be optimized for robustness and cost. Moreover, control circuits usually induce burden on cellular metabolism and impact a population's growth, where mutation becomes a critical source of perturbation to the population. Thus circuit design needs both single cell-level optimization to reduce the mutation rate such as sequence design or delay the selection by lowering gene expression load (Sleight et al., 2010; Ceroni, Boo, et al., 2018), and population-level regulation to avoid the growth advantages of mutant cells, for example, generating diverse phenotypes to compete with mutant populations (Zhou et al., 2015; Roell et al., 2019; Holland et al., 2014; Williams and Murray, 2019). In future studies, we hope to understand if cell-cell signaling-mediated state switching behaviors can be utilized to overcome mutation perturbations for more robust

population-level behaviors.

Chapter 3

DESIGN OF POPULATION INTERACTIONS IN WELL-MIXED ENVIRONMENTS

3.1   Motivation

Microbes form communities that include multiple cell species with complex interactions in natural environments such as soil, food and human gut (Fierer and Jackson, 2006; Gill et al., 2006). Compared to monocultures, multiple cell populations contain more diverse functionalities with promoted stability and robustness to fluctuations in environments (LaPara et al., 2002; Burmølle et al., 2006). Inspired by the enhanced performance of natural multicellular systems, researchers have started to engineer synthetic microbial consortia of multiple cell populations to achieve more complicated tasks (Balaban et al., 2004; Brenner, Karig, et al., 2007; Y. Chen et al., 2015; Kong et al., 2018).

Maintaining stable coexistence of multiple populations is a major challenge due to competitive exclusion. The competitive exclusion principle states that complete competitors cannot coexist upon limiting resources (Georgii Frantsevich Gause, 1932; Hardin, 1960). However, theoretical studies show that if there exist population interactions that depend on population densities and can impact cell growth, then a single resource can support coexistence in microbial consortia (Lobry and Harmand, 2006). Thus, designing proper population interactions that can support stable coexistence becomes the key question.

Cooperation and competition are fundamental population interactions that can shape population-level behaviors. Microbial consortia of cooperating cell populations have been shown to exhibit promoted biomass (Schink, 2002; Burmølle et al., 2006) and resilience to cheaters and invaders (Pande et al., 2016). Competition is another nonnegligible interaction since cells naturally compete for space and nutrients to survive. It also plays an important role in antibiotics warfare among multiple bacterial species (Clemente et al., 2015). Although population interactions have been studied for a long time, the contribution of cooperation and competition to consortia stability and functionality is an ongoing debate. Evidence in studies of cross-feeding and mutual removal of toxins show that stable and robust growth is more likely achieved in consortia based on cooperative interactions (Woyke et al.,

2006; Kato et al., 2008). On the contrary, there are also ecological studies of mixed cell populations indicating that stable coexistence of microbes is promoted when competition dominates the population interaction network and dampens other cooperative interactions (Foster and Bell, 2012; Coyte, Schluter, and Foster, 2015).

So far, the relationship between population interactions and stable coexistence remains unclear. From the theory side, it is hard to find a unified mechanistic model that characterizes diverse interaction mechanisms in microbial consortia, including metabolites exchange, antibiotics warfare by toxins, quorum sensing, and contact-based interactions. Commonly used phenomenological models, such as Lokta-Volterra equations, directly consider pairwise interactions where interaction kinetics are directly dependent on population densities. These pairwise models largely failed to predict population growth in consortia of more than three species (Levin, 1976; Tilman, 1987; Stanton, 2003). Even within two cell populations, pairwise models cannot characterize interactions achieved by different mechanisms of growth and death regulation with a mechanistic understanding (Momeni, Xie, and Shou, 2017).

From the experimental side, batch cultures and continuous cultures such as chemostats are common environments for laboratory research of microbial populations. Yet different culture conditions may result in opposite coexistence results of mixed cell populations. For example, fast growing cell populations are shown to exhibit strong dominance and outcompete other cell populations to extinction in continuous cultures with limiting nutrients (Tilman, 1977; Sommer, 1983; Passarge et al., 2006). In contrast, cell populations competing for limiting nutrients can coexistence in many batch culture experiments, since population growth dynamics are usually observed until stationary phase (Freilich et al., 2011; Kong et al., 2018; Y. Ram et al., 2019). Therefore, the conclusion of coexistence dependency on population interactions can be misleading without clarifying the specific environments (Balsa-Canto, Alonso-del-Real, and Querol, 2019).

To design synthetic microbial consortia with stable coexistence, we need to understand the role of the population interaction network topology, interaction mechanisms as well as culture environments in population growth dynamics.

In this chapter, we focus on population interactions that are mediated by chemicals, also called chemical-mediated interactions, in well-mixed environments. Chemical-mediated interactions are common in natural microbial communities (Burmølle et al., 2006; Kato et al., 2008) and widely used in engineering synthetic consortia (Y. Chen et al., 2015; Kong et al., 2018). In Section 3.2, we review the classical Lokta-

Volterra model and propose a more mechanistic model. The mechanistic model can capture dynamics of mediator chemicals as well as characterizing interactions based on mediator chemicals. In Section 3.3, we investigate why batch versus chemostat culture environments lead to opposite coexistence results using mathematical models. Results show that nutrient limitation and chemical accumulation are main reasons that batch cultures are less robust than chemostat cultures. Finally in Section 3.4, design principles of the interaction network topology and chemical mediation mechanisms are proposed that achieve stable coexistence in well-mixed environments.

3.2 Pairwise versus mechanistic models

Lotka-Volterra model

For a long time, the theoretical study of microbial cell-cell interactions have been based on pairwise modeling, such as Lotka-Volterra equations (Lotka, 1925; Volterra, 1926). The Lotka-Volterra model was first proposed to describe prey-predator systems and then generalized to resource competition of multiple species including microbial populations. In a batch environment of n cell populations with competitive interactions, the population density dynamics for $i = 1, 2, ..., n$ can be described by

$$\frac{dN_i}{dt} = N_i\left(\alpha_i - \sum_{j=1}^{n} \beta_{ji} N_j\right), \tag{3.1}$$

where α_i is the growth rate of the ith cell population and β_{ji} is the competition coefficient that describes how strongly the jth population inhibits the growth of the ith population. When modeling cell populations that competitively grow on a limited nutrient, the Lokta-Volterra model is commonly written in another form:

$$\frac{dN_i}{dt} = \alpha_i N_i\left(1 - \frac{\sum_{j=1}^{n} \eta_j N_j}{N_{\max}}\right). \tag{3.2}$$

The parameter $N_{\max}$ is interpreted as the total carrying capacity of cell population density. The parameter η_j describes the weight or proportion of the jth cell population in nutrient consumption and resource occupancy. In both equations (3.1) and (3.2), each cell population density either converges to an equilibrium $N_i^* = 0$ representing extinction or $N_i^* > 0$ corresponding to coexistence, based on parameters of growth rates and competition strengths.

The Lokta-Volterra model is phenomenological and does not refer to mechanisms of cell-cell interactions. In a single microbial population culture, the Lokta-Volterra

model can describe the exponential growth phase and population capping phenomena. By fitting the pairwise competition coefficients, we can also explain coexistence of two populations or oscillatory dynamics between prey and predator populations qualitatively as observed in natural systems. The Lokta-Volterra model is a useful conceptual tool for small systems given its simplicity.

However, it is impossible to derive a Lokta-Volterra model of more than two populations with only pairwise characterizations that are not from first principle. For example, when more than two species are competing for the same limiting nutrient, the interaction strengths among them cannot be simply considered as the sum of pairwise competition coefficients. Indirect interactions with more complicated kinetics are often hidden. Thus, the Lokta-Volterra model and pairwise modeling in general has very limited prediction and verification capacity in large-scale design of stable and coexisting microbial consortia. Moreover, in the Lokta-Volterra model, cell-cell interactions are assumed to be linearly dependent on population densities with pairwise coefficients. Such assumption does not have an explicit priority reason since the underlying mechanisms are not specified. For example, competitive consumption of a limiting nutrient and mutual killing by toxins are written in the same way in the Lokta-Volterra model, which is unrealistic since the two mechanisms lead to quite different dynamics in cell growth. Therefore, predictions from the Lokta-Volterra model are less helpful to guide the design and implementations of cell-cell interactions in synthetic populations.

Chemical-mediated interaction model

A more mechanistic class of models is based on characterization of specific interaction mechanisms (Niehaus et al., 2019). In microbial communities, chemical-mediated interactions are common, such as competitive nutrient uptake, mutual metabolites feeding, killing via antimicrobial toxins, quorum sensing systems, etc. Here, we focus on chemical-mediated interactions among cell populations, and investigate a mechanistic model that captures dynamics of both population growth and mediator chemicals.

The competition of limiting nutrients is one of the most well studied cell-cell interactions. A classical model of nutrient uptake and cell growth in a microbial population is the Monod equation (Monod, 1949), which has provided generally satisfactory fitting results to the single population growth data. Since the Monod model describes the cell growth and consumption dynamics of the nutrient, it can

be easily extended from monocultures to co-cultures of multiple populations. Other models such as the Haldane (Haldane, 1965; Andrews, 1968), Moser (Moser et al., 1958), and Contois models (Contois, 1959), are also developed based on the Monod model to describe population's growth kinetics upon nutrients (Muloiwa, Nyende-Byakika, and Dinka, 2020).

The general Monod model for the growth of n cell populations on a single nutrient M in a batch culture is given by

$$
\begin{aligned}
\text{ith cell population density:} \quad & \frac{\mathrm{d}N_i}{\mathrm{d}t} = \mu_i(M)N_i, \\
\text{limiting nutrient:} \quad & \frac{\mathrm{d}M}{\mathrm{d}t} = -\sum_{i=1}^{n} \frac{\mu_i(M)}{Y_i}N_i,
\end{aligned}
\tag{3.3}
$$

where the function $\mu_i(M)$ represents the growth rate of the ith cell population that depends on the nutrient M, and Y_i is called the yield coefficient representing the efficiency of the nutrient uptake. If we apply the Monod equation of growth kinetics where $\mu_i(M) = \alpha_i \frac{M}{K_i+M}$ and denote the nutrient uptake rate $\delta_i = \frac{\alpha_i}{Y_i}$, we can rewrite equation (3.3) as

$$
\begin{aligned}
\text{ith cell population density:} \quad & \frac{\mathrm{d}N_i}{\mathrm{d}t} = \alpha_i \frac{M}{K_i + M}N_i, \\
\text{limiting nutrient:} \quad & \frac{\mathrm{d}M}{\mathrm{d}t} = -\sum_{i=1}^{n} \delta_i \frac{M}{K_i + M}N_i.
\end{aligned}
\tag{3.4}
$$

We can interpret the parameter α_i as the maximum growth rate, K_i as the nutrient threshold that provides the half maximum growth of the ith cell population. With this model, we can easily characterize a single cell population's growth kinetics from monoculture data and predict the growth of the co-culture of n cell species. Compared with the Lotka-Volterra model, cell-cell competitive interactions are mechanistically characterized by nutrient uptake and growth dynamics instead of pairwise competition coefficients.

Similarly, we can also build general models of interactions where cell population's growth and death are mediated by chemicals. Figure 3.1A illustrates that n cell populations interact through chemicals in a well-mixed environment. The mediator chemicals can be considered either consumed by cells such as in metabolite feeding and degraded by cells such as antibiotics degraded by resistant cells (Shou, S. Ram, and Vilar, 2007; D'Onofrio et al., 2010; Mee et al., 2014), or accumulated in the environment such as quorum sensing molecules, digestive enzymes and toxins (Miller and Bassler, 2001; Scott and Hasty, 2016; Cavaliere et al., 2017). These chemicals
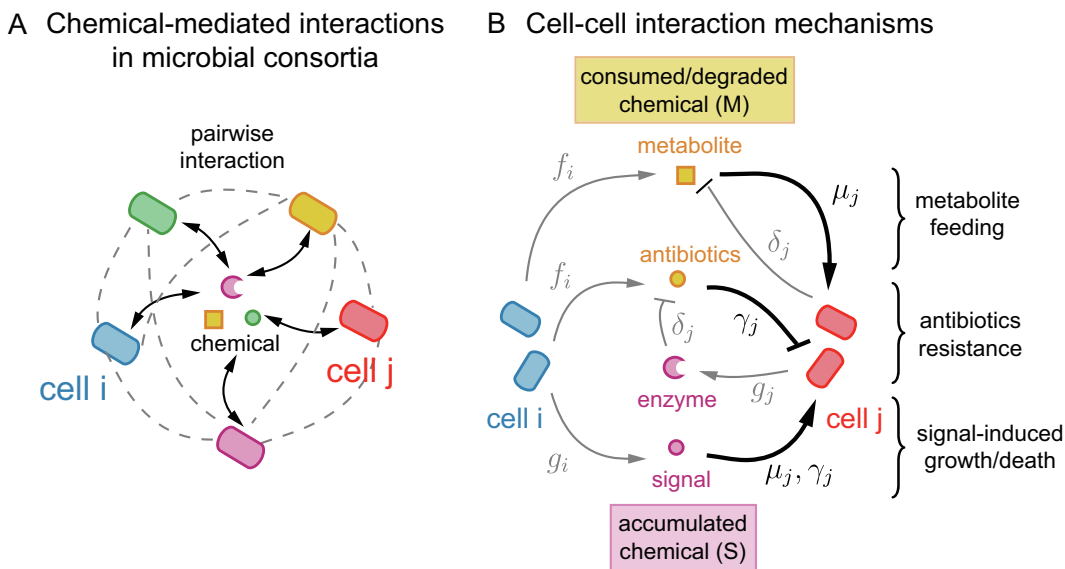
A Chemical-mediated interactions
in microbial consortia

B Cell-cell interaction mechanisms

Figure 3.1: Schematic diagram of chemical-meditated interactions. (A) Multiple cell populations that produce and sense chemicals to interact. Dashed lines between each pair of populations represent the pairwise interactions hidden in these mechanistic chemical-mediated interactions. (B) Specific interaction mechanisms of chemicals mediating cell growth/death dynamics between two cell populations. Black arrows represent chemicals modulating cells' growth or death. Grey arrows indicate that cells produce, consume, degrade or sense the chemicals.

can determine population's growth and death rates via more complicated biochemical reactions. Figure 3.1B illustrates these two types of consumed/degraded and accumulated mediator chemicals and interactions of diverse mechanisms between two cell populations.

To model the consortium of n populations with chemical mediated interactions, we denote the consumed or degraded chemical species by M and the accumulated species by S, and define functions $\mu_i(M, S)$, $\gamma_i(M, S)$ and $\delta_i(M, S)$ as the ith cell population's growth rate, death rate and consumption or degradation rate of M. More diverse interactions exist when these chemicals are produced and secreted by other cell populations. We assume that the production of M and S depend on each cell population density with rates $f_i(M, S)$ and $g_i(M, S)$. Note that these production rates may also depend on mediator chemicals. For example, consumption of nutrients provides more energy and machinery for chemical production; signaling molecules can induce transcription and translation for more chemical production. Therefore, the general model of n cell populations that interaction via chemicals M

and S becomes

ith cell population density: $\qquad \dfrac{\mathrm{d}N_i}{\mathrm{d}t} = (\mu_i(M,S) - \gamma_i(M,S))\, N_i,$

consumed or degraded chemical: $\qquad \dfrac{\mathrm{d}M}{\mathrm{d}t} = \displaystyle\sum_{i=1}^{n} f_i(M,S)N_i - \sum_{i=1}^{n} \delta_i(M,S)N_i,$

accumulated chemical: $\qquad \dfrac{\mathrm{d}S}{\mathrm{d}t} = \displaystyle\sum_{i=1}^{n} g_i(M,S)N_i.$

$$(3.5)$$

Note that the consumed or degraded chemical M has a different dynamics than the accumulated chemical S. Specifically, when chemicals M produced by the jth population induce inhibition or activation in the ith population growth, there is an extra negative feedback in M-mediated interaction strength because of the consumption or degradation of M by the ith population. Thus, it is unlikely to use the same kinetic model to capture these two types of interactions between the ith and jth populations as defined in the Lotka-Volterra model in equation (3.1).

In Figure 3.2A, we show a simple example where a cell population inhibits its own density via either a consumed or degraded chemical M and an accumulated chemical S that induces self-killing. We consider that the nutrient is not limiting and cells grow with a constant rate α and are killed by chemicals with a mass action kinetics with rate γ. Assuming the production and consumption/degradation of the chemical M is proportional to the population density with rate β_M and δ, we can write the model of the population and M chemical dynamics:

cell population density: $\qquad \dfrac{\mathrm{d}N}{\mathrm{d}t} = (\alpha - \gamma M)\, N,$

consumed or degraded chemical: $\qquad \dfrac{\mathrm{d}M}{\mathrm{d}t} = \beta_M N - \delta M N.$

$$(3.6)$$

Similarly, assuming the chemical S is produced by cells with a constant rate β_S, we can write the model of the population with the accumulated chemical-mediated interaction:

cell population density: $\qquad \dfrac{\mathrm{d}N}{\mathrm{d}t} = (\alpha - \gamma S)\, N,$

accumulated chemical: $\qquad \dfrac{\mathrm{d}S}{\mathrm{d}t} = \beta_S N.$

$$(3.7)$$

The cell population dynamics show significantly different results for these two chemical-mediated interactions, as shown in simulations in Figure 3.2B. With the consumed or degraded chemical M, the population density not only depends on its growth and death rates, but also the production and consumption/degradation rates of
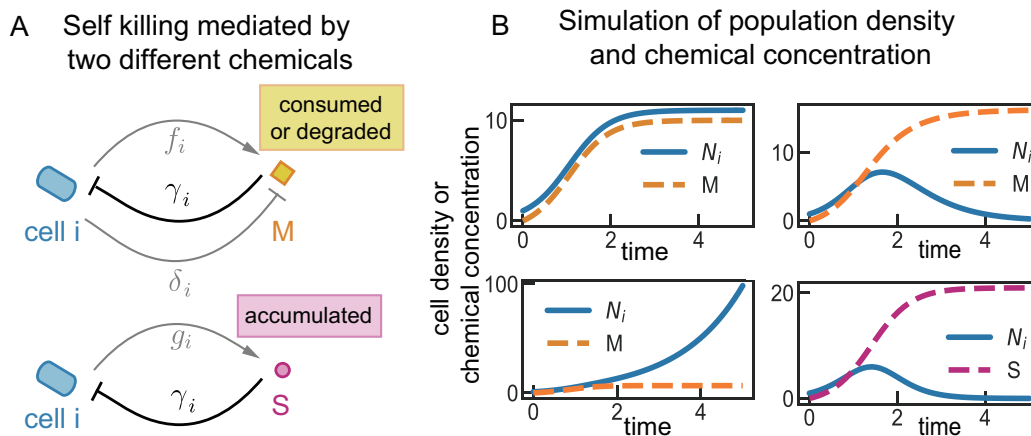
Figure 3.2: Simulation of a self-killing population via consumed/degraded and accumulated chemicals. (A) The same self-inhibition interaction with two types of mediator chemicals. (B) Simulations of population growth and chemical concentration of these two interaction mechanisms. The upper left, upper right and bottom left panels correspond to three different regimes of production and consumption/degradation rates of chemical M that lead to a constant density, zero density and an explosion in growth. The bottom right panel is the simulation of the accumulated chemical S.

the mediator M. When there is a balanced production and consumption/degradation of M, both the density and the chemical concentration reach a certain level (upper left). When there is a strong production and a weak consumption/degradation of M, the chemical concentration accumulates and kills all cells (upper right). When the production is weak and the consumption/degradation of M is strong, there leaves not enough chemical M to kill cells so the population keeps growing (bottom left). Meanwhile, the accumulated chemical S is constantly produced and accumulates, and eventually kills all cells (bottom right).

The results in this section suggest that the same interaction network implemented with different mechanisms may result in opposite growth dynamics. We will discuss detailed constraints on interactions based on these two types of chemicals to achieve stable coexistence in following sections.

3.3 Batch versus chemostat cultures

Batch culture has been a common method for characterizations of biological systems in synthetic biology because of the low cost and ease of operation. In batch cultures, microbial populations consume nutrients as they grow and enter stationary phase. Even though cells eventually die because of nutrients depletion and wastes

accumulation in batch cultures, stationary phase is often considered as the steady state of engineered populations where experimental observation stops. Therefore, theoretical studies of cell populations in batch cultures are based on models that characterize growth until stationary phase. Another common culture environment is the continuous culture, which provides a more static and controlled growth condition with diluted fresh medium. The balance between inflow and outflow of media enables specific growth rates and physiological states of cell populations. One main laboratory approach is chemostat where the nutrients are limited through a fixed dilution rate, which can be considered as a simplification of an open and well-mixed environment with a flux of energy in natural systems.

When investigating how to achieve stable coexistence of cell populations with chemical-mediated interactions in synthetic consortia, we notice that culture condition becomes a critical factor. Firstly, the fresh media in chemostat ensures a longer time of cell growth to observe interactions besides nutrient limitation, where as only fast interactions before nutrient depletion can be well characterized in batch cultures. More importantly, the dilution condition makes a huge difference to the mediator chemical's concentration. In batch cultures, chemicals secreted by cells may accumulate and become saturated when interacting with other populations. With an external dilution in chemostat, the accumulated chemical can be maintained at a relatively low concentration so strengths of interactions via the chemical still depend on population density with a higher sensitivity.

Here, we present a simple example of two cell populations that compete for a single limiting nutrient. With mathematical models, we demonstrate that batch and chemostat cultures show opposite coexistence behaviors.

Batch culture

We consider two cell populations of type I and type II are co-cultured in media, as shown in Figure 3.3A. The population densities are denoted by N_1 and N_2, and the concentration of the limiting nutrient is denoted by M. We build an ODE model based on the Monod equation of cell population growth, and assume both populations have the same nutrient uptake and consumption dynamics with rate δ and threshold K, as presented in equation (3.4). In a batch culture where cell death is not considered and stationary phase is considered as the steady state, we can obtain
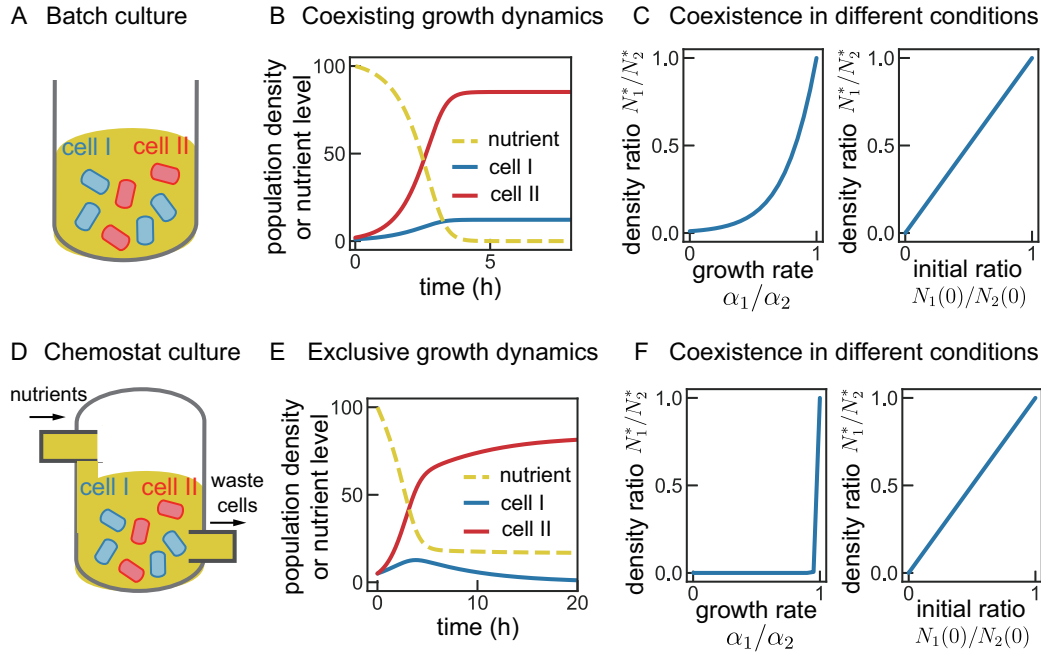
Figure 3.3: Competition for a limiting nutrient in batch versus chemostat cultures. (A) Schematic diagram of a co-culture of two cell populations in a batch culture. (B) Simulations of population densities and nutrient consumption dynamics in the batch culture. Cells stop growing and maintain a certain density when the nutrient is completely consumed. (C) Simulations of density ratio of two populations with various growth rates and initial densities. (D) Schematic diagram of a co-culture of two cell populations in a chemostat culture. (E) Simulations of population densities and nutrient consumption dynamics in the chemostat culture. Cells continuously grow and the nutrient concentration is maintained at a certain level due to cells' consumption and the continuously inflow/outflow of the media. (F) Simulations of density ratio of two populations with various growth rates and initial densities.

dynamics of the system before entering stationary phase:

$$
\begin{aligned}
\text{cell population I density:} \quad & \frac{\mathrm{d}N_1}{\mathrm{d}t} = \alpha_1 N_1 \frac{M}{M+K}, \\
\text{cell population II density:} \quad & \frac{\mathrm{d}N_2}{\mathrm{d}t} = \alpha_2 N_2 \frac{M}{M+K}, \\
\text{limiting nutrient:} \quad & \frac{\mathrm{d}M}{\mathrm{d}t} = -\delta N_1 \frac{M}{M+K} - \delta N_2 \frac{M}{M+K}.
\end{aligned}
\tag{3.8}
$$

Since the nutrient is added at the beginning of cell population growth, the nutrient concentration in the media decays while cells grow until it is depleted. Therefore, at steady state, we find $M^* = 0$ and cells stop growing, i.e., $\frac{\mathrm{d}N_1}{\mathrm{d}t} = \frac{\mathrm{d}N_2}{\mathrm{d}t} = 0$. It is easy to find that the population densities of two cell populations depend on their growth rates α_1, α_2 and initial density conditions.

Figure 3.3B shows the simulation of cell population growth and nutrient consumption. We set same initial densities for two cell populations and set a higher growth rate for cell type II, i.e., $\alpha_2 > \alpha_1$. Both populations grow and enter stationary phase when the nutrient is depleted, but the fast growing population of cell type II has a higher density than cell type I. Moreover, we alter their growth rates and find the final density ratio $\frac{N_1^*}{N_2^*}$ to be positively related to growth rate ratio $\frac{\alpha_1}{\alpha_2}$ in Figure 3.3C (left). We also simulate population growth dynamics with varying initial density ratios $\frac{N_1(0)}{N_2(0)}$ and observe a linear relationship to the final density ratio in Figure 3.3C (right). All simulations and analysis show that two cell populations that purely compete for a single nutrient can coexist in a batch culture despite the difference in their growth rates. Note that we do not model the dynamics of cell death and population decay after nutrients being used up, the steady state here only characterizes the entrance of stationary phase. In some sense, the population densities and coexistence in batch cultures only represent transient dynamics without reaching a steady state.

Chemostat culture

For chemostat cultures, there is a constant dilution of cells and media in the co-culture of two cell populations, as shown in Figure 3.3D. We also build an ODE model based on the Monod equation. Both cell populations are diluted with a constant rate D and the media is also diluted with an inflow flux M_{in} of fresh nutrients. We can write down the model:

$$\text{cell population I density:} \quad \frac{\mathrm{d}N_1}{\mathrm{d}t} = \alpha_1 N_1 \frac{M}{M + K} - D N_1,$$

$$\text{cell population II density:} \quad \frac{\mathrm{d}N_2}{\mathrm{d}t} = \alpha_2 N_2 \frac{M}{M + K} - D N_2,$$

$$\text{limiting nutrient:} \quad \frac{\mathrm{d}M}{\mathrm{d}t} = D\left(M_{in} - M\right) - \delta N_1 \frac{M}{M + K} - \delta N_2 \frac{M}{M + K}.$$

(3.9)

At equilibrium where $\frac{\mathrm{d}N_1}{\mathrm{d}t} = \frac{\mathrm{d}N_2}{\mathrm{d}t} = 0$, we find the coexistence of two cell populations, i.e., $N_1^* > 0, N_2^* > 0$, is only achieved when:

$$\alpha_1 \frac{M^*}{M^* + K} - D = \alpha_2 \frac{M^*}{M^* + K} - D = 0, \tag{3.10}$$

which is impossible when $\alpha_1 \neq \alpha_2$. In other words, two cell populations with different growth rates cannot coexist in a chemostat culture with a single limiting nutrient.

Figure 3.3E shows the simulation of co-cultured cell populations. The fast growing cell type II outcompetes cell type I, and cell type I goes extinct at steady state.

It is more clear in Figure 3.3F (left panel) that as long as the growth rates are different, only one cell population can survive in the chemostat culture. Figure 3.3F (right panel) demonstrates that when both cell populations grow at the same rate, the density ratio at steady state depends on their initial densities in a proportional manner.

The chemostat model leads to an opposite coexistence prediction as the batch culture. In the chemostat culture, only one cell population can survive and dominate. In fact, such phenomenon has been well studied back in the 20th century in ecology. It is first proposed as the competitive exclusion principle (CEP) which states that multiple species cannot coexist with single limiting resource, and has been one of the central themes in ecology (Georgii Frantsevich Gause, 1932; George Francis Gause, 2019). A few decades after the competitive exclusion principle, theorists used the Monod equation of microbial growth and substrate consumption to explain the exclusion in microorganisms co-cultured in chemostat conditions (Herbert, Elsworth, and Telling, 1956; S.-B. Hsu, Hubbell, and Waltman, 1977; S. Hsu, 1978).

We show more examples of two cell population systems with cooperative and competitive interactions using similar models as in equation (3.10). For example, as shown in Figure 3.4A,D, we consider cell populations involving mutual competition via bactericidal and bacteriostatic antibiotics in a batch culture. We assume bactericidal antibiotics induce cell death while bacteriostatic antibiotics inhibit cell growth. Detailed mathematical models can be found in Appendix A. Simulations in Figure 3.4B,C show that mutual competition by killing via bactericidal antibiotics cannot support coexistence of two populations, and the density ratio depends on initial densities. Interestingly, two populations can coexist until stationary phase if they only inhibit each other's growth via bacteriostatic antibiotics, as shown in Figure 3.4E,F. This is consistent with the previous result that a batch culture of fast and slowly growing populations does not exhibit competitive exclusion, since both modeling and experimental settings only characterize transient dynamics until stationary phase. However, the coexistence is not stable since the ratio density large depends on the initial densities of the two populations.

In contrast to the batch culture, populations in the chemostat culture has a more robust and consistent coexistence results in different antibiotics and various initial densities, as shown in Figure 3.5. In simulations shown in Figure 3.5B,E, with competitive interactions, two populations cannot coexist and only one population dominates no matter specific chemicals of bactericidal or bacteriostatic antibiotics
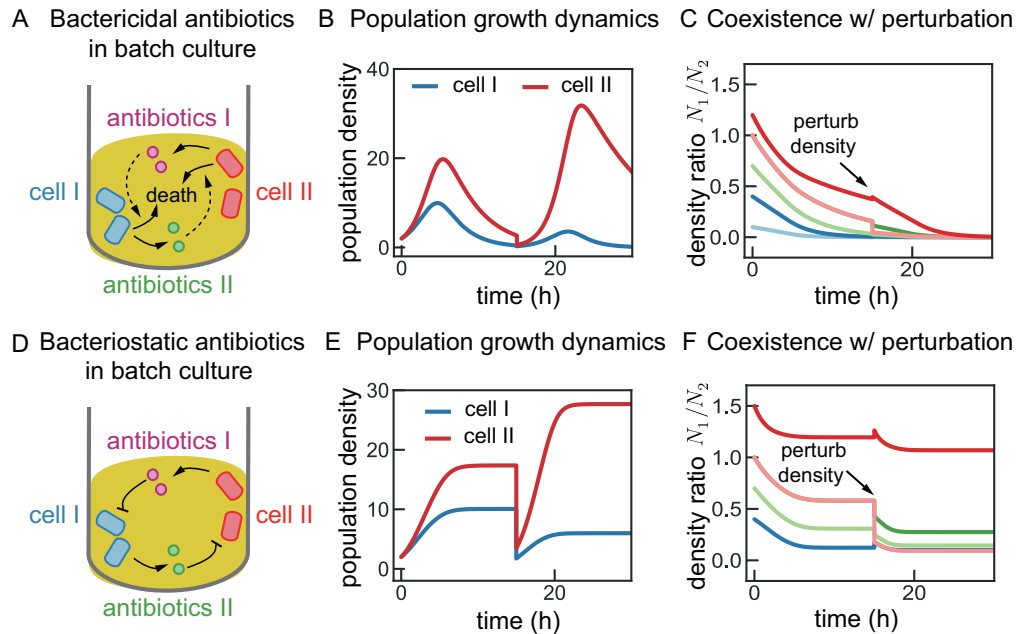
Figure 3.4: Competition via bactericidal and bacteriostatic antibiotics in a batch culture. (A)(D) Schematic diagrams of a co-culture of two cell populations with competitive interactions via bactericidal or bacteriostatic antibiotics in a batch culture. (B)(E) Simulations of population densities in the batch culture. At 15hr in the simulation, we dilute the cell populations to a low initial densities and show their growth dynamics in fresh media. (C)(F) Simulations of the density ratio of two populations with various initial densities. At 15hr, we perturb the densities to show the convergence of the density ratio.

mediate the interaction. Moreover, the density ratio at steady state is stable and not dependent on initial densities since the ratio converges to zero in all conditions, as shown in Figure 3.5C,F.

Besides the example of competitive interactions shown in Figure 3.4 and 3.5, we also model and simulate co-cultures with cooperative interactions in both batch and chemostat cultures. More examples can be found in Figure A.1 and A.2 in Appendix A. Cooperative interaction example include different mechanisms of crossfeeding of metabolites, mutual growth activation by quorum sensing signaling molecules and toxin removal. Simulations of population growth show that cooperative interactions can support coexistence in both batch and chemostat cultures. However, only the coexistence is stable in the chemostat culture with a robust density ratio at steady state despite the initial condition or perturbations to densities.

Compared to the chemostat culture environment, the major limitation of the batch culture is that essentially only transient growth dynamics can be characterized since
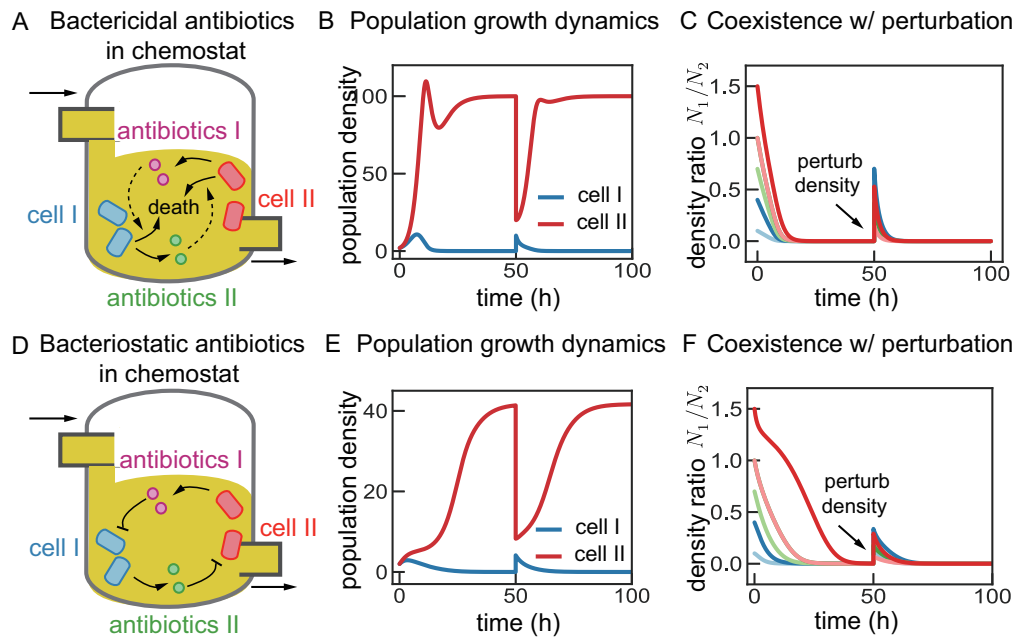
Figure 3.5: Competition via bactericidal and bacteriostatic antibiotics in a chemostat culture. (A)(D) Schematic diagrams of a co-culture of two cell populations with competitive interactions via bactericidal or bacteriostatic antibiotics in a chemostat culture. There is a constant inflow/outflow of media. (B)(E) Simulations of population densities in the chemostat culture. At 50hr in the simulation, we dilute the cell populations to a low initial densities and show their growth dynamics in fresh media. (C)(F) Simulations of the density ratio of two populations with various initial densities. At 50hr, we perturb the densities to show the convergence of the density ratio.

it is a closed system. Therefore, it is hard to quantify the stability of population coexistence in long terms in batch cultures.

Previous results from Section 3.2 and 3.3 suggest that both chemical-mediated interaction mechanisms and culture conditions play a critical role in population interaction dynamics. Particularly, the same interaction network topology between populations might lead to opposite stability and coexistence results without specifications. Therefore, the contradictory results on either cooperation or competition supports stable coexistence in previous theoretical and experimental studies might be understood. From the engineering perspective, it is also important to use the more appropriate mechanistic models and culture environments when designing and testing population interaction networks.

3.4 Stable coexistence of two cell populations

Now we use the mechanistic model of chemical-mediated interactions proposed in Section 3.2 to explore what interactions lead to stable coexistence of cell populations. Here, coexistence is achieved when all cell population densities are above zero at steady state. The coexistence is stable if the same steady state of cell population densities is maintained despite perturbations in cell numbers or chemical concentrations.

We consider a microbial consortium of two cell populations co-cultured in the chemostat condition. The population densities of cell type I and II are denoted by N_1 and N_2. Each population can produce and secret a chemical species that regulates growth or induces death of itself and the other population. We denote the chemical produced by the ith population by M_i if it is consumed/degraded by recipient populations, or by S_i if it accumulates in the environment. For simplicity, we assume all growth and death rates of cell populations linearly depend on these chemicals' concentrations, and all consumption and degradation rates of chemicals linearly depend on the recipient cell densities.

Interaction network via accumulated chemicals

First, we consider all interactions between N_1 and N_2 are mediated by two accumulated chemicals S_1 and S_2. We assume these chemical species either promote or inhibit cells' growth and death, and use parameter $d_{ij}S_j$ to represent the effected growth or death rate on the ith population by chemical S_j. Then we write down an ODE model of the two population system:

$$
\begin{aligned}
\text{cell population I density:} \quad & \frac{dN_1}{dt} = (\alpha_1 + d_{11}S_1 + d_{12}S_2 - D)\, N_1, \\
\text{cell population II density:} \quad & \frac{dN_2}{dt} = (\alpha_2 + d_{21}S_1 + d_{22}S_2 - D)\, N_2, \\
\text{mediator chemical I:} \quad & \frac{dS_1}{dt} = \beta_1 N_1 - DS_1, \\
\text{mediator chemical II:} \quad & \frac{dS_2}{dt} = \beta_2 N_2 - DS_2,
\end{aligned}
\tag{3.11}
$$

where α_i is the basal cell growth rate and D is the dilution rate in the chemostat. We assume the dilution rate D is small to have a reasonable population density, i.e., $D < \alpha_i$. Note that if $d_{ij} > 0$, then S_j promotes the ith population's growth rate. In opposite, if $d_{ij} < 0$, then S_j inhibits growth or induces death of the ith population.

Now we solve for the steady state. Since the mediator chemicals are not consumed or degraded by cells, they accumulate and reach concentrations at steady state

depending on the population densities and the dilution rate:

$$S_1^* = \frac{\beta_1}{D} N_1^*, \ S_2^* = \frac{\beta_2}{D} N_2^*. \tag{3.12}$$

If we apply equation (3.12) to (3.11), we can obtain a reduced population model:

cell population I density: $\dfrac{dN_1}{dt} = \left(\alpha_1 + d_{11}\dfrac{\beta_1}{D}N_1 + d_{12}\dfrac{\beta_2}{D}N_2 - D\right)N_1,$

cell population II density: $\dfrac{dN_2}{dt} = \left(\alpha_2 + d_{21}\dfrac{\beta_1}{D}N_1 + d_{22}\dfrac{\beta_2}{D}N_2 - D\right)N_2,$
$$\tag{3.13}$$

which is similar to the Lotka-Volterra model. Then we can find the steady states of cell densities by setting $\frac{dN_1}{dt} = 0$, $\frac{dN_2}{dt} = 0$. To reach coexistence of both populations, i.e., $N_1^* > 0, N_2^* > 0$, the equilibrium should satisfy:

$$\begin{aligned}
d_{11}\frac{\beta_1}{D}N_1^* + d_{12}\frac{\beta_2}{D}N_2^* = D - \alpha_1 < 0, \\
d_{21}\frac{\beta_1}{D}N_1^* + d_{22}\frac{\beta_2}{D}N_2^* = D - \alpha_2 < 0.
\end{aligned} \tag{3.14}$$

It is easy to find the steady state of coexisting cell densities:

$$\begin{aligned}
N_1^* &= \frac{d_{22}(D - \alpha_1) - d_{12}(D - \alpha_2)}{d_{11}d_{22} - d_{12}d_{21}} \frac{D}{\beta_1}, \\
N_2^* &= \frac{d_{11}(D - \alpha_2) - d_{21}(D - \alpha_1)}{d_{11}d_{22} - d_{12}d_{21}} \frac{D}{\beta_2}.
\end{aligned} \tag{3.15}$$

Next we investigate sufficient conditions for stable coexistence. We can define the matrix J according to equation (3.13):

$$J = \frac{1}{D} \begin{bmatrix} d_{11}\beta_1 & d_{12}\beta_2 \\ d_{21}\beta_1 & d_{22}\beta_2 \end{bmatrix} \tag{3.16}$$

The matrix J can be regarded as a measurement of cell-cell interactions. Since $\beta_i > 0, D > 0$, then signs of d_{ij} can indicate cooperation(+) or competition(-) and values of $\frac{d_{ij}\beta_j}{D}$ can represent interaction strengths. We show that the coexistence is globally stable under certain conditions on the matrix J by introducing the following theorem for Lotka-Volterra models. Detailed proof can be found in (Goh, 1977).

Theorem 1 *If the nontrivial equilibrium of equation (3.13) is feasible and there exist a constant positive diagonal matrix P such that $PJ + J^T P$ is negative definite, then equation (3.13) is globally stable in the feasible region.*

Now we look for sufficient conditions that satisfy Theorem 1. For a two population system with interactions mediated by accumulated chemicals, we consider a constant positive diagonal matrix $P = \begin{bmatrix} p_1 & 0 \\ 0 & p_2 \end{bmatrix}$ where $p_1 d_{12} \beta_2 = p_2 d_{21} \beta_1$. It is only feasible when $d_{12} d_{21} > 0$ since p_i, β_i are positive. Then $PJ + J^T P$ becomes a symmetric matrix:

$$PJ + J^T P = \frac{2}{D} \begin{bmatrix} p_1 d_{11} \beta_1 & p_1 d_{12} \beta_2 \\ p_2 d_{21} \beta_1 & p_2 d_{22} \beta_2 \end{bmatrix}. \tag{3.17}$$

A symmetric matrix is negative definite if and only if all of its eigenvalues are negative. This condition implies:

$$
\begin{aligned}
& p_1 d_{11} \beta_1 + p_2 d_{22} \beta_2 < 0, \\
& p_1 p_2 \beta_1 \beta_2 \left(d_{11} d_{22} - d_{12} d_{21} \right) > 0.
\end{aligned}
\tag{3.18}
$$

Since p_i, β_i are all positive, we can derive a sufficient condition for globally stable coexistence:

$$
\begin{aligned}
& d_{11} < 0, \ d_{22} < 0, \\
& d_{11} d_{22} - d_{12} d_{21} > 0, \\
& d_{12} d_{21} > 0.
\end{aligned}
\tag{3.19}
$$

In addition, the coexistence is feasible when $N_1^* > 0, N_2^* > 0$. According to equation (3.15), the feasible solution condition depends on d_{ij} and growth rates α_i. We define $\gamma = \frac{D - \alpha_1}{D - \alpha_2} > 0$, then derive feasible solution condition as

$$\frac{d_{12}}{d_{22}} < \gamma, \ \frac{d_{21}}{d_{11}} < \frac{1}{\gamma}. \tag{3.20}$$

Note that for accumulated chemical-mediated interactions, the globally stable co-existence condition in equation (3.19) and the feasible solution condition in equation (3.20) do not depend on chemical production rates β_i. Meanwhile, the growth and death rates of cell populations induced by chemicals d_{ij} are more important in these constraints.

Following these conditions, we can design two interaction networks via accumulated chemicals. The first network include both populations inhibiting growth of themselves and each other, as shown in Figure 3.6A. Two cell populations can maintain a stable coexistence as long as the overall self-inhibition is stronger than mutual inhibition. The second network involves two populations mutually promoting each other's growth while inhibiting their own growth, as shown in Figure 3.6B. We also show the general stable coexistence condition for a simpler case where the
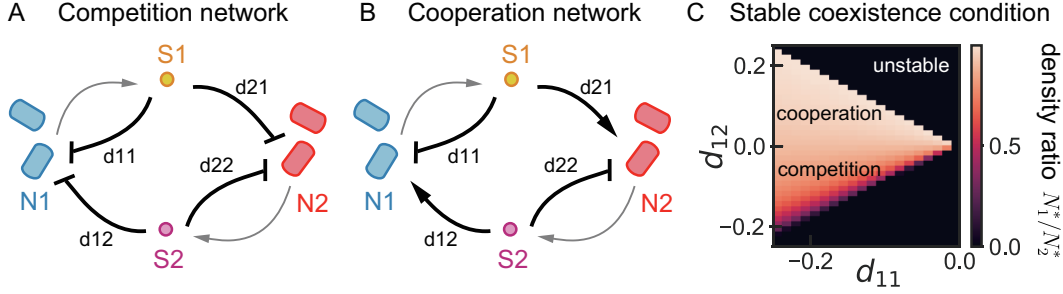
Figure 3.6: Stability condition on interactions via accumulated chemicals in well-mixed environments. (A)(B) Schematic diagrams of a mutual competition or a mutual cooperation interaction between two populations via two accumulated chemicals S_1, S_2. Black arrows represent activation/inhibition of cell growth/death. Grey arrows represent cells producing the chemicals. (C) The steady state population density ratio between two populations with varying d_{ij}.

interaction network is symmetric, i.e., $d_{11} = d_{22}, d_{12} = d_{21}$ in Figure 3.6C. We set the growth rate of cell population II to be faster than cell population I, and simulate for the steady state density ratio with a wide range of d_{ij} values. Only when both populations maintain nonzero densities are marked as stable. The simulation result also shows that with interactions that satisfy the conditions in equations (3.19) and (3.20), both mutual competition and cooperation can support two coexisting populations with different growth rates.

Interaction network via consumed/degraded chemicals

Next, we consider all interactions between N_1 and N_2 are mediated by two chemicals M_1 and M_2 that are actively consumed or degraded by cells. Similarly, we describe the growth or death rate of the ith population modulated by chemical M_j by $d_{ij}M_j$. Then we write down an ODE model of the two population system:

$$
\begin{aligned}
\text{cell population I density:} \quad & \frac{\mathrm{d}N_1}{\mathrm{d}t} = (\alpha_1 + d_{11}M_1 + d_{12}M_2 - D)\, N_1, \\[4pt]
\text{cell population II density:} \quad & \frac{\mathrm{d}N_2}{\mathrm{d}t} = (\alpha_2 + d_{21}M_1 + d_{22}M_2 - D)\, N_2, \\[4pt]
\text{mediator chemical I:} \quad & \frac{\mathrm{d}M_1}{\mathrm{d}t} = \beta_1 N_1 - (\delta_1 N_1 + \delta_2 N_2 + D)\, M_1, \\[4pt]
\text{mediator chemical II:} \quad & \frac{\mathrm{d}M_2}{\mathrm{d}t} = \beta_2 N_2 - (\delta_1 N_1 + \delta_2 N_2 + D)\, M_2,
\end{aligned}
\tag{3.21}
$$

where α_i is the basal cell growth rate and D is the dilution rate in chemostat. Note that chemicals M_1, M_2 modulate populations' growth and death rates while being consumed or degraded by cells. Compared with accumulated chemicals, the

consumed or degraded chemical has a population density-dependent decay with the consumption rate δ_i.

Now we solve for the steady state of chemical concentrations:

$$M_1^* = \frac{\beta_1 N_1^*}{\delta_1 N_1^* + \delta_2 N_2^* + D}, \quad M_2^* = \frac{\beta_2 N_2^*}{\delta_1 N_1^* + \delta_2 N_2^* + D}. \tag{3.22}$$

We find that chemical concentrations are not only dependent on cell population densities through production but also through consumption or degradation. We can find a bound of M_1^*, M_2^*:

$$0 \leq M_1^* \leq \frac{\beta_1}{\delta_1}, \ 0 \leq M_2^* \leq \frac{\beta_2}{\delta_2}. \tag{3.23}$$

Then we solve for the equilibrium of M_i^* by setting $\frac{dN_1}{dt} = 0, \frac{dN_2}{dt} = 0$. If two populations can coexist at steady state, i.e., $N_1^* > 0, N_2^* > 0$, then system should satisfy the following condition:

$$0 \leq M_1^* = \frac{d_{22}(D - \alpha_1) - d_{12}(D - \alpha_2)}{d_{11}d_{22} - d_{12}d_{21}} \leq \frac{\beta_1}{\delta_1},$$
$$0 \leq M_2^* = \frac{d_{11}(D - \alpha_2) - d_{21}(D - \alpha_1)}{d_{11}d_{22} - d_{12}d_{21}} \leq \frac{\beta_2}{\delta_2}. \tag{3.24}$$

Compared with interactions mediated by accumulated chemicals, there is a upper bound for the concentration of consumed/degraded chemicals that depend on their production and decay rates. In this scenario, the feasible solution for stable coexistence has more constraints.

Next, we explore the stability condition. We consider the competition interaction network as an example. The schematic diagram is shown in Figure 3.7A. Then we find the stable regime of parameters d_{ij} by simulation. For simplicity, we set $d_{11} = d_{22}, d_{12} = d_{21}$. Unlike the large region of stable coexistence in the case with accumulated chemicals, the stable coexistence condition lies in a small region, as shown in Figure 3.7B. Compared to the stable regime with accumulated chemicals in Figure 3.6C, the absolute values of d_{11} and d_{12} cannot be too small. This is because the present chemical concentrations are not as high as accumulated chemicals. For example,chemicals that are slowly produced but decay fast only induce weak effects on cells' growth or death. In this case, high rates of d_{11} and d_{12} are required to provide strong enough interaction strengths. Moreover, when we increase the chemical production rates β_i of M_i, the stable region becomes larger, as shown in Figure 3.7C. The increasing stable region in simulation results are consistent with the upper bound result in equation (3.24).
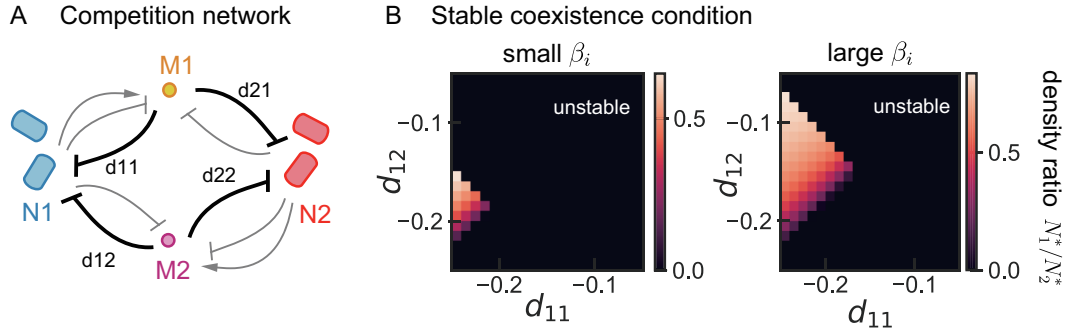
Figure 3.7: Stability condition on interactions via consumed/degraded chemicals in well-mixed environments. (A) Schematic diagrams of a mutual competition interaction between two populations via two consumed/degraded chemicals S_1, S_2. Black arrows represent activation/inhibition of cell growth/death. Grey arrows represent cells producing and consuming/degrading the chemicals. (B) The steady state population density ratio between two populations with varying d_{ij} and a small or big chemical production rate β_i.

The example here illustrates that different mechanisms between accumulated and consumed/degraded chemicals have a big impact on the coexistence stability even in a two population-system with the same interaction network topology. The strengths of interactions via accumulated chemicals can be approximated as proportional to population densities. Thus, the interaction network topology and corresponding stability conditions to maintain stable coexistence are similar to predictions from the Lotka-Volterra model. However, when interactions are mediated by consumed/degraded chemicals, more constraints are found using the mechanistic model. Note that the model here is simple with linear kinetics for most processes, so more work needs to be done to consider saturation in growth/death regulation as well as chemical kinetics. Moreover, so far we only focus on stability of coexistence at steady state without characterizing transient dynamics, delay and stochasticity in cell populations. Detailed mechanisms of chemical-mediated interactions can govern these properties and need more investigation from theoretical studies. Primary simulations of two population systems show that interactions via consumed/degraded chemicals have a faster convergence to steady state, while accumulated chemicals induce more oscillatory growth dynamics, shown in Figure A.3. It suggests that there is a tradeoff in designs between stability and convergence speed. Therefore, the combination of two types of chemicals may improve both transient and steady state properties of interactive microbial populations in consortia.

DESIGN OF POPULATION INTERACTIONS IN SPATIALLY STRUCTURED CONSORTIA

4.1 Motivation

Engineering microbial consortia can enrich the potential of synthetic gene circuits in various applications, including bioproduction (Minty et al., 2013; D. Y. Zhang et al., 2007) and therapeutic applications in human gut microbiome (Riglar et al., 2017). These applications often involve complex and fluctuating environments and the functions depend on robust behaviors of engineered consortia. Thus, to design stable consortia with robust functions not only requires control of cellular and population-level dynamics, but also depends on population-environment interactions.

Unlike homogeneous environments in laboratory studies, many complex environments are spatially heterogeneous. For example, microbes in human gut are not uniformly distributed and can be redistributed through interactions with the host during disease (Tropini et al., 2017). Given the limited range of physical connections via direct contact, signal diffusion or cell migration, the spatial heterogeneity can have a significant effect to the efficiency of population interactions, and further determine stability and robustness properties of microbial consortia (Nadell, Drescher, and Foster, 2016). In an experimental study of synthetic microbial consortia, microbial populations are distributed in separate colonies in a defined spatial environment, and results show that the separation distance can balance competitive and cooperative interactions and promote stable coexistence (Kim et al., 2008). More experimental evidence suggests that aggregated distribution of cell populations can improve persistence of consortia and allow a better adaptation to environmental disruptions (Brenner and Arnold, 2011).

Besides spatially heterogeneous environments, microbes can self-organize into certain spatial structures. For example, microbial populations form biofilm with spatial structures. The spatial structure can provide shield and protection against antimicrobial treatment and promote survival and functionality of microbial populations (Burmølle et al., 2006; Elias and Banin, 2012). The self-organized spatial structure is significantly shaped by population interactions. Different types of interactions lead to diverse spatial patterns that reflect cell populations' relative positioning

(Momeni, Brileya, et al., 2013; Kong et al., 2018), usually exhibiting segregating (Nielsen et al., 2000; Hallatschek et al., 2007), aggregating or intermixing (Rickard et al., 2006) and layering structures (Hansen et al., 2007).

In summary, population interactions facilitate self-organized spatial structures in microbial consortia. On the other hand, population interaction efficiency is strongly impacted by defined spatial environments. Many theoretical and experimental work have studied the relationship between population interactions and spatial structures (Momeni, Brileya, et al., 2013; Kong et al., 2018; Yanni et al., 2019). However, there are not many general guiding rules to achieve certain spatial patterns by engineering interactions and defining spatial environments. In particular, we are lack of design principles that can achieve stable coexistence and robust functions of synthetic microbial consortia in a spatial environment.

In this chapter, we consider two design questions for microbial consortia in spatial context. Firstly in Section 4.2, We discuss what spatial distribution of cell populations can promote stability and robustness in population-level behaviors. Secondly in Section 4.3, we investigate how to design population interactions to achieve certain spatial structures that improve stability and robustness.

4.2   Robust population behaviors in defined spatial environments

In microbial consortia of multiple cell populations, each population is expected to maintain a certain density fraction to ensure the overall functionality is achieved collectively. Here, we consider a two population system and present a control strategy for robust density ratio in spatial context [1].

Synthetic interaction and circuit design

We adopt the circuit design for population density ratio control presented in Section 2.4, as shown in Figure 4.1A. Consider two different cell types of N_1 and N_2 cells. Cell type I and II inhibit their own density by activating a toxin (ccdB) production via constitutively synthesized quorum sensing signals S_1, S_2. Meanwhile, they promote each other's growth by activating an anti-toxin (ccdA) production via quorum sensing signals. The interaction network includes self-competitive and mutually cooperative interactions.

In spatial context, we consider there are n microcolonies of each cell type I and II, distributed in $2n$ wells on an agar plate, as shown in Figure 4.1B. Microcolonies

---

[1] *A version of this section has been published as (Ren and Murray, 2018).*

A   Schematic of interaction and circuit design
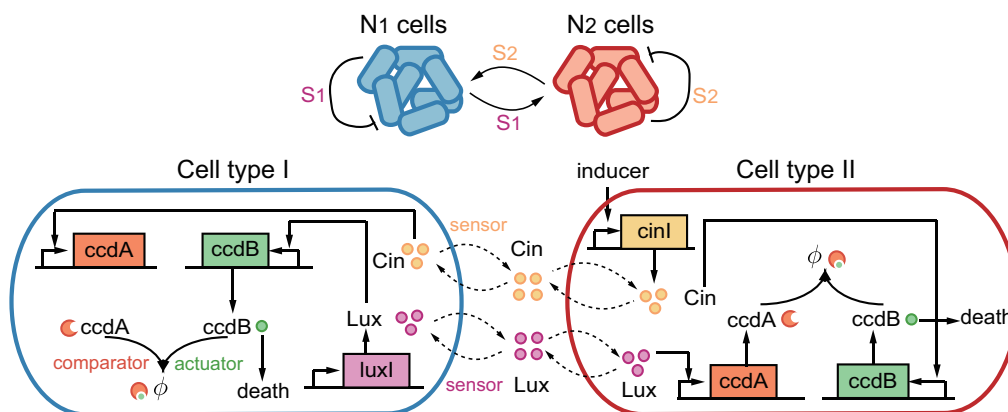
B   Defined spatial distribution of populations

C   Diffusion of quorum sensing signals

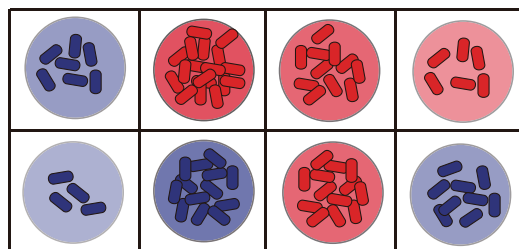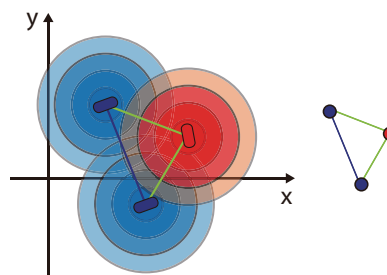Figure 4.1: Schematic diagram of the synthetic circuit design and defined spatial environment. (A) The circuit design of population density ratio control between two populations. (B) Schematic diagram of the defined environment. Microcolines of two cell strains are distributed in wells on a 2D agar plate. Quorum sensing molecules can diffuse on the plate and reach cells in all wells. (C) Illustation of the diffusion and concentration distribution of quorum sensing signaling molecules. Cell populations interact based on sensing the signaling molecules. The simplified interaction network in the right demonstrates that two cell type I microcolonies (blue circles) interact via Lux-AHL (blue line), and any cell type I and II microcolonies (blue, red circles) interact via Lux-AHL and Cin-AHL (green line).

are shaped in circles centered at each well and grow within the well boundary. We assume that cells cultured in the same well have identical growth dynamics and can be represented by one agent. In this two population-system, cells interact via quorum sensing signals that diffuse fast and freely on the agar plate, therefore the concentration of signaling molecules forms a spatial distribution. Figure 4.1C illustrates the diffusion of signaling molecules from each microcolony. The region with lighter color represents a lower concentration of signaling molecules since it is further from the colony center.

Reaction-diffusion model

To model dynamics of $2n$ microcolonies and signaling molecules, we propose $2n$ sets of ODEs describing intracellular chemical reactions and 2 sets of PDEs describing signal diffusion in the environment. The model assumptions for the synthetic circuit are the same as in Section 2.4.

For cells in the ith microcolony of cell type I, we denote its population density by $N_i^{(1)}$, its intracellular concentrations of toxin and anti-toxin by $T_i^{(1)}, A_i^{(1)}$, and its position by $\mathbf{r}_i^{(1)}$. Since both signaling molecules have a spatial distribution across the 2D space, we denote the concentrations of signaling molecules S_1, S_2 at the position $\mathbf{r}$ by $S^{(1)}(\mathbf{r}), S^{(2)}(\mathbf{r})$. The population growth and intracellular dynamics model of the ith microcolony of cell type I is written as

$$
\text{population density:} \quad \frac{dN_i^{(1)}}{dt} = k_{N_1}\left(1 - \frac{N_i^{(1)}}{N_{\max}}\right) N_i^{(1)} - d_N T_i^{(1)} N_i^{(1)},
$$

$$
\text{toxin ccdB:} \quad \frac{dT_i^{(1)}}{dt} = \beta_T \frac{\left(S^{(1)}\left(\mathbf{r}_i^{(1)}\right)\right)^2}{K_{S_1} + \left(S^{(1)}\left(\mathbf{r}_i^{(1)}\right)\right)^2} - \gamma T_i^{(1)} A_i^{(1)} - d T_i^{(1)}, \quad (4.1)
$$

$$
\text{anti-toxin ccdA:} \quad \frac{dA_i^{(1)}}{dt} = \beta_A \frac{\left(S^{(2)}\left(\mathbf{r}_i^{(1)}\right)\right)^2}{K_{S_2} + \left(S^{(2)}\left(\mathbf{r}_i^{(1)}\right)\right)^2} - \gamma T_i^{(1)} A_i^{(1)} - d A_i^{(1)},
$$

where $i = 1, 2, ..., n$.

We can obtain the dynamical model for the signaling molecule S_1 as

$$
\frac{\partial S^{(1)}(\mathbf{r}, t)}{\partial t} = \sum_{i=1}^{n} \beta_{S_1} N_i^{(1)} \mathbf{1}_{\{\mathbf{r}=\mathbf{r}_i^{(1)}\}}(\mathbf{r}) + k_{dif} \nabla^2 S^{(1)} - d_S S^{(1)},
$$
$$
0 \le \mathbf{r} \le L, \ S^{(1)}(\mathbf{r}, 0) = 0, \ S^{(1)}\left(L\frac{\mathbf{r}}{|\mathbf{r}|}, t\right) = 0. \quad (4.2)
$$

Function $\mathbf{1}_{\{\mathbf{r}=\mathbf{r}_i^{(1)}\}}(\mathbf{r})$ is an indicator function defined as

$$
\mathbf{1}_{\{\mathbf{r}=\mathbf{r}_i^{(1)}\}}(\mathbf{r}) = \begin{cases} 1, & \mathbf{r} = \mathbf{r}_i^{(1)}, \\ 0, & \mathbf{r} \ne \mathbf{r}_i^{(1)}, \end{cases} \quad (4.3)
$$

We can also write similar models of cell type II by changing the superscript (1) in equation (4.1) to (2) for all $N_j^{(2)}, T_j^{(2)}, A_j^{(2)}$, where $j = 1, 2, ..., n$. For signaling molecules S_2, its concentration dynamics is similar to equation (4.2) with changed

Parameters	Description
k_{N_1}, k_{N_2}	Population growth rate of cell type I and II
$N_{\max}$	Carrying capacity in each well
d_N	Population death rate by toxin of cell type I and II
β_T, β_A	Activated production rate of toxin ccdB and antitoxin ccdA by AHL
γ	Sequestration rate of toxin ccdB and antitoxin ccdA
d	Dilution rate of intracellular species in cell type I and II
K_{S_1}, K_{S_2}	Dissociation coefficient of Lux-AHL and Cin-AHL activation
β_{S_1}, β_{S_2}	Production rate of Lux-AHL and Cin-AHL
d_S	degradation rate of AHLs
K_{dif}	diffusion rate of AHLs
L	boundaries of the space

Table 4.1: Parameters of the reaction-diffusion model.

subscript and superscript. The full model can be found in equation (B.1). The parameters are listed in Table 4.1.

Note that to describe the populations in a well-mixed environment, We can reduce the reaction-diffusion model to only ODEs, by setting the distance between wells to be value 0 and having identical dynamics of all cells of the same type.

For spatially distributed consortia, we can reduce the full model into a simplified model that captures population interactions. We first reduce the PDEs using quasi-steady state assumptions, and then reduce the ODEs by linearization. Quorums sensing molecules diffuse fast on an agar plate compared to celluar processes (Decho, Frey, and Ferry, 2011), so the timescale of S_1, S_2 dynamics is relatively fast. We assume that the spatial distribution of signaling molecules reaches quasi-steady state. Since signaling molecules only affect cell growth when they are sensed by cells and react with intracellular chemicals, we only need to solve for quasi-steady states of S_1, S_2 concentrations at each microcolony center position. Thus, we can obtain the simplified model from PDE reduction:

$$S^{(1)}\left(\mathbf{r}_i^{(1)}\right) = \frac{K_{dif}}{r_y} \sum_{p=1}^{n} f\left(\mathbf{r}_p^{(1)} - \mathbf{r}_i^{(1)}\right) N_p^{(1)},$$

$$S^{(2)}\left(\mathbf{r}_i^{(1)}\right) = K_{dif} \sum_{q=1}^{n} f\left(\mathbf{r}_q^{(2)} - \mathbf{r}_i^{(1)}\right) N_q^{(2)}, \qquad (4.4)$$

$$K_{dif} = \frac{\beta_S}{2\sqrt{k_{dif}d_S}}, \quad f\left(\mathbf{r}\right) = \exp\left(-\sqrt{\frac{d_S}{k_{dif}}}\mathbf{r}\right).$$

The parameter r_y is defined by $r_y = \frac{\beta_{S_1}}{\beta_{S_2}}$, which represents the relative production

rate of two signaling molecules. By tuning r_y, we can obtain different population density ratio at steady state.

The growth and death kinetics of cell populations are regulated by the toxin and antitoxin. Since the toxin-antitoxin pair performs strong sequestration, there is a timescale separation of toxin dynamics from cell growth (Qian, Grunberg, and Del Vecchio, 2018). By performing quasi-steady state approximation and linearization on ODEs in equation (4.1), we obtain the linearized model in forms of:

$$
\begin{aligned}
\frac{\mathrm{d}N_i^{(1)}}{\mathrm{d}t} &= \frac{\beta_T d_N}{d} \left(-\frac{1}{r_y} S^{(1)}\left(\mathbf{r}_i^{(1)}\right) + S^{(2)}\left(\mathbf{r}_i^{(1)}\right) \right), \\
\frac{\mathrm{d}N_j^{(2)}}{\mathrm{d}t} &= \frac{\beta_T d_N}{d} \left(\frac{1}{r_y} S^{(1)}\left(\mathbf{r}_j^{(2)}\right) - S^{(2)}\left(\mathbf{r}_j^{(2)}\right) \right).
\end{aligned}
\tag{4.5}
$$

We plug equation (4.4) into equation (4.5), and obtain the reduced model:

$$
\begin{aligned}
\frac{\mathrm{d}N_i^{(1)}}{\mathrm{d}t} &= K_N \left(-\frac{1}{r_y} \sum_{p=1}^{n} f\left(\mathbf{r}_p^{(1)} - \mathbf{r}_i^{(1)}\right) N_p^{(1)} + \sum_{q=1}^{n} f\left(\mathbf{r_q}^{(2)} - \mathbf{r}_i^{(1)}\right) N_q^{(2)} \right), \\
\frac{\mathrm{d}N_j^{(2)}}{\mathrm{d}t} &= K_N \left(+\frac{1}{r_y} \sum_{p=1}^{n} f\left(\mathbf{r}_p^{(1)} - \mathbf{r}_j^{(2)}\right) N_p^{(1)} - \sum_{q=1}^{n} f\left(\mathbf{r}_q^{(2)} - \mathbf{r}_j^{(2)}\right) N_q^{(2)} \right),
\end{aligned}
\tag{4.6}
$$

where $K_N = \frac{K_{dif} \beta_T d_N}{d}$.

The reduced model in equation (4.6) only contains cell populations at discrete well positions as variables. The parameter K_N is a lumped parameter characterizing cell growth rate. In both N_1 and N_2 dynamics, there is a negative term representing self-inhibition because cells of the same type inhibit their own density via toxins; there is a positive term representing mutual interaction because cells are rescued by signaling molecules from the other cell type to keep growing. All interaction strengths are functions of the distance between involved microcolonies, so it is natural to derive a network model based on the spatial distribution of these microcolonies.

Spatial distribution and control performance

Given a fixed set of parameters, we can find the dynamics in equation (4.6) is determined by the spatial distribution of each population. We define a state vector $X = [X^{(1)}, X^{(2)}]^T = [N_1^{(1)}, \cdots, N_n^{(1)}, N_1^{(2)}, \cdots, N_n^{(2)}]^T \in \mathbb{R}^{2n}$ to represent densities of microcolonies. We also define a matrix $D \in \mathbb{R}^{2n \times 2n}$ to represent interactions among

microcolonies. The matrix D can be partitioned into four $n \times n$ block matrices:

$$
\begin{aligned}
\text{cell I self-interaction strength:}\quad & D_{11} = [d_{ij}],\ d_{ij} = K_N f\left(\mathbf{r}_j^{(1)} - \mathbf{r}_i^{(1)}\right), \\
\text{cell II to I interaction strength:}\quad & D_{12} = [d_{ij}],\ d_{ij} = K_N f\left(\mathbf{r}_j^{(2)} - \mathbf{r}_i^{(1)}\right), \\
\text{cell I to II interaction strength:}\quad & D_{21} = [d_{ij}],\ d_{ij} = K_N f\left(\mathbf{r}_j^{(1)} - \mathbf{r}_i^{(2)}\right), \\
\text{cell II self-interaction strength:}\quad & D_{22} = [d_{ij}],\ d_{ij} = K_N f\left(\mathbf{r}_j^{(2)} - \mathbf{r}_i^{(2)}\right).
\end{aligned}
\tag{4.7}
$$

The reduced model in equation (4.6) can be written in a network model:

$$
\begin{aligned}
\frac{\mathrm{d}}{\mathrm{d}t}\begin{bmatrix} X^{(1)} \\ X^{(2)} \end{bmatrix} &= \begin{bmatrix} -\frac{1}{r_y}D_{11} & D_{12} \\ \frac{1}{r_y}D_{21} & -D_{22} \end{bmatrix}\begin{bmatrix} X^{(1)} \\ X^{(2)} \end{bmatrix}, \\
y &= \frac{\left\lVert X^{(1)} \right\rVert}{\left\lVert X^{(2)} \right\rVert} = \frac{\sum_{i=1}^{n} N_i^{(1)}}{\sum_{j=1}^{n} N_j^{(2)}}.
\end{aligned}
\tag{4.8}
$$

Defined spatial distribution corresponds to values of matrices $D_{11}, D_{12}, D_{21}, D_{22}$. To investigate what spatial distributions can maintain stable and robust density ratio control, we first run simulations of all potential distributions using the full reaction-diffusion model in equation (B.1). In the simulation, we set $n = 4$ and $r_y = 1$.

Firstly, we present three different spatial distributions that show the desired density ratio $y^* = 1$ at steady state in Figure 4.2A. Note that the microcolony distribution of cell type I and II is symmetrical, i.e., $D_{11} = D_{22}, D_{12} = D_{21}$. Then we test asymmetrical distributions and find that the density ratio deviates from value 1, as shown in Figure 4.2B. Moreover, the deviation is increased when the absolute value of the self-interaction strengths difference between two populations $||D_{11}|| - ||D_{22}||$ increases, as shown in Figure 4.3A. We alter the absolute distance between adjacent wells and find the same trend on self-interaction strengths. In this simulation, the distribution shown in Figure 4.2B (left) exhibits the largest deviation. Since all cell type II microcolonies are closely distributed in the middle while cell type I microcolonies are far from each other, self-inhibition of cell type II is much higher given its own signal accumulation, leading to a higher density of N_1 than N_2.

To investigate the robustness performance of density ratio control, we introduce a disturbance to cell growth rates and assess the system output's adaptation performance as a measure of robustness. The adaptation error is defined by the steady state error between density ratios with and without the disturbance. We assume the disturbance is homogeneous to all type I cells and leads to a decreased growth
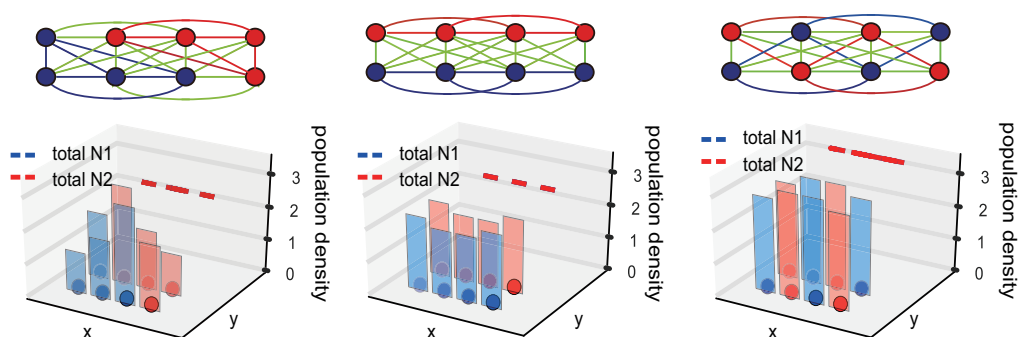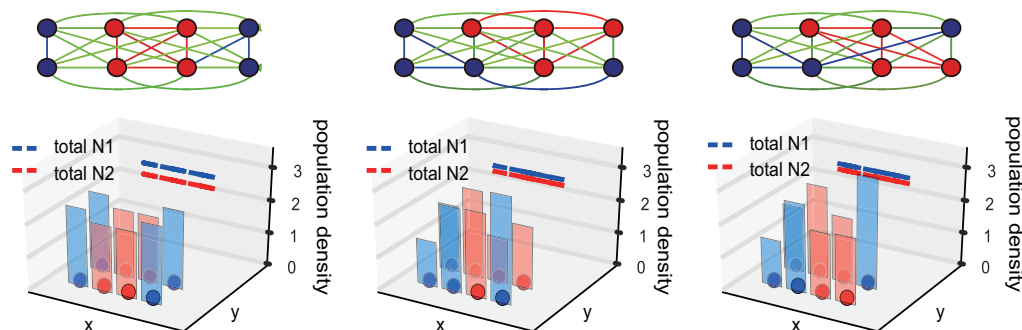
Figure 4.2: Simulation of densities of spatially distributed populations. (A) Schematic diagrams of symmetrical spatial distributions of microcolonies, and corresponding simulations of steady state density of all microcolonies. Dashed lines(overlapping) in the simulation plots are average population density of two cell types. (B) Schematic diagrams of symmetrical spatial distributions of micro-colonies, and corresponding simulations of steady state density of all microcolonies.

rate. Figure 4.3B shows that colony distributions that has larger mutual interaction strengths $||D_{12}|| + ||D_{21}||$ are more adaptive to perturbations. The most robust distribution corresponds to the network shown in 4.2A (right), where all microcolonies of cell type I and II are more intermixing. The intermixing distribution enhances the mutual promotion in cell growth with a stronger cooperation via high signal concentrations.

To improve the design of spatial distributions for stable and robust population density ratio, we have following principles for the system in equation (4.8):

If $D_{11} = D_{22}, D_{12} = D_{21}$, then the system has coexistence of two cell populations with ratio r_y at steady state.

The deviation of the steady state population ratio from r_y increases when $||D_{11}|| - ||D_{22}||$ increases.

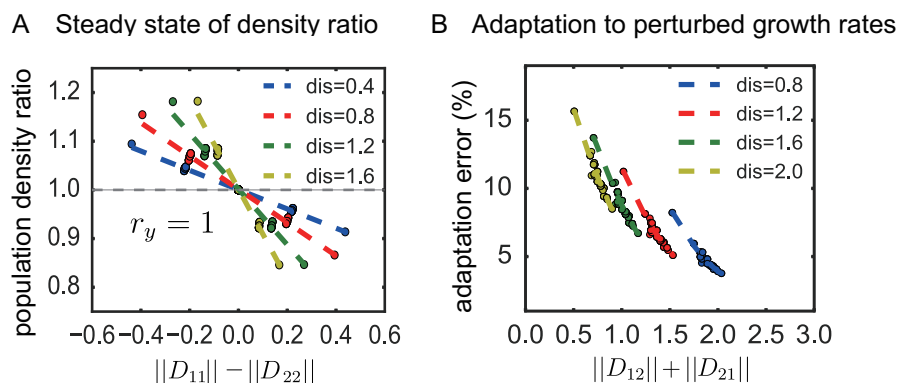A Steady state of density ratio   B Adaptation to perturbed growth rates

Figure 4.3: Steady state density ratio and adaptation performance of spatially distributed populations. (A) Simulation results of population density ratio versus calculated self-interaction strength difference between two populations. We screen all spatial distributions with varied absolute distances between wells. Dots correspond to results of each distribution and dashed lines show the linear relationship from interpolation. (B) Simulation results of adaptation error in density ratio versus calculated mutual interaction strength.

The steady state population ratio adapts better after perturbation on growth rates when $\|D_{12}\| + \|D_{21}\|$ increases.

Discussion

For a two population consortium in a defined spatial environment, we propose a model that can predict steady state properties of interactive populations by characterizing their interaction strengths. The interaction strengths depend on spatial distributions of microbial colonies. Therefore, by optimizing the spatial distribution, we can build a consortium with stable and robust functionalities. Specifically, to maintain a relatively high density ratio between two populations, a more intermixing colony distribution of two cell types can promote robustness. Although this work is based on a a specific synthetic circuit for density ratio control, the theory and analysis approach can be adopted to a more generalized problem in synthetic consortia design in spatial context. For functionalities that require population interactions, our approach is useful for finding limitations on control performance and exploring optimal spatial structures of colony distributions.

4.3 Stable coexistence of two cell populations with spatial structures

Stable coexistence is a critical property for microbial consortia. In Section 3.4, we discussed how to design population interactions for stable coexistence in well-mixed environments. In spatial environments, microbial populations can self-organize

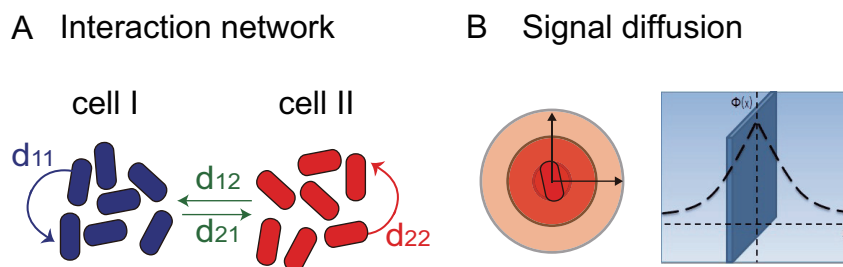A   Interaction network   B   Signal diffusion

Figure 4.4: Schematic diagram of interactive populations in spatial context. (A) Two cell populations with mutual interactions and self-interactions of certain strengths. The interactions are fulfilled by regulation on cell growth and death dynamics via signaling molecules. (B) Illustration of the diffusion and concentration distribution of quorum sensing signaling molecules in a 2D space.

into spatial structures. Spatial structures are found to be beneficial to population survival in studies of natural consortia. It suggests that engineering synthetic consortia to form certain spatial structures may improve stability and robustness of their functionalities. Here, we investigate design principles of synthetic microbial consortia for stable coexistence, and explore: 1) how self-organized spatial patterns depend on population interactions; 2) what spatial structures and interactions support stable coexistence [2].

Synthetic interaction design

We consider a two population system, where cell type I and II interact and mediate cell growth and death via quorum sensing signaling molecules. As discussed in Section 3.1 and 3.3, signaling molecules are accumulated chemicals and we can use a simple pairwise description to characterize population interactions. The schematic of the two population system is shown in Figure 4.4A. We denote self-interaction strengths by $d_{ii}, i = 1, 2$ and mutual interaction strengths by $d_{ij}, i \neq j$. Negative interaction strengths correspond to inhibition in cell growth and positive interaction strengths correspond to promotion in cell growth.

In spatial context, we assume cells are cultured on an agar plate. Quorum sensing signaling molecules are produced by cells and diffuse on the 2D space, forming a spatial distribution of their concentrations. Figure 4.4B illustrates that each single cell is a point source and the concentration of signaling molecules decreases at further positions from the source.

---

[2]*A version of this section has been published as (Ren and Murray, 2019).*
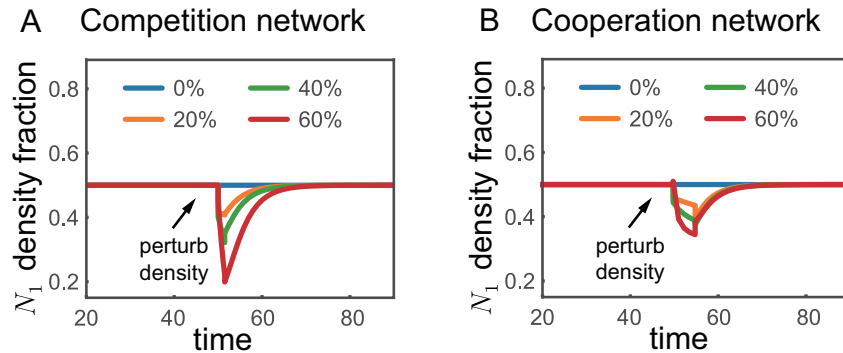
Figure 4.5: Simulation of populations with competition and cooperation in well-mixed environments. (A)(B) Simulations of density dynamics of mutually competitive and cooperative populations. At 50hr, we perturb the density of cell type I with varying amplitude and show the adaptation in N_1 density fraction.

Stable coexistence in well-mixed environments

In well-mixed environments, we find cell populations can maintain stable coexistence as long as the conditions in equations (3.19) and (3.20) are satisfied. The condition suggests two interaction networks that involve self-inhibition ($d_{ii} < 0$) and either mutual promotion ($d_{ij} > 0$) or mutual inhibition ($d_{ij} < 0$) on cell growth. Here, we specify these two interaction networks by their difference in mutual interactions and call them cooperation and competition networks.

We build an ODE model for two cell populations in a well-mixed batch environment:

$$\frac{dN_1}{dt} = k_N \left(1 - \frac{N_1 + N_2}{N_{max}}\right) N_1 + (d_{11}N_1 + d_{12}N_2) N_1,$$
$$\frac{dN_2}{dt} = k_N \left(1 - \frac{N_1 + N_2}{N_{max}}\right) N_2 + (d_{21}N_1 + d_{22}N_2) N_2,$$
(4.9)

where k_N is the basal growth rate and N_{max} is the carrying capacity.

To test if two populations can coexist in both cooperation and competition networks, we run simulations of population density dynamics. We set parameters $d_{11} = d_{22}, d_{12} = d_{21}, |d_{12}| = 0.8|d_{11}|$, which satisfies the stable coexistence condition for both cooperation and competition networks. In the simulation, we start with random nonzero initial densities. After reaching steady state, we perturb the population density by diluting out 20%, 40%, 60% of cell type I population. For both interaction networks, Figure 4.5 shows that population densities converge to $N_1^* = N_2^*$ and maintain a stable density ratio $\frac{N_1^*}{N_2^*} = 1$.

Spatial model with nonlocal reactions

Now we build models for the same cooperation and competition networks in spatial environments.

All interactions are realized via quorum sensing yet the diffusible signaling molecules can only reach cells in the neighborhood within some range. Therefore, the interactions are nonlocal behaviors that depend on the spatial distribution of cells and of signaling molecules in the neighborhood. We assume cells are point sources of diffusible signaling molecules on 2D space. Adding source production and self decay in signaling molecules diffusion equations, we derive the signaling molecules concentration ϕ at the radius r of a single source at steady state with appropriate boundary conditions:

$$\phi\left(r\right) = \begin{cases} S_0 & r = 0, \\ \dfrac{S_0}{2\pi d} K_0\left(\dfrac{r}{L}\right) & r > 0, \end{cases} \tag{4.10}$$

where S_0 is the production rate of signaling molecules, d is the diffusion rate of signaling molecules, L is the diffusion range calculated as $L = \frac{d}{\gamma}$, γ is the degradation rate of signaling molecules. Parameter K_0 is the modified Bessel function of the second kind of order zero, which can be approximated as the inverse of a log function when r is small. Therefore, the strengths of interactions mediated by signaling molecules are no longer linear functions of cell population densities as in the well-mixed model in equation (4.9), but instead are weighted by a decreasing distance kernel $\phi(r)$.

To be consistent with the parameters in the well-mixed model, we set

$$\int_0^\infty 2\pi r \phi\left(r\right) dr = 1. \tag{4.11}$$

We denote population densities of cell type I and II at position $\boldsymbol{p} = (x_p, y_p) \in \mathbb{R}^2$ and time t by $N_i(\boldsymbol{p}, t), i = 1, 2$. The population interactions between cells at position $\boldsymbol{p}$, denoted by $I_{N_i}(\boldsymbol{p}), i = 1, 2$, are nonlocal and can be written in the following form:

$$I_{N_i}\left(\boldsymbol{p}\right) = \int \phi\left(|\boldsymbol{p} - \boldsymbol{q}|\right) N_i\left(\boldsymbol{q}, t\right) \cdot d\boldsymbol{q}, \ \boldsymbol{p} \in \mathbb{R}^2. \tag{4.12}$$

We assume cells also diffuse to access more space and resource when growing. When the growth is activated, cells diffuse faster. Nonlocal interactions also have an impact on cell diffusion dynamics, since cell growth and motility depends on

interactions via signaling molecules. We denote the diffusion rate of type I and II cells at position $\boldsymbol{p}$ by $D_i(\boldsymbol{p}), i = 1, 2$:

$$D_i(\boldsymbol{p}) = D_0 \left(\kappa + a_{ii} I_{N_i}(\boldsymbol{p}) + a d_{ij} I_{N_j}(\boldsymbol{p}) \right) \geq 0, i \neq j, \tag{4.13}$$

where κ is a basal diffusion scaled by D_0. Model of cell diffusion by motility in 2D space (x, y) can be found in literature (Painter and Sherratt, 2003).

We can build the spatial model of cell population dynamics based on characterization of cell diffusion and growth/death kinetics mediated by nonlocal interactions. The model is written in PDEs:

$$\begin{aligned}
\frac{\partial N_1}{\partial t} &= \Delta(D_1 N_1) + k_N \left(1 - \frac{N_1 + N_2}{N_{\max}} \right) N_1 + \left(d_{11} I_{N_1} + d_{12} I_{N_2} \right) N_1, \\
\frac{\partial N_2}{\partial t} &= \Delta(D_2 N_2) + k_N \left(1 - \frac{N_1 + N_2}{N_{\max}} \right) N_2 + \left(d_{21} I_{N_1} + d_{22} I_{N_2} \right) N_2.
\end{aligned} \tag{4.14}$$

Spatial patterns and coexistence stability

To obtain a straightforward understanding of how interaction networks lead to self-organized spatial patterns, we run simulations using an agent-based simulator gro (Jang et al., 2012). We set the initial condition of a homogeneous distribution of both cell populations and use the same parameters in the well-mixed model for better comparison. As shown in Figure 4.6A,B, cooperation leads to a more intermixing spatial pattern while competition tends to self-organize into small patches of segregated colonies. Both competition and cooperation networks support coexistence of two cell populations.

Then we test if the coexistence is stable in spatial environments. We perturb cell density of cell type I by killing cells within a square region of antibiotics dispersal. The range of the perturbation region is measured by r_{dis}. As shown in Figure 4.6A,B, cooperation helps recovery of cell type I population but competition lets cell type II dominates the antibiotics dispersal area and extincts cell type I completely. Figure 4.6C,D demonstrate the population fraction dynamics when r_{dis} is altered. All simulations show that only cooperation network maintains stable coexistence after perturbation in the spatial environment.

From the simulation, we find that the stability of coexistence depends on interaction networks. In contrast to well-mixed environments, competition network becomes unstable. We find the opposite coexistence properties emerging from the spatial patterns. When cell type I in the perturbed area is depleted, cells outside this area can diffuse in. With the cooperation network, the other existing population of cell
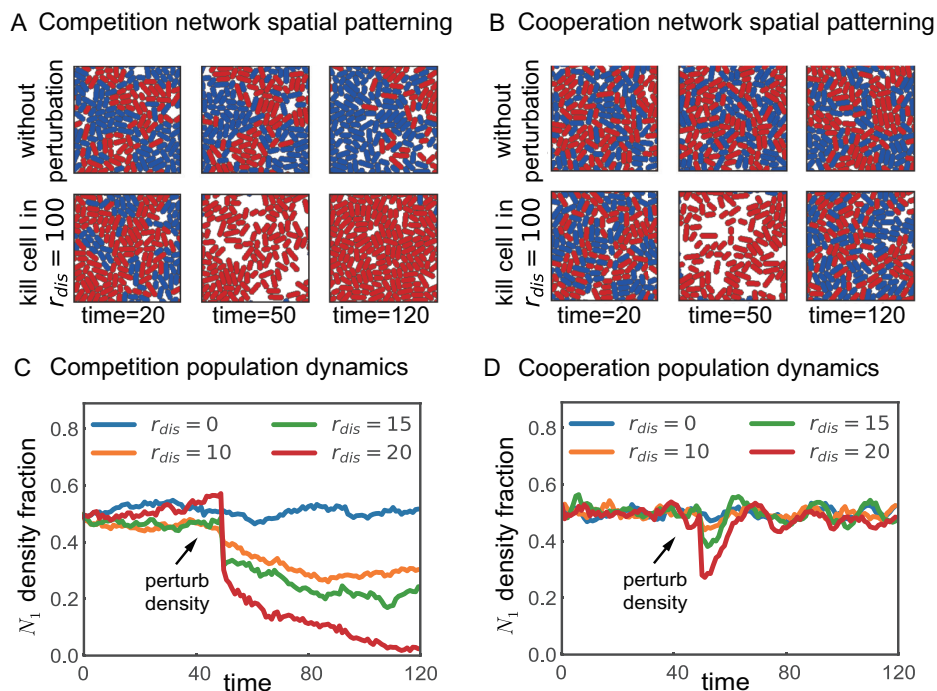
Figure 4.6: Simulation of populations with competition and cooperation in spatial environments. (A)(B) Simulations in gro that show self-organized spatial patterns from competition and cooperation networks. The upper row is without perturbation and the bottom row is when cells of type I in a region is depleted at 50hr. (C)(D) Trajectories of the population density fraction from simulations in gro. Different colors represent a range of perturbed region size.

type II would promote cell type I's growth to recover coexistence in the perturbed region. However, in the competition network, two cell populations inhibit each other's growth. Once cell type I population sense the signaling molecules from cell type II, they die more until the decrease in their density from mutual interaction balances with the self-inhibition. Thus, it is harder for two populations to mix in spatial environment, but instead they form more segregated colonies. When cell type I is depleted, only cell type II grows and further prevents cell type I from growing in the perturbed region. Eventually cell type II is outcompeted and only one dominant population of cell type I cannot recover coexistence after the perturbation.

Spatial conditions for stable coexistence

According to the nonlocal model, we give theoretical explanations of the significant difference of coexistence stability under spatial conditions between cooperation and competition. We linearize equation (4.14) around the equilibrium, apply Fourier
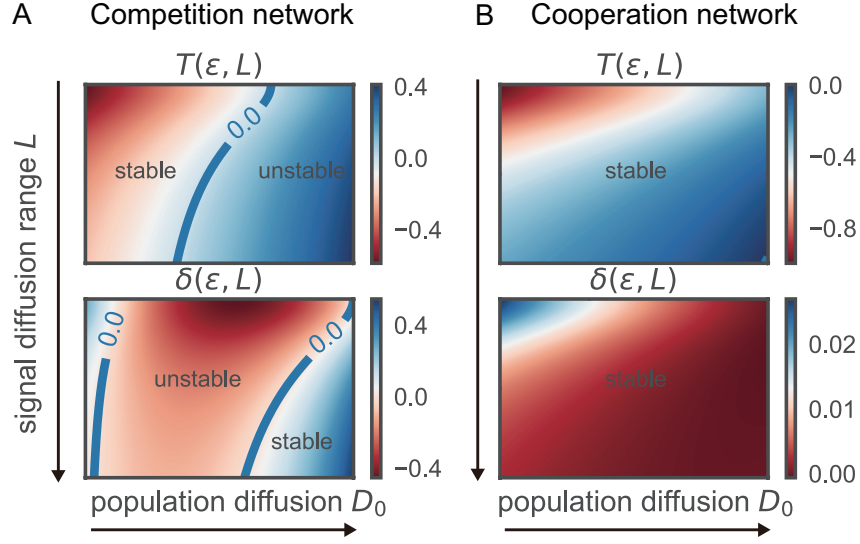
Figure 4.7: Stability condition on signal and population diffusion. (A)(B) Calculation of $T(\epsilon, L)$ and $\delta(\epsilon, L)$ to identify stable regions for competition and cooperation networks.

transform and obtain the following characteristic equation:

$$H = \begin{bmatrix} d_{11} & d_{12} \\ d_{21} & d_{22} \end{bmatrix} \bar{\phi}\left(1 - D_0\epsilon^2\right) - \frac{k_N}{N_{\max}} - \begin{bmatrix} 1 & 0 \\ 0 & 1 \end{bmatrix} \kappa' D_0\epsilon^2, \qquad (4.15)$$

where $\kappa' = d_{11} + d_{12} + \frac{\kappa}{N^*} \geq 0$. The Fourier transform of ϕ is $\bar{\phi} = \frac{1}{\sqrt{(\epsilon L)^2 + 1}}$ according to equations (4.10) and (4.11). Thus, the local stability requires the following conditions:

$$T(\epsilon, L) = 2\left(d_{11}\bar{\phi}\left(1 - D_0\epsilon^2\right) - \kappa' D_0\epsilon^2 - \frac{k_N}{N_{\max}}\right) < 0,$$

$$\delta(\epsilon, L) = \left((d_{11} + d_{12})\bar{\phi}\left(1 - D_0\epsilon^2\right) - \kappa' D_0\epsilon^2 - 2\frac{k_N}{N_{\max}}\right) \qquad (4.16)$$

$$\cdot \left((d_{11} - d_{12})\bar{\phi}\left(1 - D_0\epsilon^2\right) - \kappa' D_0\epsilon^2\right) > 0.$$

Equation (4.16) is equivalent to stable conditions in well-mixed model when there is no cell and signaling molecule diffusion. In other words, well-mixed stability conditions can be derived from equation (4.16) when $L = 0$ and $D_0 = 0$.

Given parameters satisfying the well-mixed stability conditions, the spatial conditions are different for cooperative and competitive interactions. In Figure 4.7, we alter the population diffusion rate D_0 and quorum sensing signaling molecules diffusion range L, and calculate T and δ to identify stable regions. For competitive

interactions, Figure 4.7A shows that the stability condition may not be satisfied for some parameter regimes. Large population diffusion rates indicate the strong repression on cell motility from competitive interactions, and small signal diffusion ranges stress the impact of spatial heterogeneity of signaling molecules on population dynamics. Thus, spatial perturbations can break the coexistence stability when D_0 increases and L is small. Meanwhile, the cooperation network ensures a more robust and stable coexistence in a wide regime of parameters, as shown in Figure 4.7B.

Discussion

The results of the two population system show that cooperative interaction is beneficial because it maintains stable coexistence via intermixing spatial patterning. While competition networks are more likely to be unstable, a potential advantage of competition interactions lies in performing localized functions since cells self-organize into spatially segregated patterns. For example, the human gut microbiome consists of hundreds of microbial species and they are grouped to perform complicated functions (Tropini et al., 2017). It is important to keep stable and robust coexistence within groups and avoid cross-talk and interference from unrelated groups at the same time. Another application could be spatial-temporal control on cell differentiation. The rate of evolution depends on spatial organization and interactions among the population in nontrivial ways.

From modeling and theoretical analysis, we find that the diffusion range and rate of signaling molecules has a big role in determine interaction strengths. For design purposes, we can improve the the stability and robustness performance of synthetic consortia by manipulating these properties.

Chapter 5

CONCLUSION

This thesis mainly contributes to the modeling, design and analysis of synthetic microbial consortia. It is our hope to develop helpful principles based on theoretical analysis and computation, and promote model-based design approach for more controllable dynamics across single level-level to population-level in multicellular systems.

In Chapter 2, we propose model-based design principles for achieving robust control of population density and density-dependent functions. Theoretical analysis and simulation results show that the population-level design via cell-cell signaling systems significantly improves robust behaviors to environmental disturbances. Especially in heterogeneous populations, cell-cell signaling systems can coordinate behaviors of phenotypes to generate a collective adaptation to disturbances. We also explore the performance of a layered control circuit. Results of a population dosage and cellar expression control example suggest that the layered feedback structure aids robustness across single cell-level to population-level.

Future work involves following directions that will hopefully further improve robust control of population-level dynamics. From the implementation perspective, it is helpful to find components and to construct synthetic circuits following the design principles proposed in Chapter 2. For both the signal integral feedback and the bistable stable switching feedback, cell-cell signaling system is the key component. We introduce general regulation networks of control circuits, yet implementation constraints on cell-cell signaling systems haven't been fully discussed. The production, diffusion and degradation kinetics of signaling molecules, as well as cross-talk between signaling systems need to be considered in implementations (Scott and Hasty, 2016).

From the design perspective, we find that heterogeneity in cell populations can be utilized for robust control of population-level dynamics, and propose the population-level design principle based on bistable switching circuits. Based on this observation, we can extend the design to multi-stable state switching circuits and couple them with cell-cell signaling systems (Angeli, Ferrell, and Sontag, 2004; Santos-Moreno et al., 2020). Another interesting topic is to explore fitness benefits of

populations that exhibit heterogeneous phenotypes. Natural microbial populations exhibit heterogeneous phenotypes to better survive environmental stress (Balaban et al., 2004; Kussell and Leibler, 2005; Holland et al., 2014). Thus, heterogeneity can also be harnessed as a fitness advantage to design synthetic microbial populations for robust survival and functionality in long terms.

From the control theory perspective, it is worth reconsidering the concept of robustness in a cell population control context (Del Vecchio, Dy, and Qian, 2016). In our studies, we find population-level robustness does not require single cell's robustness mechanism, and can even emerge from the instability and fragility of single cell's dynamics (Doyle and Csete, 2011). Thus, it is natural to consider layered control structures to overcome intracellular noises at single cell-level and to deal with environmental disturbances at population-level. More theoretical work can be done to understand tradeoffs in such multi-layered distributed yet centralized control structures in microbial consortia.

In Chapter 3, we study design principles of population interaction networks to maintain stable coexistence in well-mixed environments. In a system of two populations, we show that stable coexistence can be achieved in both mutually competitive and cooperative populations. Yet the stability condition depends on specific mechanisms of chemical-mediated interactions. Results suggest that the stability condition for accumulated chemicals, such as quorum sensing signals, is less constrained than by consumed or degraded chemicals, such as metabolites.

In Chapter 4, we investigate design principles of population interaction networks and defined spatial distributions for robust and stable microbial consortia in spatial context. Results suggest that mutually cooperative populations form more intermixing spatial patterns while competitive populations self-organize into segregated patterns. Moreover, more intermixing spatial patterns or distributions of microcolonies can improve the coexistence stability and robustness of density ratio in two population-systems.

There remain more challenges in developing design principles of population interactions and defined environments based on theory and modeling. One challenge is model identifiability, which is a general problem in model-based design in synthetic biology. We hope the unknown parameters of the chemical-mediated interaction model can be determined from experimental data of growth data for each single population. Thus the mechanistic model can have more prediction power for larger systems that consist of multiple populations with chemical-mediated interactions.

One future work is to identify the chemical-mediated interaction model with single population growth data and predict coexistence of two or more populations in co-cultures using identified parameters.

Another challenge lies in the computational aspect. In general, it is hard to analytically solve for population densities of multiple populations from either high dimension ODE or PDE models. We can use simulation tools to predict densities and behaviors of microbial populations in consortia (Jang et al., 2012; Swaminathan et al., 2019; Bauer et al., 2017; Harcombe et al., 2014). However, these tools are developed to answer different biological questions and have their own specializations, such as fast simulation of chemical reactions, metabolic dynamics, cell lineages or spatial organizations in 2D/3D spaces. Therefore, developing computational tools that aim for prediction and analysis of coexisting microbial populations with chemical-mediated interactions is a potential direction in future work.

In order for design principles of synthetic microbial consortia to be truly useful, the proposed circuits should be implemented in experiments and we should test if they indeed exhibit predicted behaviors. Such progress requires a tighter integration between work on theory, modeling and experiments. Circuit designs proposed in Section 2.4 of population density control, density ratio control and fractional control are also implemented in experiments and being tested by collaborators (McCardell et al., 2017). In addition, recent experimental results of bistable switch implementations have shown surprisingly ultrasensitive responses (Gerhardt et al., 2021), which is consistent with our theoretical predictions in Section 2.6. In the future, we hope to integrate these experimental results with our modeling and theory to further improve the design of synthetic microbial consortia.

BIBLIOGRAPHY

Ackermann, Martin (2015). "A functional perspective on phenotypic heterogeneity in microorganisms". In: *Nature Reviews Microbiology* 13.8, pp. 497–508.

Agrawal, Deepak K et al. (2019). "In vitro implementation of robust gene regulation in a synthetic biomolecular integral controller". In: *Nature communications* 10.1, pp. 1–12.

Ajo-Franklin, Caroline M et al. (2007). "Rational design of memory in eukaryotic cells". In: *Genes & development* 21.18, pp. 2271–2276.

Alper, Hal and Gregory Stephanopoulos (2009). "Engineering for biofuels: exploiting innate microbial capacity or importing biosynthetic potential?" In: *Nature Reviews Microbiology* 7.10, pp. 715–723.

Anderson, J Christopher et al. (2006). "Environmentally controlled invasion of cancer cells by engineered bacteria". In: *Journal of molecular biology* 355.4, pp. 619–627.

Andrews, John F (1968). "A mathematical model for the continuous culture of microorganisms utilizing inhibitory substrates". In: *Biotechnology and Bioengineering* 10.6, pp. 707–723.

Ang, Jordan, Sangram Bagh, et al. (2010). "Considerations for using integral feedback control to construct a perfectly adapting synthetic gene network". In: *Journal of theoretical biology* 266.4, pp. 723–738.

Ang, Jordan and David R McMillen (2013). "Physical constraints on biological integral control design for homeostasis and sensory adaptation". In: *Biophysical journal* 104.2, pp. 505–515.

Angeli, David, James E Ferrell, and Eduardo D Sontag (2004). "Detection of multistability, bifurcations, and hysteresis in a large class of biological positive-feedback systems". In: *Proceedings of the National Academy of Sciences* 101.7, pp. 1822–1827.

Aoki, Stephanie K et al. (2019). "A universal biomolecular integral feedback controller for robust perfect adaptation". In: *Nature* 570.7762, pp. 533–537.

Arai, Takamitsu et al. (2007). "Synthesis of Clostridium cellulovorans minicellulosomes by intercellular complementation". In: *Proceedings of the National Academy of Sciences* 104.5, pp. 1456–1460.

Aström, Karl Johan and Richard M Murray (2010). *Feedback systems: an introduction for scientists and engineers*. Princeton university press.

Balaban, Nathalie Q et al. (2004). "Bacterial persistence as a phenotypic switch". In: *Science* 305.5690, pp. 1622–1625.

Balagaddé, Frederick K et al. (2008). "A synthetic Escherichia coli predator–prey ecosystem". In: *Molecular Systems Biology* 4.1.

Balsa-Canto, Eva, Javier Alonso-del-Real, and Amparo Querol (2019). "Mixed growth curve data do not suffice to fully characterize the dynamics of mixed cultures". In: *Proceedings of the National Academy of Sciences*.

Basu, Subhayu et al. (2005). "A synthetic multicellular system for programmed pattern formation". In: *Nature* 434.7037, pp. 1130–1134.

Bauer, Eugen et al. (2017). "BacArena: individual-based metabolic modeling of heterogeneous microbes in complex communities". In: *PLoS computational biology* 13.5, e1005544.

Becskei, Attila, Bertrand Séraphin, and Luis Serrano (2001). "Positive feedback in eukaryotic gene networks: cell differentiation by graded to binary response conversion". In: *The EMBO journal* 20.10, pp. 2528–2535.

Belair, David G, Ngoc Nhi Le, and William L Murphy (2014). "Design of growth factor sequestering biomaterials". In: *Chemical Communications* 50.99, pp. 15651–15668.

Borkowski, Olivier et al. (2016). "Overloaded and stressed: whole-cell considerations for bacterial synthetic biology". In: *Current opinion in microbiology* 33, pp. 123–130.

Brenner, Katie and Frances H Arnold (2011). "Self-organization, layered structure, and aggregation enhance persistence of a synthetic biofilm consortium". In: *PloS one* 6.2, e16791.

Brenner, Katie, David K Karig, et al. (2007). "Engineered bidirectional communication mediates a consensus in a microbial biofilm consortium". In: *Proceedings of the National Academy of Sciences* 104.44, pp. 17300–17304.

Brenner, Katie, Lingchong You, and Frances H Arnold (2008). "Engineering microbial consortia: a new frontier in synthetic biology". In: *Trends in biotechnology* 26.9, pp. 483–489.

Briat, Corentin, Ankit Gupta, and Mustafa Khammash (2016). "Antithetic integral feedback ensures robust perfect adaptation in noisy biomolecular networks". In: *Cell systems* 2.1, pp. 15–26.

Buchler, Nicolas E and Frederick R Cross (2009). "Protein sequestration generates a flexible ultrasensitive response in a genetic network". In: *Molecular systems biology* 5.1, p. 272.

Burmeister, Alina and Alexander Grünberger (2020). "Microfluidic cultivation and analysis tools for interaction studies of microbial co-cultures". In: *Current opinion in biotechnology* 62, pp. 106–115.

Burmølle, Mette et al. (2006). "Enhanced biofilm formation and increased resistance to antimicrobial agents and bacterial invasion are caused by synergistic interactions in multispecies biofilms". In: *Applied and environmental microbiology* 72.6, pp. 3916–3923.

Burrill, Devin R et al. (2012). "Synthetic memory circuits for tracking human cell fate". In: *Genes & development* 26.13, pp. 1486–1497.

Cavaliere, Matteo et al. (2017). "Cooperation in microbial communities and their biotechnological applications". In: *Environmental microbiology* 19.8, pp. 2949–2963.

Ceroni, Francesca, Rhys Algar, et al. (2015). "Quantifying cellular capacity identifies gene expression designs with reduced burden". In: *Nature methods* 12.5, p. 415.

Ceroni, Francesca, Alice Boo, et al. (2018). "Burden-driven feedback control of gene expression". In: *Nature methods* 15.5, pp. 387–393.

Charbonneau, Mark R et al. (2020). "Developing a new class of engineered live bacterial therapeutics to treat human diseases". In: *Nature Communications* 11.1, pp. 1–11.

Chen, David and Adam P Arkin (2012). "Sequestration-based bistability enables tuning of the switching boundaries and design of a latch". In: *Molecular systems biology* 8.1, p. 620.

Chen, Ye et al. (2015). "Emergent genetic oscillations in a synthetic microbial consortium". In: *Science* 349.6251, pp. 986–989.

Clemente, Jose C et al. (2015). "The microbiome of uncontacted Amerindians". In: *Science advances* 1.3, e1500183.

Contois, DE (1959). "Kinetics of bacterial growth: relationship between population density and specific growth rate of continuous cultures". In: *Microbiology* 21.1, pp. 40–50.

Coyte, Katharine Z, Jonas Schluter, and Kevin R Foster (2015). "The ecology of the microbiome: networks, competition, and stability". In: *Science* 350.6261, pp. 663–666.

Cuba Samaniego, Christian and Elisa Franco (2018). "Ultrasensitive molecular controllers for quasi-integral feedback". In: *bioRxiv*.

D'Onofrio, Anthony et al. (2010). "Siderophores from neighboring organisms promote the growth of uncultured bacteria". In: *Chemistry & biology* 17.3, pp. 254–264.

Decho, Alan W, Rebecca L Frey, and John L Ferry (2011). "Chemical challenges to bacterial AHL signaling in the environment". In: *Chemical reviews* 111.1, pp. 86–99.

Del Vecchio, Domitilla, Aaron J Dy, and Yili Qian (2016). "Control theory meets synthetic biology". In: *Journal of The Royal Society Interface* 13.120, p. 20160380.

Doyle, John C and Marie Csete (2011). "Architecture, constraints, and behavior". In: *Proceedings of the National Academy of Sciences* 108.Supplement 3, pp. 15624–15630.

Drengstig, T et al. (2012). "A basic set of homeostatic controller motifs". In: *Biophysical journal* 103.9, pp. 2000–2010.

Eiteman, Mark A, Sarah A Lee, and Elliot Altman (2008). "A co-fermentation strategy to consume sugar mixtures effectively". In: *Journal of Biological Engineering* 2.1, pp. 1–8.

Elias, Sivan and Ehud Banin (2012). "Multi-species biofilms: living with friendly neighbors". In: *FEMS microbiology reviews* 36.5, pp. 990–1004.

Elowitz, Michael B and Stanislas Leibler (2000). "A synthetic oscillatory network of transcriptional regulators". In: *Nature* 403.6767, pp. 335–338.

Escalante, Ana E et al. (2015). "Ecological perspectives on synthetic biology: insights from microbial population biology". In: *Frontiers in microbiology* 6, p. 143.

Ferrell, James E and Eric M Machleder (1998). "The biochemical basis of an all-or-none cell fate switch in Xenopus oocytes". In: *Science* 280.5365, pp. 895–898.

Fierer, Noah and Robert B Jackson (2006). "The diversity and biogeography of soil bacterial communities". In: *Proceedings of the National Academy of Sciences* 103.3, pp. 626–631.

Foster, Kevin R and Thomas Bell (2012). "Competition, not cooperation, dominates interactions among culturable microbial species". In: *Current biology* 22.19, pp. 1845–1850.

Fraser, Dawn and Mads Kaern (2009). "A chance at survival: gene expression noise and phenotypic diversification strategies". In: *Molecular microbiology* 71.6, pp. 1333–1340.

Freilich, Shiri et al. (2011). "Competitive and cooperative metabolic interactions in bacterial communities". In: *Nature communications* 2.1, pp. 1–7.

Fuqua, W Claiborne, Stephen C Winans, and E Peter Greenberg (1994). "Quorum sensing in bacteria: the LuxR-LuxI family of cell density-responsive transcriptional regulators." In: *Journal of bacteriology* 176.2, p. 269.

Gardner, Timothy S, Charles R Cantor, and James J Collins (2000). "Construction of a genetic toggle switch in Escherichia coli". In: *Nature* 403.6767, pp. 339–342.

Gause, George Francis (2019). *The Struggle for Existence: A Classic of Mathematical Biology and Ecology*. Courier Dover Publications.

Gause, Georgii Frantsevich (1932). "Experimental studies on the struggle for existence: I. Mixed population of two species of yeast". In: *Journal of experimental biology* 9.4, pp. 389–402.

Gerhardt, Karl P et al. (2021). "Independent control of mean and noise by convolution of gene expression distributions". In: *bioRxiv*.

Gestel, Jordi Van, Hera Vlamakis, and Roberto Kolter (2015). "Division of labor in biofilms: the ecology of cell differentiation". In: *Microbial Biofilms*, pp. 67–97.

Gill, Steven R et al. (2006). "Metagenomic analysis of the human distal gut microbiome". In: *science* 312.5778, pp. 1355–1359.

Goh, Bo S (1977). "Global stability in many-species systems". In: *The American Naturalist* 111.977, pp. 135–143.

Grandclément, Catherine et al. (2016). "Quorum quenching: role in nature and applied developments". In: *FEMS microbiology reviews* 40.1, pp. 86–116.

Haldane, JBS (1965). "Enzymes MIT Press". In: *Cambridge, Massachusetts* 84.

Hallatschek, Oskar et al. (2007). "Genetic drift at expanding frontiers promotes gene segregation". In: *Proceedings of the National Academy of Sciences* 104.50, pp. 19926–19930.

Hansen, Susse Kirkelund et al. (2007). "Characterization of a Pseudomonas putida rough variant evolved in a mixed-species biofilm with Acinetobacter sp. strain C6". In: *Journal of bacteriology* 189.13, pp. 4932–4943.

Harcombe, William R et al. (2014). "Metabolic resource allocation in individual microbes determines ecosystem interactions and spatial dynamics". In: *Cell reports* 7.4, pp. 1104–1115.

Hardin, Garrett (1960). "The competitive exclusion principle". In: *science* 131.3409, pp. 1292–1297.

Hennig, Stefan et al. (2018). "New approaches in bioprocess-control: Consortium guidance by synthetic cell-cell communication based on fungal pheromones". In: *Engineering in Life Sciences* 18.6, pp. 387–400.

Herbert, Denis, R Elsworth, and RC Telling (1956). "The continuous culture of bacteria; a theoretical and experimental study". In: *Microbiology* 14.3, pp. 601–622.

Hermsen, Rutger, David W Erickson, and Terence Hwa (2011). "Speed, sensitivity, and bistability in auto-activating signaling circuits". In: *PLoS Comput Biol* 7.11, e1002265.

Hogenesch, John B and Erik D Herzog (2011). "Intracellular and intercellular processes determine robustness of the circadian clock". In: *FEBS letters* 585.10, pp. 1427–1434.

Holland, Sara L et al. (2014). "Phenotypic heterogeneity is a selected trait in natural yeast populations subject to environmental stress". In: *Environmental microbiology* 16.6, pp. 1729–1740.

Hsiao, Victoria et al. (2015). "Design and implementation of a biomolecular concentration tracker". In: *ACS synthetic biology* 4.2, pp. 150–161.

Hsu, SB (1978). "Limiting behavior for competing species". In: *SIAM Journal on Applied Mathematics* 34.4, pp. 760–763.

Hsu, Sze-Bi, S Hubbell, and Paul Waltman (1977). "A mathematical theory for single-nutrient competition in continuous cultures of micro-organisms". In: *SIAM Journal on Applied Mathematics* 32.2, pp. 366–383.

Isaacs, Farren J et al. (2003). "Prediction and measurement of an autoregulatory genetic module". In: *Proceedings of the National Academy of Sciences* 100.13, pp. 7714–7719.

Jang, Seunghee S et al. (2012). "Specification and simulation of synthetic multicelled behaviors". In: *ACS Synthetic Biology* 1.8, pp. 365–374.

Jawed, Kamran, Syed Shams Yazdani, and Mattheos AG Koffas (2019). "Advances in the development and application of microbial consortia for metabolic engineering". In: *Metabolic engineering communications* 9, e00095.

Johns, Nathan I et al. (2016). "Principles for designing synthetic microbial communities". In: *Current Opinion in Microbiology* 31, pp. 146–153.

Jones, J Andrew and Xin Wang (2018). "Use of bacterial co-cultures for the efficient production of chemicals". In: *Current opinion in biotechnology* 53, pp. 33–38.

Kaern, Mads et al. (2005). "Stochasticity in gene expression: from theories to phenotypes". In: *Nature Reviews Genetics* 6.6, pp. 451–464.

Kato, Souichiro et al. (2008). "Network relationships of bacteria in a stable mixed culture". In: *Microbial ecology* 56.3, pp. 403–411.

Keren, Iris et al. (2004). "Specialized persister cells and the mechanism of multidrug tolerance in Escherichia coli". In: *Journal of bacteriology* 186.24, pp. 8172–8180.

Khalil, Ahmad S and James J Collins (2010). "Synthetic biology: applications come of age". In: *Nature Reviews Genetics* 11.5, pp. 367–379.

Kim, Hyun Jung et al. (2008). "Defined spatial structure stabilizes a synthetic multispecies bacterial community". In: *Proceedings of the National Academy of Sciences* 105.47, pp. 18188–18193.

Kong, Wentao et al. (2018). "Designing microbial consortia with defined social interactions". In: *Nature Chemical Biology* 14.8, pp. 821–829.

Kramer, Beat P et al. (2004). "An engineered epigenetic transgene switch in mammalian cells". In: *Nature biotechnology* 22.7, pp. 867–870.

Kuramitsu, Howard K et al. (2007). "Interspecies interactions within oral microbial communities". In: *Microbiology and molecular biology reviews* 71.4, pp. 653–670.

Kussell, Edo and Stanislas Leibler (2005). "Phenotypic diversity, population growth, and information in fluctuating environments". In: *Science* 309.5743, pp. 2075–2078.

LaPara, Timothy M et al. (2002). "Functional and structural adaptations of bacterial communities growing on particulate substrates under stringent nutrient limitation". In: *Microbial ecology* 44.4, pp. 317–326.

Lee, Sang Jun et al. (2002). "Genes encoding the N-acyl homoserine lactone-degrading enzyme are widespread in many subspecies of Bacillus thuringiensis". In: *Appl. Environ. Microbiol.* 68.8, pp. 3919–3924.

Lee, Soo Chan et al. (2010). "The evolution of sex: a perspective from the fungal kingdom". In: *Microbiology and Molecular Biology Reviews* 74.2, pp. 298–340.

Levin, Simon A (1976). "Population dynamic models in heterogeneous environments". In: *Annual review of ecology and systematics*, pp. 287–310.

Lindemann, Stephen R et al. (2016). "Engineering microbial consortia for controllable outputs". In: *The ISME journal* 10.9, pp. 2077–2084.

Lobry, Claude and Jérôme Harmand (2006). "A new hypothesis to explain the coexistence of n species in the presence of a single resource". In: *Comptes rendus biologies* 329.1, pp. 40–46.

Lu, Timothy K and James J Collins (2007). "Dispersing biofilms with engineered enzymatic bacteriophage". In: *Proceedings of the National Academy of Sciences* 104.27, pp. 11197–11202.

Ma, Wenzhe et al. (2009). "Defining network topologies that can achieve biochemical adaptation". In: *Cell* 138.4, pp. 760–773.

Ma, Yitong et al. (2020). "Synthetic mammalian signaling circuits for robust cell population control". In:

McCardell, Reed D et al. (2017). "Control of bacterial population density with population feedback and molecular sequestration". In: *bioRxiv*, p. 225045.

McCarty, Nicholas S and Rodrigo Ledesma-Amaro (2019). "Synthetic biology tools to engineer microbial communities for biotechnology". In: *Trends in biotechnology* 37.2, pp. 181–197.

Mee, Michael T et al. (2014). "Syntrophic exchange in synthetic microbial communities". In: *Proceedings of the National Academy of Sciences* 111.20, E2149–E2156.

Meyer, Andreas et al. (2015). "Optimization of a whole-cell biocatalyst by employing genetically encoded product sensors inside nanolitre reactors". In: *Nature chemistry* 7.8, pp. 673–678.

Miller, Melissa B and Bonnie L Bassler (2001). "Quorum sensing in bacteria". In: *Annual Reviews in Microbiology* 55.1, pp. 165–199.

Minty, Jeremy J et al. (2013). "Design and characterization of synthetic fungal-bacterial consortia for direct production of isobutanol from cellulosic biomass". In: *Proceedings of the National Academy of Sciences* 110.36, pp. 14592–14597.

Momeni, Babak, Kristen A Brileya, et al. (2013). "Strong inter-population cooperation leads to partner intermixing in microbial communities". In: *elife* 2, e00230.

Momeni, Babak, Li Xie, and Wenying Shou (2017). "Lotka-Volterra pairwise modeling fails to capture diverse pairwise microbial interactions". In: *Elife* 6, e25051.

Monod, Jacques (1949). "The growth of bacterial cultures". In: *Annual review of microbiology* 3.1, pp. 371–394.

Moser, Hermann et al. (1958). "The dynamics of bacterial populations maintained in the chemostat." In: *The dynamics of bacterial populations maintained in the chemostat.*

Muloiwa, Mpho, Stephen Nyende-Byakika, and Megersa Dinka (2020). "Comparison of unstructured kinetic bacterial growth models". In: *South African Journal of Chemical Engineering*.

Nadell, Carey D, Knut Drescher, and Kevin R Foster (2016). "Spatial structure, cooperation and competition in biofilms". In: *Nature Reviews Microbiology* 14.9, pp. 589–600.

Nakada, Daisuke, Boaz P Levi, and Sean J Morrison (2011). "Integrating physiological regulation with stem cell and tissue homeostasis". In: *Neuron* 70.4, pp. 703–718.

Niehaus, Lori et al. (2019). "Microbial coexistence through chemical-mediated interactions". In: *Nature communications* 10.1, pp. 1–12.

Nielsen, Alex T et al. (2000). "Role of commensal relationships on the spatial structure of a surface-attached microbial consortium". In: *Environmental microbiology* 2.1, pp. 59–68.

Olsman, Noah et al. (2019). "Hard limits and performance tradeoffs in a class of antithetic integral feedback networks". In: *Cell systems* 9.1, pp. 49–63.

Ozbudak, Ertugrul M et al. (2004). "Multistability in the lactose utilization network of Escherichia coli". In: *Nature* 427.6976, p. 737.

Ozdemir, Tanel et al. (2018). "Synthetic biology and engineered live biotherapeutics: toward increasing system complexity". In: *Cell systems* 7.1, pp. 5–16.

Painter, Kevin J and Jonathan A Sherratt (2003). "Modelling the movement of interacting cell populations". In: *Journal of theoretical biology* 225.3, pp. 327–339.

Pande, Samay et al. (2016). "Privatization of cooperative benefits stabilizes mutualistic cross-feeding interactions in spatially structured environments". In: *The ISME journal* 10.6, pp. 1413–1423.

Passarge, Jutta et al. (2006). "Competition for nutrients and light: stable coexistence, alternative stable states, or competitive exclusion?" In: *Ecological Monographs* 76.1, pp. 57–72.

Ptashne, Mark (1992). "A genetic switch: phage and higher organisms". In:

Ptashne, Mark et al. (1980). "How the λ repressor and cro work". In: *Cell* 19.1, pp. 1–11.

Qian, Yili and Domitilla Del Vecchio (2018). "Realizing 'integral control' in living cells: how to overcome leaky integration due to dilution?" In: *Journal of The Royal Society Interface* 15.139, p. 20170902.

Qian, Yili, Theodore W Grunberg, and Domitilla Del Vecchio (2018). "Multi-time-scale biomolecular 'quasi-integral' controllers for set-point regulation and trajectory tracking". In: *2018 Annual American Control Conference (ACC)*. IEEE, pp. 4478–4483.

Ram, Yoav et al. (2019). "Predicting microbial growth in a mixed culture from growth curve data". In: *Proceedings of the National Academy of Sciences* 116.29, pp. 14698–14707.

Relman, David A (2012). "The human microbiome: ecosystem resilience and health". In: *Nutrition reviews* 70.suppl_1, S2–S9.

Ren, Xinying, Ania-Ariadna Baetica, et al. (2017). "Population regulation in microbial consortia using dual feedback control". In: *2017 IEEE 56th Annual Conference on Decision and Control (CDC)*. IEEE, pp. 5341–5347.

Ren, Xinying and Richard M Murray (2018). "Role of interaction network topology in controlling microbial population in consortia". In: *2018 IEEE Conference on Decision and Control (CDC)*. IEEE, pp. 2691–2697.

– (2019). "Cooperation enhances robustness of coexistence in spatially structured consortia". In: *2019 18th European Control Conference (ECC)*. IEEE, pp. 2651–2656.

Ren, Xinying, Christian Cuba Samaniego, et al. (2020). "Bistable State Switch Enables Ultrasensitive Feedback Control in Heterogeneous Microbial Populations". In: *bioRxiv*.

Rickard, Alexander H et al. (2006). "Autoinducer 2: a concentration-dependent signal for mutualistic bacterial biofilm growth". In: *Molecular microbiology* 60.6, pp. 1446–1456.

Riglar, David T et al. (2017). "Engineered bacteria can function in the mammalian gut long-term as live diagnostics of inflammation". In: *Nature biotechnology* 35.7, pp. 653–658.

Roell, Garrett W et al. (2019). "Engineering microbial consortia by division of labor". In: *Microbial Cell Factories* 18.1, pp. 1–11.

Sabnis, Akshay et al. (2018). "Antibiotic interceptors: creating safe spaces for bacteria". In: *PLoS pathogens* 14.4.

Sabra, Wael et al. (2010). "Biosystems analysis and engineering of microbial consortia for industrial biotechnology". In: *Engineering in Life Sciences* 10.5, pp. 407–421.

Samaniego, Christian Cuba and Elisa Franco (2017). "An ultrasensitive biomolecular network for robust feedback control". In: *IFAC-PapersOnLine* 50.1, pp. 10950–10956.

Santos-Moreno, Javier et al. (2020). "Multistable and dynamic CRISPRi-based synthetic circuits". In: *Nature communications* 11.1, pp. 1–8.

Satija, Rahul and Alex K Shalek (2014). "Heterogeneity in immune responses: from populations to single cells". In: *Trends in immunology* 35.5, pp. 219–229.

Schink, Bernhard (2002). "Synergistic interactions in the microbial world". In: *Antonie Van Leeuwenhoek* 81.1-4, pp. 257–261.

Schreiber, Frank et al. (2016). "Phenotypic heterogeneity driven by nutrient limitation promotes growth in fluctuating environments". In: *Nature microbiology* 1.6, p. 16055.

Scott, Spencer R and Jeff Hasty (2016). "Quorum sensing communication modules for microbial consortia". In: *ACS synthetic biology* 5.9, pp. 969–977.

Shou, Wenying, Sri Ram, and Jose MG Vilar (2007). "Synthetic cooperation in engineered yeast populations". In: *Proceedings of the National Academy of Sciences* 104.6, pp. 1877–1882.

Sleight, Sean C et al. (2010). "Designing and engineering evolutionary robust genetic circuits". In: *Journal of biological engineering* 4.1, p. 12.

Sommer, Ulrich (1983). "Nutrient competition between phytoplankton species in multispecies chemostat experiments". In: *Archiv für hydrobiologie* 96, pp. 399–416.

Stallaert, Wayne et al. (2019). "Bistable switches as integrators and actuators during cell cycle progression". In: *FEBS letters* 593.20, pp. 2805–2816.

Stanton, Maureen L (2003). "Interacting guilds: moving beyond the pairwise perspective on mutualisms". In: *The American Naturalist* 162.S4, S10–S23.

Stelling, Jörg et al. (2004). "Robustness of cellular functions". In: *Cell* 118.6, pp. 675–685.

Swaminathan, Anandh et al. (2019). "Fast and flexible simulation and parameter estimation for synthetic biology using bioscrape". In: *bioRxiv*, p. 121152.

Swift, Simon et al. (1996). "Quorum sensing: a population-density component in the determination of bacterial phenotype". In: *Trends in biochemical sciences* 21.6, pp. 214–219.

Tabata, Tetsuya and Yuki Takei (2004). "Morphogens, their identification and regulation". In: *Development* 131.4, pp. 703–712.

Thattai, Mukund and Alexander Van Oudenaarden (2004). "Stochastic gene expression in fluctuating environments". In: *Genetics* 167.1, pp. 523–530.

Tian, Liangfei et al. (2019). "Artificial morphogen-mediated differentiation in synthetic protocells". In: *Nature communications* 10.1, pp. 1–13.

Tilman, David (1977). "Resource competition between plankton algae: an experimental and theoretical approach". In: *Ecology* 58.2, pp. 338–348.

– (1987). "The importance of the mechanisms of interspecific competition". In: *The American Naturalist* 129.5, pp. 769–774.

Toyofuku, Masanori et al. (2016). "Environmental factors that shape biofilm formation". In: *Bioscience, biotechnology, and biochemistry* 80.1, pp. 7–12.

Travisano, Michael and Gregory J Velicer (2004). "Strategies of microbial cheater control". In: *Trends in microbiology* 12.2, pp. 72–78.

Tropini, Carolina et al. (2017). "The gut microbiome: connecting spatial organization to function". In: *Cell host & microbe* 21.4, pp. 433–442.

Veening, Jan-Willem, Wiep Klaas Smits, and Oscar P Kuipers (2008). "Bistability, epigenetics, and bet-hedging in bacteria". In: *Annu. Rev. Microbiol.* 62, pp. 193–210.

Venayak, Naveen et al. (2015). "Engineering metabolism through dynamic control". In: *Current opinion in biotechnology* 34, pp. 142–152.

West, Stuart A and Guy A Cooper (2016). "Division of labour in microorganisms: an evolutionary perspective". In: *Nature Reviews Microbiology* 14.11, pp. 716–723.

Widmaier, Daniel M et al. (2009). "Engineering the Salmonella type III secretion system to export spider silk monomers". In: *Molecular systems biology* 5.1, p. 309.

Wilhelm, Thomas (2009). "The smallest chemical reaction system with bistability". In: *BMC systems biology* 3.1, p. 90.

Williams, Rory L and Richard M Murray (2019). "Tunable integrase-mediated differentiation facilitates improved output of burdensome functions in E. coli". In:

Woyke, Tanja et al. (2006). "Symbiosis insights through metagenomic analysis of a microbial consortium". In: *Nature* 443.7114, pp. 950–955.

Wu, Fuqing, David J Menn, and Xiao Wang (2014). "Quorum-sensing crosstalk-driven synthetic circuits: from unimodality to trimodality". In: *Chemistry & biology* 21.12, pp. 1629–1638.

Xiao, Fangzhou and John C Doyle (2018). "Robust perfect adaptation in biomolecular reaction networks". In: *2018 IEEE Conference on Decision and Control (CDC)*. IEEE, pp. 4345–4352.

Xiu, Yu et al. (2017). "Naringenin-responsive riboswitch-based fluorescent biosensor module for Escherichia coli co-cultures". In: *Biotechnology and Bioengineering* 114.10, pp. 2235–2244.

Yanni, David et al. (2019). "Drivers of spatial structure in social microbial communities". In: *Current Biology* 29.11, R545–R550.

You, Lingchong et al. (2004). "Programmed population control by cell–cell communication and regulated killing". In: *Nature* 428.6985, pp. 868–871.

Youk, Hyun and Wendell A Lim (2014). "Secreting and sensing the same molecule allows cells to achieve versatile social behaviors". In: *Science* 343.6171, p. 1242782.

Zhang, David Yu et al. (2007). "Engineering entropy-driven reactions and networks catalyzed by DNA". In: *Science* 318.5853, pp. 1121–1125.

Zhang, Haoran et al. (2015). "Engineering Escherichia coli coculture systems for the production of biochemical products". In: *Proceedings of the National Academy of Sciences* 112.27, pp. 8266–8271.

Zhang, Shu et al. (2018). "Interkingdom microbial consortia mechanisms to guide biotechnological applications". In: *Microbial biotechnology* 11.5, pp. 833–847.

Zhou, Kang et al. (2015). "Distributing a metabolic pathway among a microbial consortium enhances production of natural products". In: *Nature biotechnology* 33.4, pp. 377–383.

MODELS AND SIMULATIONS OF CHEMICAL-MEDIATED INTERACTIONS

This section contains more modeling and simulation results for populations with chemical-mediated interactions discussed in Chapter 3.

A.1 Competitive interactions in batch versus chemostat cultures

Here are models for populations with competitive interactions via bactericidal and bacteriostatic antibiotics, discussed in Section 3.3.

We assume that bactericidal antibiotics induce death while bacteriostatic antibiotics inhibit cell growth. Meanwhile, both populations grow on the same nutrient. We denote the population densities of cell type I and II by N_1 and N_2, concentrations of antibiotics I and II by T_1 and T_2, and the nutrient concentration by M. We assume that the production of antibiotics depend on population densities as well as the nutrient uptake, to avoid infinite production even when the nutrient is used up.

For a batch culture, we can first write down an ODE model of interactive populations via bactericidal antibiotics, assuming that the antibiotics kill cells with a Hill-type function kinetics:

$$
\begin{aligned}
\text{cell I population density:} \quad & \frac{\mathrm{d}N_1}{\mathrm{d}t} = \left(\alpha_1 \frac{M}{K_M + M} - \gamma \frac{T_2}{K_T + T_2} \right) N_1, \\[2mm]
\text{cell II population density:} \quad & \frac{\mathrm{d}N_2}{\mathrm{d}t} = \left(\alpha_2 \frac{M}{K_M + M} - \gamma \frac{T_1}{K_T + T_1} \right) N_2, \\[2mm]
\text{antibiotics I concentration:} \quad & \frac{\mathrm{d}T_1}{\mathrm{d}t} = \beta_1 \frac{M}{K_M + M} N_1, \\[2mm]
\text{antibiotics II concentration:} \quad & \frac{\mathrm{d}T_2}{\mathrm{d}t} = \beta_2 \frac{M}{K_M + M} N_2, \\[2mm]
\text{nutrient concentration:} \quad & \frac{\mathrm{d}M}{\mathrm{d}t} = -\delta \frac{M}{K_M + M} \left(N_1 + N_2 \right).
\end{aligned}
\tag{A.1}
$$

Parameters α_1, α_2 are cell growth rates, γ is cell death rate, K_M is the dissociation rate in nutrient consumption, K_T is the dissociation rate in antibiotics killing, β_1, β_2 are production rates of antibiotics, and δ is the nutrient consumption rate. For simplicity, some parameters are set to be the same rate for two cell populations.

Similarly, we can write down an ODE model of interactive populations via bacterio-static antibiotics, assuming that the antibiotics inhibit cells' growth with a Hill-type function kinetics:

$$
\begin{aligned}
\text{cell I population density:} \quad & \frac{\mathrm{d}N_1}{\mathrm{d}t} = \alpha_1 \frac{M}{K_M + M} \frac{K_T}{K_T + T_2} N_1, \\
\text{cell II population density:} \quad & \frac{\mathrm{d}N_2}{\mathrm{d}t} = \alpha_2 \frac{M}{K_M + M} \frac{K_T}{K_T + T_1} N_2, \\
\text{antibiotics I concentration:} \quad & \frac{\mathrm{d}T_1}{\mathrm{d}t} = \beta_1 \frac{M}{K_M + M} N_1, \\
\text{antibiotics II concentration:} \quad & \frac{\mathrm{d}T_2}{\mathrm{d}t} = \beta_2 \frac{M}{K_M + M} N_2, \\
\text{nutrient concentration:} \quad & \frac{\mathrm{d}M}{\mathrm{d}t} = -\delta \frac{M}{K_M + M} \left(N_1 + N_2 \right).
\end{aligned}
\tag{A.2}
$$

Parameters are the same as in equation (A.1), except that K_T is the dissociation rate of antibiotics inhibiting cell growth.

For a chemostat culture, we assume there is a constant dilution rate D in the media and inflow rate of nutrient M_0. We can obtain an ODE model for the interaction mediated by bactericidal antibiotics:

$$
\begin{aligned}
\text{cell I population density:} \quad & \frac{\mathrm{d}N_1}{\mathrm{d}t} = \left(\alpha_1 \frac{M}{K_M + M} - \gamma \frac{T_2}{K_T + T_2} - D \right) N_1, \\
\text{cell II population density:} \quad & \frac{\mathrm{d}N_2}{\mathrm{d}t} = \left(\alpha_2 \frac{M}{K_M + M} - \gamma \frac{T_1}{K_T + T_1} - D \right) N_2, \\
\text{antibiotics I concentration:} \quad & \frac{\mathrm{d}T_1}{\mathrm{d}t} = \beta_1 \frac{M}{K_M + M} N_1 - D T_1, \\
\text{antibiotics II concentration:} \quad & \frac{\mathrm{d}T_2}{\mathrm{d}t} = \beta_2 \frac{M}{K_M + M} N_2 - D T_2, \\
\text{nutrient concentration:} \quad & \frac{\mathrm{d}M}{\mathrm{d}t} = D(M_0 - M) - \delta \frac{M}{K_M + M} \left(N_1 + N_2 \right).
\end{aligned}
\tag{A.3}
$$

Similarly, the ODE model of interactive populations with bacteriostatic antibiotics

in the chemostat culture becomes

cell I population density: $\qquad \dfrac{\mathrm{d}N_1}{\mathrm{d}t} = \left(\alpha_1 \dfrac{M}{K_M + M} \dfrac{K_T}{K_T + T_2} - D \right) N_1,$

cell II population density: $\qquad \dfrac{\mathrm{d}N_2}{\mathrm{d}t} = \left(\alpha_2 \dfrac{M}{K_M + M} \dfrac{K_T}{K_T + T_1} - D \right) N_2,$

antibiotics I concentration: $\qquad \dfrac{\mathrm{d}T_1}{\mathrm{d}t} = \beta_1 \dfrac{M}{K_M + M} N_1 - DT_1,$

antibiotics II concentration: $\qquad \dfrac{\mathrm{d}T_2}{\mathrm{d}t} = \beta_2 \dfrac{M}{K_M + M} N_2 - DT_2,$

nutrient concentration: $\qquad \dfrac{\mathrm{d}M}{\mathrm{d}t} = D(M_0 - M) - \delta \dfrac{M}{K_M + M} (N_1 + N_2).$

$$(A.4)$$

A.2 Cooperative interactions in batch versus chemostat cultures

We show more examples of different chemical-mediation mechanisms for cooperative interactions, and show population density dynamics and coexistence in batch and chemostat cultures.

The first cooperation mechanism is via crossfeeding of metabolites, as shown in Figure A.1A. The metabolites produced by one population can be considered as nutrients to the other population and promote their growth. Meanwhile, both populations grow on another shared nutrient. We denote the population densities of cell type I and II by N_1 and N_2, concentrations of nutrient I and II by M_1 and M_2, and the shared nutrient concentration by M. We assume that the production of M_1 and M_2 depend on population densities as well as the shared nutrient uptake, to avoid infinite production even when the nutrient is used up. In a batch culture, we can write down an ODE model:

cell I population density: $\qquad \dfrac{\mathrm{d}N_1}{\mathrm{d}t} = \alpha_1 \dfrac{M_2}{K_M + M_2} N_1,$

cell II population density: $\qquad \dfrac{\mathrm{d}N_2}{\mathrm{d}t} = \alpha_1 \dfrac{M_1}{K_M + M_1} N_2,$

nutrient I concentration: $\qquad \dfrac{\mathrm{d}M_1}{\mathrm{d}t} = \beta_1 \dfrac{M}{K_M + M} N_1 - \delta \dfrac{M_1}{K_M + M_1} N_2, \qquad (A.5)$

nutrient II concentration: $\qquad \dfrac{\mathrm{d}M_2}{\mathrm{d}t} = \beta_2 \dfrac{M}{K_M + M} N_2 - \delta \dfrac{M_2}{K_M + M_2} N_1,$

nutrient concentration: $\qquad \dfrac{\mathrm{d}M}{\mathrm{d}t} = -\delta \dfrac{M}{K_M + M} (N_1 + N_2).$

Parameters α_1, α_2 are cell growth rates, K_M is the dissociation rate in nutrient consumption, β_1, β_2 are production rates of nutrients, and δ is the nutrient consumption
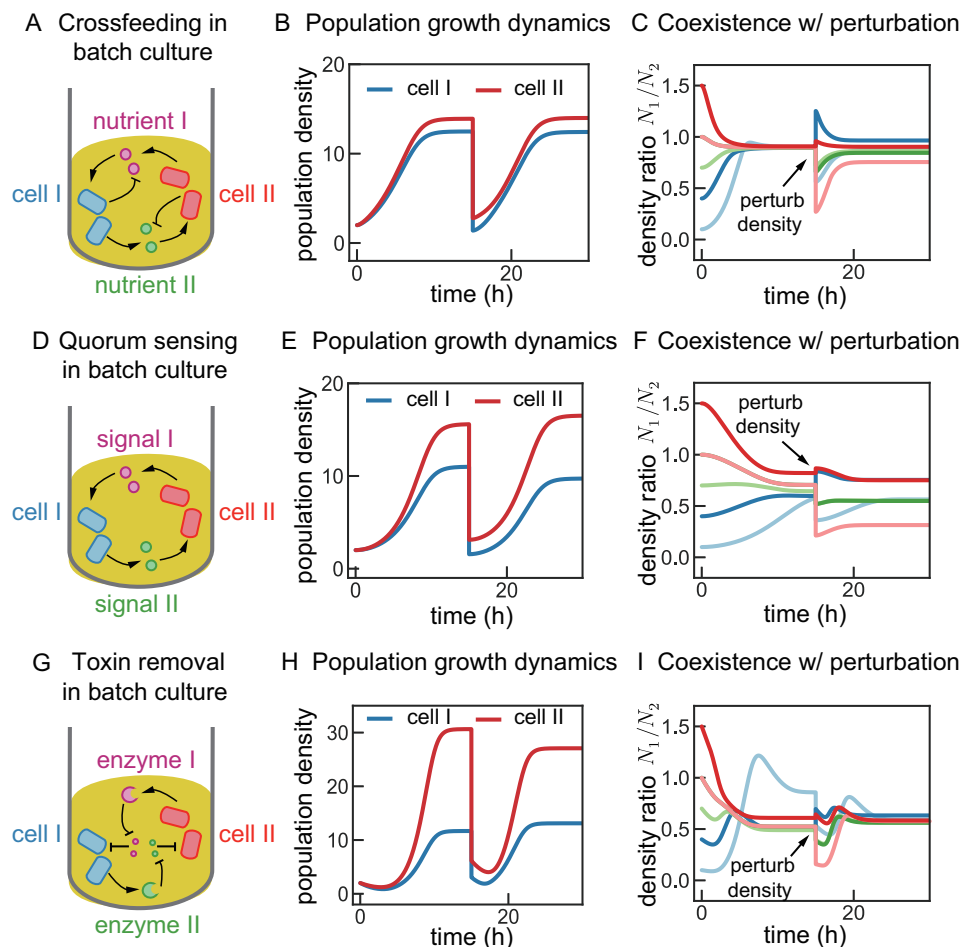
Figure A.1: Cooperation via cross-feeding, quorum sensing and toxin removal in the batch culture. (A)(D)(G) Schematic diagrams of a co-culture of two cell populations with cooperative interactions in a batch culture. There is a constant inlow/outflow of media. (B)(E)(H) Simulations of population densities in the batch culture. At 15hr in the simulation, we dilute the cell populations to a low initial densities and show their growth dynamics in fresh media. (C)(F)(I) Simulations of the density ratio of two populations with various initial densities. At 15hr, we perturb the densities to show the convergence of the density ratio.

rate. For simplicity, some parameters are set to be the same rate for two cell populations.

The second cooperation mechanism is via growth activation via quorum sensing molecules, as shown in Figure A.1B. The quorum sensing molecules can activate growth without being consumed. We denote concentrations of signal I and II by S_1 and S_2, and assume that the production of S_1 and S_2 depend on population densities as well as the shared nutrient uptake. In a batch culture, we can write down an ODE

model:

cell I population density:
$$\frac{\mathrm{d}N_1}{\mathrm{d}t} = \alpha_1 \frac{M}{K_M + M} \frac{S_2}{K_S + S_2} N_1,$$

cell II population density:
$$\frac{\mathrm{d}N_2}{\mathrm{d}t} = \alpha_2 \frac{M}{K_M + M} \frac{S_1}{K_S + S_1} N_2,$$

signal I concentration:
$$\frac{\mathrm{d}S_1}{\mathrm{d}t} = \beta_1 \frac{M}{K_M + M} N_1,$$

antibiotics II concentration:
$$\frac{\mathrm{d}S_2}{\mathrm{d}t} = \beta_2 \frac{M}{K_M + M} N_2,$$

nutrient concentration:
$$\frac{\mathrm{d}M}{\mathrm{d}t} = -\delta \frac{M}{K_M + M} (N_1 + N_2).$$

(A.6)

The parameter K_S is the dissociation rate in signal-induced growth activation.

The third cooperation mechanism is via toxin removal by secretion of enzymes that degrade toxins, as shown in Figure A.1C. We assume there are two toxins in the media, denoted by T_1 and T_2. The enzyme I secreted by cell II population can degrade toxin I and relieve the death of cell I population, and vice versa. We denote concentrations of enzyme I and II by R_1 and R_2, and assume that the production of R_1 and R_2 depend on population densities as well as the shared nutrient uptake. In a batch culture, we can write down an ODE model, assuming Hill-type functions of toxin removal kinetics by the enzyme:

cell I population density:
$$\frac{\mathrm{d}N_1}{\mathrm{d}t} = \left(\alpha_1 \frac{M}{K_M + M} - \gamma \frac{T_1}{K_T + T_1} \right) N_1,$$

cell II population density:
$$\frac{\mathrm{d}N_2}{\mathrm{d}t} = \left(\alpha_2 \frac{M}{K_M + M} - \gamma \frac{T_2}{K_T + T_2} \right) N_2,$$

toxin I concentration:
$$\frac{\mathrm{d}T_1}{\mathrm{d}t} = -\eta \frac{R_1}{K_R + R_1} T_1,$$

toxin II concentration:
$$\frac{\mathrm{d}T_2}{\mathrm{d}t} = -\eta \frac{R_2}{K_R + R_2} T_2,$$

enzyme I concentration:
$$\frac{\mathrm{d}R_1}{\mathrm{d}t} = \beta_1 \frac{M}{K_M + M} N_2,$$

enzyme II concentration:
$$\frac{\mathrm{d}R_2}{\mathrm{d}t} = \beta_2 \frac{M}{K_M + M} N_1,$$

nutrient concentration:
$$\frac{\mathrm{d}M}{\mathrm{d}t} = -\delta \frac{M}{K_M + M} (N_1 + N_2).$$

(A.7)

The parameter γ is cell death rate, K_T is the dissociation rate in toxin killing, η is toxin degradation rate by enzymes, K_R is the dissociation rate in enzymatic degradation.

Similarly, we can derive ODE models for populations in the chemostat culture by adding dilution and inflow of nutrient in the media.
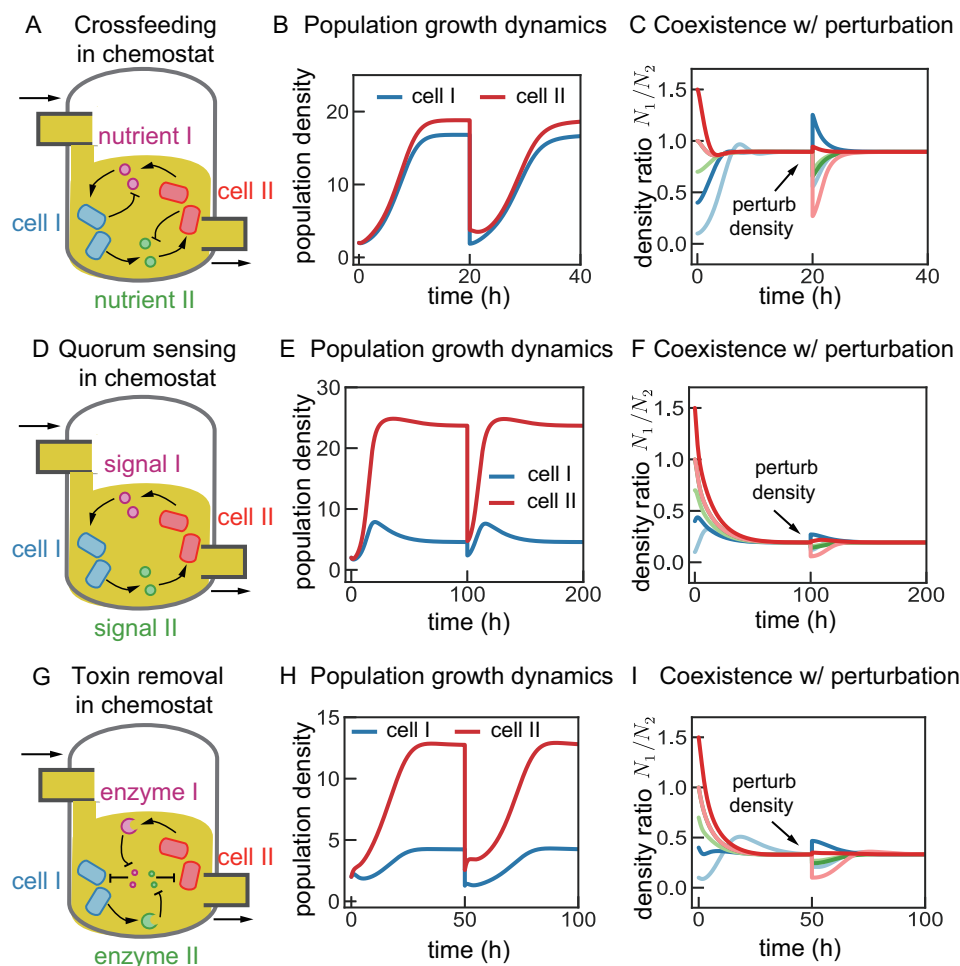
Figure A.2: Cooperation via cross-feeding, quorum sensing and toxin removal in the chemostat culture. (A)(D)(G) Schematic diagrams of a co-culture of two cell populations with cooperative interactions in a chemostat culture. There is a constant inlow/outflow of media. (B)(E)(H) Simulations of population densities in the chemostat culture. At 20hr/100hr/50hr in the simulation, we dilute the cell populations to a low initial densities and show their growth dynamics in fresh media. (C)(F)(I) Simulations of the density ratio of two populations with various initial densities. At 20hr/100hr/50hr, we perturb the densities to show the convergence of the density ratio.

We show simulations of population growth dynamics and density ratio of the batch culture in Figure A.1, and of the chemostat culture in Figure A.2. In Figure A.1, simulations of cell growth dynamics show coexistence of two populations with cooperative interactions, yet the steady state densities at stationary phase depend on initial cell densities as well as nutrients. When diluting and regrowing cells in fresh media, the new steady state at stationary phase is steered to different levels. The same two population system in chemostat culture can maintain a stable coexistence

with cooperative interactions despite initial condition and perturbations in densities, shown in Figure A.2.

A.3   Competition via accumulated versus consumed/degraded chemicals

In this section, we compare the transient dynamical properties of the competition network mediated by two types of chemicals in the two population-system, discussed in Section 3.4. We show simulations of population density dynamics of competitively interactive populations in Figure A.3. The trajectories show that with accumulated chemicals, the transient dynamics of population densities become more oscillatory, compared to the fast convergence with consumed/degraded chemicals.
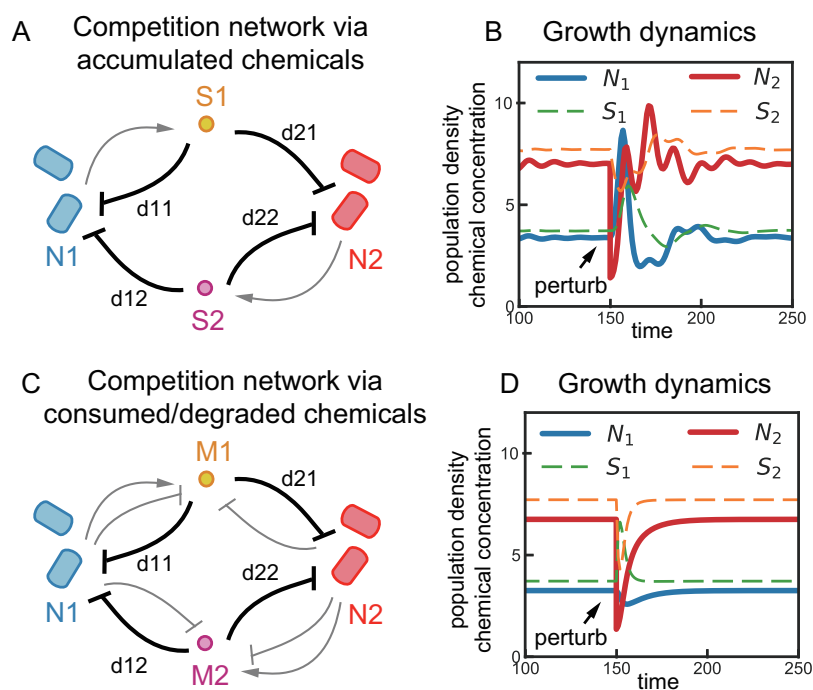

Figure A.3: Dynamics of populations with competition via accumulated and consumed/degraded chemicals. (A)(C) Schematic diagrams of competition network mediated by accumulated and consumed/degraded chemicals between two populations. (B)(D) Simulations of population density and chemical concentration dynamics. At 150min, we perturb the population density and show oscillatory and dampened convergence.

DETAILED MODELS OF SPATIALLY DISTRIBUTED POPULATIONS

This section contains a detailed model of of spatially distributed populations discussed in Chapter 4.

cell I density:
$$\frac{dN_i^{(1)}}{dt} = k_{N_1}\left(1 - \frac{N_i^{(1)}}{N_{\max}}\right)N_i^{(1)} - d_N T_i^{(1)} N_i^{(1)},$$

cell I toxin:
$$\frac{dT_i^{(1)}}{dt} = \beta_T \frac{\left(S^{(1)}\left(\mathbf{r}_i^{(1)}\right)\right)^2}{K_{S_1} + \left(S^{(1)}\left(\mathbf{r}_i^{(1)}\right)\right)^2} - \gamma T_i^{(1)} A_i^{(1)} - dT_i^{(1)},$$

cell I anti-toxin:
$$\frac{dA_i^{(1)}}{dt} = \beta_A \frac{\left(S^{(2)}\left(\mathbf{r}_i^{(1)}\right)\right)^2}{K_{S_2} + \left(S^{(2)}\left(\mathbf{r}_i^{(1)}\right)\right)^2} - \gamma T_i^{(1)} A_i^{(1)} - dA_i^{(1)},$$

cell II density:
$$\frac{dN_i^{(1)}}{dt} = k_{N_2}\left(1 - \frac{N_j^{(2)}}{N_{\max}}\right)N_j^{(2)} - d_N T_j^{(2)} N_j^{(2)},$$

cell II toxin:
$$\frac{dT_j^{(2)}}{dt} = \beta_T \frac{\left(S^{(2)}\left(\mathbf{r}_j^{(2)}\right)\right)^2}{K_{S_j} + \left(S^{(2)}\left(\mathbf{r}_j^{(2)}\right)\right)^2} - \gamma T_j^{(2)} A_j^{(2)} - dT_j^{(2)}, \quad (\text{B.1})$$

cell II anti-toxin:
$$\frac{dA_j^{(2)}}{dt} = \beta_A \frac{\left(S^{(1)}\left(\mathbf{r}_j^{(2)}\right)\right)^2}{K_{S_1} + \left(S^{(1)}\left(\mathbf{r}_j^{(2)}\right)\right)^2} - \gamma T_j^{(2)} A_j^{(2)} - dA_j^{(2)},$$

S_1 signal:
$$\frac{\partial S^{(1)}(\mathbf{r}, t)}{\partial t} = \sum_{i=1}^{n} \beta_{S_1} N_i^{(1)} \mathbf{1}_{\{\mathbf{r}=\mathbf{r}_i^{(1)}\}}(\mathbf{r}) + k_{dif}\nabla^2 S^{(1)} - d_S S^{(1)},$$
$$0 \le \mathbf{r} \le L,\ S^{(1)}(\mathbf{r}, 0) = 0,\ S^{(1)}\left(L\frac{\mathbf{r}}{|\mathbf{r}|}, t\right) = 0,$$

S_2 signal:
$$\frac{\partial S^{(2)}(\mathbf{r}, t)}{\partial t} = \sum_{j=1}^{n} \beta_{S_2} N_j^{(2)} \mathbf{1}_{\{\mathbf{r}=\mathbf{r}_j^{(2)}\}}(\mathbf{r}) + k_{dif}\nabla^2 S^{(2)} - d_S S^{(2)},$$
$$0 \le \mathbf{r} \le L,\ S^{(2)}(\mathbf{r}, 0) = 0,\ S^{(2)}\left(L\frac{\mathbf{r}}{|\mathbf{r}|}, t\right) = 0.$$